Electrolyte- and Transport-Enhanced Thermogalvanic Energy Conversion

by

Andrey Gunawan

A Dissertation Presented in Partial Fulfillment
of the Requirements for the Degree
Doctor of Philosophy

Approved November 2015 by the
Graduate Supervisory Committee:

Patrick E. Phelan, Chair
Daniel A. Buttry
Vladimiro Mujica
Candace K. Chan
Robert Y. Wang

ARIZONA STATE UNIVERSITY

December 2015

ABSTRACT

Waste heat energy conversion remains an inviting subject for research, given the renewed emphasis on energy efficiency and carbon emissions reduction. Solid-state thermoelectric devices have been widely investigated, but their practical application remains challenging because of cost and the inability to fabricate them in geometries that are easily compatible with heat sources. An intriguing alternative to solid-state thermoelectric devices is thermogalvanic cells, which include a generally liquid electrolyte that permits the transport of ions. Thermogalvanic cells have long been known in the electrochemistry community, but have not received much attention from the thermal transport community. This is surprising given that their performance is highly dependent on controlling both thermal and mass (ionic) transport. This research will focus on a research project, which is an interdisciplinary collaboration between mechanical engineering (i.e. thermal transport) and chemistry, and is a largely experimental effort aimed at improving fundamental understanding of thermogalvanic systems. The first part will discuss how a simple utilization of natural convection within the cell doubles the maximum power output of the cell. In the second part of the research, some of the results from the previous part will be applied in a feasibility study of incorporating thermogalvanic waste heat recovery systems into automobiles. Finally, a new approach to enhance Seebeck coefficient by tuning the configurational entropy of a mixed-ligand complex formation of copper sulfate aqueous electrolytes will be presented. Ultimately, a summary of these results as well as possible future work that can be formed from these efforts is discussed.

To Mom, Dad, and Sis for teaching me what love, forgiveness and respect truly are

To Alyssa and the Salas family for their unconditional love and support

To Mother Mary for her divine grace through the Novenas

ACKNOWLEDGMENTS

I am most thankful to my advisor Patrick Phelan for giving me the opportunity to work on this challenging, yet exciting and fulfilling research project. I greatly appreciate his trust in me to explore and pursue my scientific interest. And I am deeply grateful to him for bringing me into the 'family'. It has given me a perspective unlike any other, and provided me with lifelong friends. There is no way I could have accomplished this goal of mine without the support and guidance I have received from him. Thank you Pat!

Next, I would like to thank my electrochemistry guru Daniel Buttry, without whom this work would have never happened. Dan has shown tremendous patience with me and has taught me much about the finer points of physical chemistry world. Thanks to Dan, I have improved my electrochemistry skills from zero to something. I know I must have driven him crazy! But his steadfast encouragement and direction have seen me through this process. I am eternally grateful for his counsel and advice and know his words of wisdom will serve me well in my career.

I would like to especially thank Candace Chan who served as a mentor and role model for me. She pushed me to a higher academic standard and, at the same time, stood by me through every twist and turn of my graduate school experience. She has always looked out for me as if I was her student. She reminded me to remain focused on my PhD without which I know I would have been lost. I truly hope I am able to keep up to her standard and follow her example becoming a successful academia in the future.

I would also like to thank Vladimiro Mujica and Robert Wang for their contributions, friendliness, advice and encouragement on my research. A portion of

Chapter 5 is derived from Vladimiro's ideas. I couldn't have finished without you guys!

I would also like to express my gratitude to the entire Phelan Lab: Robert Taylor, Mark Miner, Carlos Ortiz, Soochan Lee, Chao-Han Lin, Nicholas Fette, Sami Al-Elyani, Turki Alajmi, Jessica Johnson, Noah Wilson, Weston Bertrand and Jonathan Sherbeck. I would also like to thank my good friends in other labs: Rafeed Chaudhury, Hechao Li, David Hanigan, Levi Straka, Tylan Watkins, Poonam Singh, Telpriore 'Greg' Tucker, Mingmeng Zhang, and Wei Lv. A special thanks goes to my best buddy and partner in crime, Adrianus Indrat Aria, for the morale support and for keeping me sane the last few years. In addition, I would like to thank numerous advisors and mentors who have supported and encouraged me, most notably, Liping Wang, Ravi Prasher, Ronald Adrian, Himanshu Tyagi, Todd Otanicar, Merlyna Lim, Lavi Zuhal, and Shannon Yee.

Last, but not least, I would like to express my most sincere and deepest gratitude to my family for the freedom to pursue my dreams for the last seven years. To Alyssa, te amo y más! Thank you for your patience and love as I finished my degree. I know that I have been cranky throughout this rollercoaster ride that has been my PhD. Your support and encouragement made it possible for me to be where I am today. You and your family have always been there for me, and I am forever grateful.

Finally I would like to acknowledge the support from The Electrochemical Society 2014 Joseph W. Richards Summer Fellowship, American Society of Mechanical Engineers Power Division 2015 Best Student Paper Award, and 2014-2015 Graduate Research Support Program from ASU Graduate & Professional Student Association. This research has been supported by the National Science Foundation through Award CBET-1236571.

TABLE OF CONTENTS

Page

Page

Page

LIST OF TABLES

Table Page

LIST OF FIGURES

Figure Page

Figure Page

Figure Page

Figure Page

Figure Page

NOMENCLATURE

A	cross-sectional area of the electrode, and of the salt bridge [m^{-2}]
C	concentration [mol L^{-1}]
E	potential difference [V]
F	Faraday constant
I	current [A]
j	current density [A m^{-2}]
k	thermal conductivity [W m^{-1} K^{-1}]
n	number of electrons involved in the reaction
P	power output [W]
R	universal gas constant, resistance [Ω]
S	partial molar entropy [J mol^{-1} K^{-1}]
S^*	Eastman entropy [J mol^{-1} K^{-1}]
$\bar{\bar{S}}_e$	total transported entropy of the electrons in metal leads [J mol^{-1} K^{-1}]
T	temperature [K]
x	inter-electrode spacing [m]
Z	figure of merit of thermoelectric devices [K^{-1}]

Greek symbols

α	Seebeck coefficient [V K^{-1}]
γ	activity coefficient
σ	electrical (ionic) conductivity [S m^{-1}]

η	power conversion efficiency [%]
Ω	ohmic

Subscripts

a	activation
amb	ambient
ext	external
int	internal
m	mass transport
oc	open-circuit
op	operating
sc	short-circuit
th	thermal
∞	steady state

1. INTRODUCTION

Thermogalvanic cells have recently received significant attention because of their immense potential in converting low-temperature waste heat to electricity (see, e.g., [1-26]). There is a huge amount of waste heat available from industrial sources [27], automobiles [28], buildings [29], etc., as well as heat available from solar thermal energy. The $ value of such waste heat conversion is difficult to estimate, but the International Energy Agency projects that world-wide demand for energy will increase by one third from 2010 to 2035, and will require an investment of $38 *trillion* [30]. Indeed, the United Nations has declared the decade 2014-2024 as the "Decade of Sustainable Energy for All" [31].

A thermogalvanic cell is defined by Agar [32] as "a galvanic cell in which the temperature is not uniform. In practice, such cell will consist of two metallic electrodes, not necessarily reversible or chemically identical, immersed in electrolyte, which may or may not be homogenous in composition, and in which selectively permeable membranes might be interposed." (p. 32) Figure 1 on the next page shows schematically a cell system using copper (Cu) electrodes in an aqueous solution of copper sulfate ($CuSO_4$).

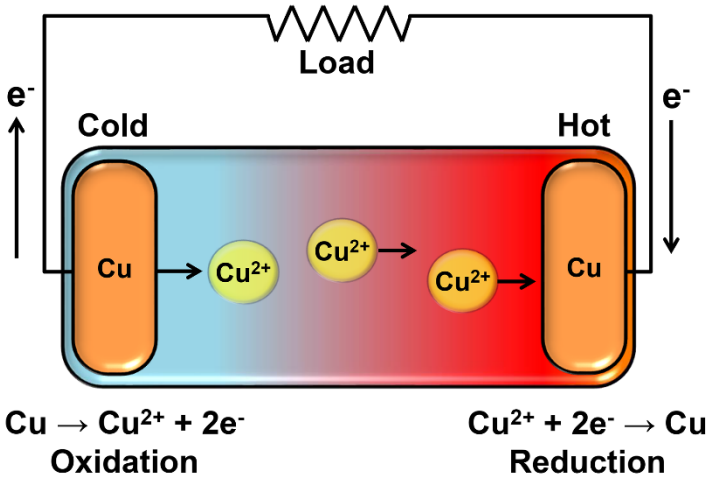

Figure 1. Schematic Drawing of a Thermogalvanic Cell Using Cu Electrodes in an Aqueous Solution of $CuSO_4$.

The temperature difference between the cold and the hot Cu electrodes creates a potential difference that is directly proportional to the change in entropy of the redox reaction in the cell. If these electrodes are connected to a load, this potential difference drives the oxidation of Cu on the cold electrode (anode) [1]:

$$Cu \rightarrow Cu^{2+} + 2\,e^{-} \qquad (1)$$

and the reduction of Cu^{2+} cations on the hot electrode (cathode):

$$Cu^{2+} + 2\,e^{-} \rightarrow Cu \qquad (2)$$

so that electrical current and power can be delivered, thus converting thermal energy into electrical energy (see Figure 2 in the next page). History notes that the first experiments of thermogalvanic cells in 1825, which were performed on the electrode-electrolyte Cu-$CuSO_4$ and Zn-$ZnSO_4$ systems, were inspired by the principle of the first solid metal/metal junction thermocouple invented by Thomas Johann Seebeck four years earlier in 1821 [33]. However, at the interface between the electrodes and the electrolyte, the passage of current will change from an electronic to an ionic current, which

distinguishes such cells from their solid-state siblings [32]. Although the nature of the effects are different, this temperature dependence of the electrode potential is often referred to as the Seebeck coefficient.

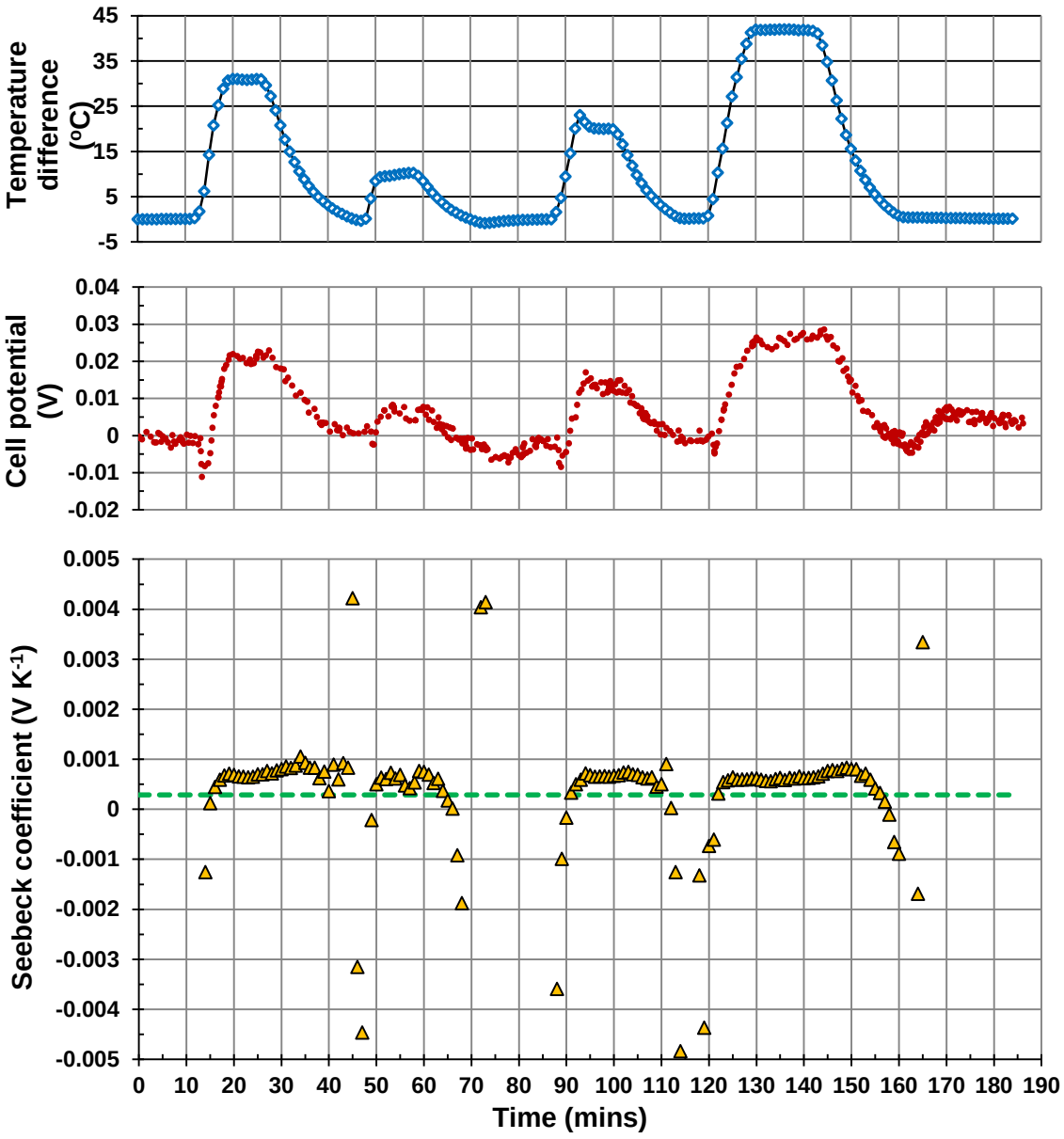

Figure 2. Plots of Temperature Difference ΔT (top), Corresponding Potential Difference Across the Cell ΔE (middle), and Corresponding Temperature Dependence of the Potential—that is, Seebeck Coefficient $\alpha = \Delta E/\Delta T$ (bottom) vs. Time, for a Thermogalvanic Cell with Cu Electrodes in 0.01 M $CuSO_4$ + 0.1 M H_2SO_4 Aqueous Electrolyte. The Dotted Straight Green Line is the Seebeck Coefficient for a Bi_2Te_3/Sb_2Te_3 Superlattice Solid-State Thermoelectric, which is ~0.243 mV K^{-1} [34].

Indeed, the scientific community has recently discussed the larger role thermogalvanic cells should have in harvesting low-grade thermal energy, such as waste heat co-generation [5] and low-temperature geothermal resources [35], but also in solar thermal energy conversion systems [2, 36]. Most of the time, the Seebeck coefficient of thermogalvanic cells reaches three or four times that of solid thermoelectrics (Figure 3). It has a quadratic effect on the maximum power output of the cell, which will be described in Section 2.2. Therefore, the Seebeck coefficient is an essential factor in the operation of a practical device.

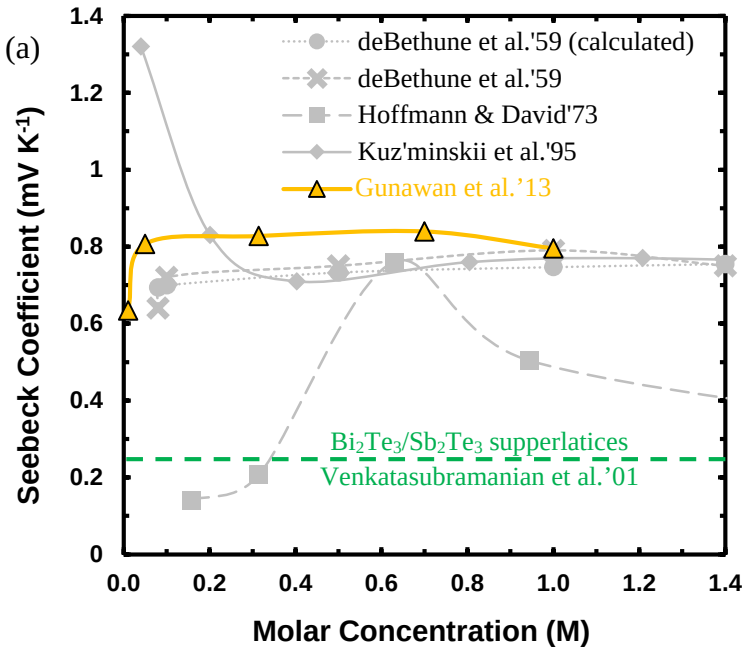

(b)

Concentration (M)	S_e (mV K^{-1})
0.01	0.63
0.05	0.80
0.3	0.83
0.7	0.84
1.0	0.79

Figure 3. Seebeck Coefficient of a Cu-$CuSO_4$ Thermogalvanic Cell System Taken from [4]: (a) Plotted against Data from Literature and Data for a Bi_2Te_3/Sb_2Te_3 Superlattice Solid-State Thermoelectric [34], and (b) Tabulated for Comparison.

1.1 Why Aren't We Using Thermogalvanic Cells Today?

Unfortunately, the performance of thermogalvanic cells depends not only on the Seebeck coefficient, but also on the internal and thermal resistances of the cell. Even

though thermogalvanic cells have very promising Seebeck coefficients, the high internal resistances of the cell systems inhibit the maximum power outputs of such cells [4, 8, 37-40]. In theory, as long as the system is in thermal and electrochemical equilibrium, the choice of electrode materials and cell configurations should not affect the Seebeck coefficient of the cell, as the thermodynamic factor, i.e. the change in entropy of the redox reaction in the cell, is the governing factor [5, 6]. This will be detailed in Section 2.1. Nevertheless, the value of the internal resistance highly depends on the cell configuration [8, 38, 41].

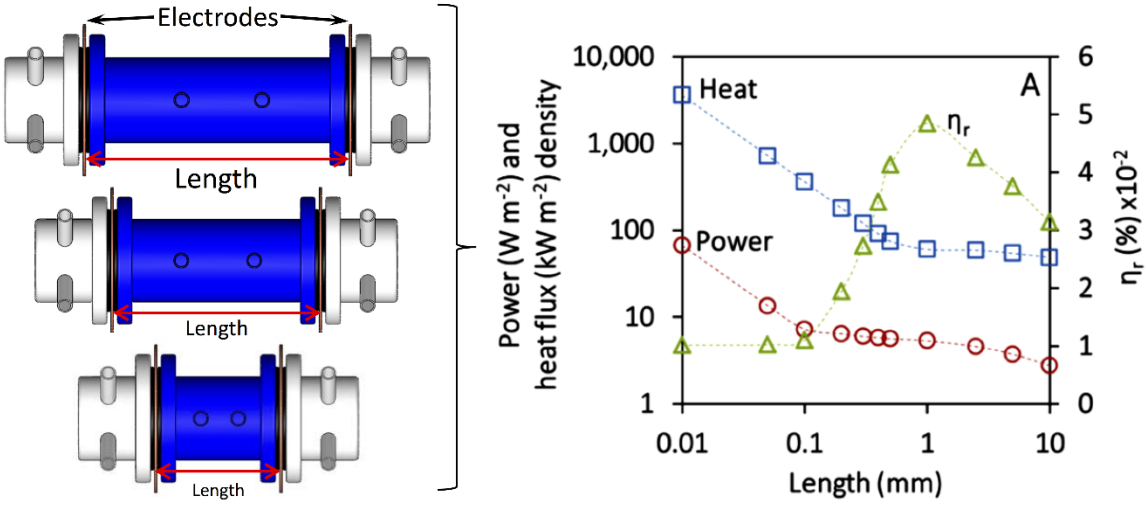

Figure 4. Reducing the Length between the Electrodes, L (left figure) Reduces the Internal Resistance (R_{int}), thus Increases the Power Output of the Cell (right figure). However, It also Reduces the Thermal Resistance, which Increases the Heat Flux Across the Cell and Eventually Lowers the Power Conversion Efficiency η_r of the Cell. The Right Figure is Taken from a Parametric Study for a Ferro/Ferricyanide Thermogalvanic Cell that Shows as L Increases, η_r Reach a Peak Value, where the Positive Effect of Natural Convection in Suppressing R_{int} Balances the Negative Effect of the Increased Electrode Spacing in Building Up the R_{int} (see Chapter 3 for details). Thus, further Enhancing the Convection by Increasing L Beyond this Point would not Improve η_r, instead, It would Decrease It [40, 42].

Ideally, a thermogalvanic cell will use an electrolyte with the largest Seebeck coefficient, and a cell configuration that has the lowest intrinsic internal resistance. The ideal cell will also be capable of maintaining current flow continuously. Reducing the distance between the electrodes, for example, reduces the internal resistance (see Figure 4). However, one should note that the thermal resistance will also be reduced at the same time, which eventually lowers the power conversion efficiency of the cell system. Alternatively, one can increase the electrolyte concentration, which would not significantly impact the thermal resistance.

On the other hand, thermal transport is just as important as ionic transport for a thermogalvanic cell to generate electric power efficiently. As pictured schematically in Figure 1, maintaining a temperature difference between the hot and cold electrodes is fundamental to the operation of a thermogalvanic cell. Keeping the thermal resistance high, however, runs counter to the goal of decreasing the internal resistance. Thus, the challenge is to do both simultaneously.

1.2 Motivation

Indeed, it has been two decades since Kuzminskii et al. [3] and Quickenden and Mua [2] published their review articles on various thermogalvanic cells. However, since Hu and Cola's seminal publication in 2010 [5], the annual amount of published work dealing with thermogalvanic cells has increased rapidly—growing at an average of around 45% per year for the past five years. Figure 5 shows the growth in thermogalvanic research since 1995 (based on a 2015 Google Scholar search). However, it is only a conservative estimate of the body of thermogalvanic research, because a

variety of other terms, such as ‘thermoelectrochemical cells’, ‘thermo-electrochemical cells’, and ‘thermocells’, are also used to describe thermogalvanic cells.

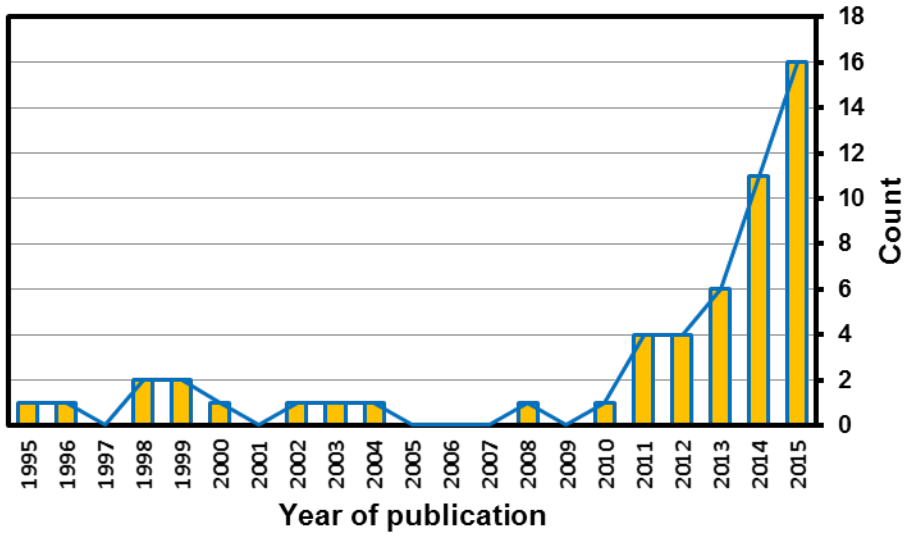

Figure 5. Significant Growth in Thermogalvanic Publications for the Past Five Years (2010 – 2015), as Indicated by Google Scholar.

Thermogalvanic cells remain intriguing and largely unexploited, in part because of the lack of fundamental understanding concerning some aspects of their operation. Although they have been the object of considerable study (Figure 5), a number of questions remain to be addressed before their practical application can be realized. Some of these questions were brought up in a 1995 seminal review article [2], and many of those remain relevant today. How can mass (ionic) transport be enhanced, while limiting thermal transport? Can a practical, inexpensive electrode be found (or developed) that can deliver high surface area and low activation energy, while allowing for good heat transfer with the heat source and sink, and good mass transfer with the electrolyte? Is there an advantage to “one-way” flow of ions, as compared to “two-way” flow? Can the

Soret effect (the diffusion of ions in response to a thermal gradient) be enhanced so that it adds significantly to the generated power? And finally, as mentioned in [2], can the thermogalvanic effect be reversed by inputting electric current, enabling a thermogalvanic cell to generate cooling rather than electric power? Answering this last question could result in the novel application of a flowing liquid that provides both convective and thermogalvanic cooling.

The great attraction of thermogalvanic cells is not that their power conversion efficiency will eventually exceed that of conventional solid-state thermoelectric devices, but rather that their fluid nature and potential to be manufactured inexpensively will lead to widespread applications. The fluid (liquid) nature of the electrolyte enables a thermogalvanic device to conform to the shape of the heat source, much more readily than a solid-state thermoelectric device. For example, an annular thermogalvanic cell has already been demonstrated that can be affixed to the outside of a hot pipe, such as an automotive exhaust pipe [5, 43, 44].

Its power level—currently on the order of microwatts—is sufficient to power low-power applications, such as wrist watches [45]. Im et al. recently demonstrated that a $Fe(CN)_6^{4-}/Fe(CN)_6^{3-}$ thermogalvanic cell can be embedded on a T-shirt and is flexible enough to optimally harness heat from a human body and store it into a capacitor for later use [43]. Motivated by this result, more studies on flexible thermogalvanic devices have been published in the past year [46-50].

In addition, with the development of nanotechnology, researchers have become interested again in not just focusing on increasing the system's efficiency, but also in finding cheaper electrolyte/electrode materials to make systems cost competitive with

solid thermoelectric devices. Hu et al. [5] has set a benchmark of five dollars per Watt ($5.14/W). That is, the benchmark is the cost per Watt of active materials, i.e. electrode and electrolyte only, for thermogalvanic devices with carbon-multiwalled nanotube buckypaper electrodes in a ferro/ferricyanide ($Fe(CN)_6^{4-}/Fe(CN)_6^{3-}$) aqueous electrolyte operating at a temperature difference of 60 ^oC. They estimated that this price will go down to $2.76/W based on the future projected prices of multiwalled carbon nanotube electrode materials. They also set a notable (highest) maximum power output density of 1.8 W m^{-2} corresponding to a power conversion efficiency relative to that of a Carnot engine operating between the same temperatures, $\eta_r = \eta/(1 - T_{cold}/T_{hot}) = 1.4\%$, as highlighted by Nature Materials [51]. Their results have helped pave the way for many published works using carbon-nanomaterial electrodes in the past five years. On the other hand, MacFarlane et al. have consistently pursued and reported new experimental data for ionic liquid thermogalvanic cells [6, 11, 14, 52-55]. Expensive, clean-room-based manufacturing processes are not required for these thermogalvanic cells, meaning that their production costs are likely to be substantially lower than for high-performance solid-state thermoelectrics.

1.3 Research Objective

Recent development of new electrolytes and electrode materials has shifted the research focus away from other routes to improved thermogalvanic cells. The objective of this interdisciplinary research is therefore to explore those alternative routes to improve the performance of thermogalvanic systems, namely the Seebeck coefficient and maximum power output. More recently, Kang and Baughman [8] stated that

"experimental measurements may be the only reliable way to determine power generation rates and efficiency of a thermocell." (p. 478) Therefore this thesis is focused on a largely experimental approach, but with appropriate application of theory to analyze the data and to suggest new directions for research, with the goal being to make possible future practical energy conversion devices. The following research questions will be addressed:

1. How does incorporating natural convection within a cell improve the maximum power output of the cell? Does it enhance the mass (ionic) transport, while limiting thermal transport? Is there an advantage to "one-way" flow of ions, as compared to "two-way" flow[1]?
2. What is the potential for applying a thermogalvanic cell to harvest waste heat energy from a vehicle's exhaust pipe?
3. How does adding polyelectrolytes or mixed-ligand complexes to conventional electrolytes affect the Seebeck coefficient?

Each of the above questions is essentially answered as a complete chapter in this dissertation. Chapter 2 will present several important definitions. Consecutively, chapter 3 presents how a simple utilization of natural convection within the cell doubles the maximum power output of the cell. Chapter 4 uses some of the results from the previous chapter in a feasibility study of incorporating thermogalvanic waste heat recovery systems into automobiles. Along the same lines as chapter 3, chapter 5 presents a novel approach to enhance Seebeck coefficient, up to 160% improvement, by tuning the

[1] Cu-$CuSO_4$ (or Cu/Cu^{2+}) system, which as shown schematically in Figure 1 results in a "one-way" flow of Cu^{2+} ions from the cold to the hot electrode. Conversely, the $Fe(CN)_6^{4-}/Fe(CN)_6^{3-}$ redox reaction yields a "two-way" flow of ions: $Fe(CN)_6^{4-}$ from the cold to the hot electrode, and $Fe(CN)_6^{3-}$ in the other direction.

configurational entropy of polyelectrolytes or mixed-ligand complex formation of $CuSO_4$ electrolytes. Finally, chapters 6 and 7 will discuss the conclusions and possible future work that can be formed from these efforts.

2. THEORETICAL BACKGROUND

Thermogalvanic cells are typically compared using the Seebeck coefficient (α) and the maximum power output (P_{max}) of the cells. Before this study is described further, these two important metrics will first be presented.

2.1 Seebeck Coefficient

For a practical thermogalvanic cell, a reasonable approximation of Seebeck coefficient is determined by the difference between the standard molar entropies of products and reactants [56]. If one considers a cell where the hypothetical reduction-oxidation (redox) reaction is

$$\mathrm{A} + \mathrm{n\ e^-} \rightleftharpoons \mathrm{B}$$

Then, the Seebeck coefficient α is given by [2]:

$$\alpha = \frac{\partial E}{\partial T} = \frac{(S_B + S_B{}^*) - (S_A + S_A{}^*) - n\bar{\bar{S}}_e}{nF} \tag{3}$$

where E is the potential difference, T the temperature, S_A and S_B the partial molar entropies of species A and B, $S_A{}^*$ and $S_B{}^*$ the respective Eastman entropies of the designated ions, n the number of electrons involved in the redox reaction above, F the Faraday constant, and $\bar{\bar{S}}_e$ the total transported entropy of the electrons in the metal leads. The latter is usually negligible, since it usually contributes only 1% of α [56, 1]. The contributions of $S_A{}^*$ and $S_B{}^*$ are also relatively small. Consequently, a simpler approximation of α can be derived by neglecting those three parameters [1, 2, 56, 57]:

$$\alpha \cong \frac{S_B - S_A}{nF} \tag{4}$$

Figure 6, for example, shows some experimental results of Seebeck coefficients for various $CuSO_4$ concentrations taken from [4]. For the investigated ΔT of 10 – 50 °C, the open circuit potential (E_{oc}) increased linearly with ΔT, suggesting that α was constant for every concentration tested. E_{oc} is therefore expressed as $\alpha \cdot \Delta T$.

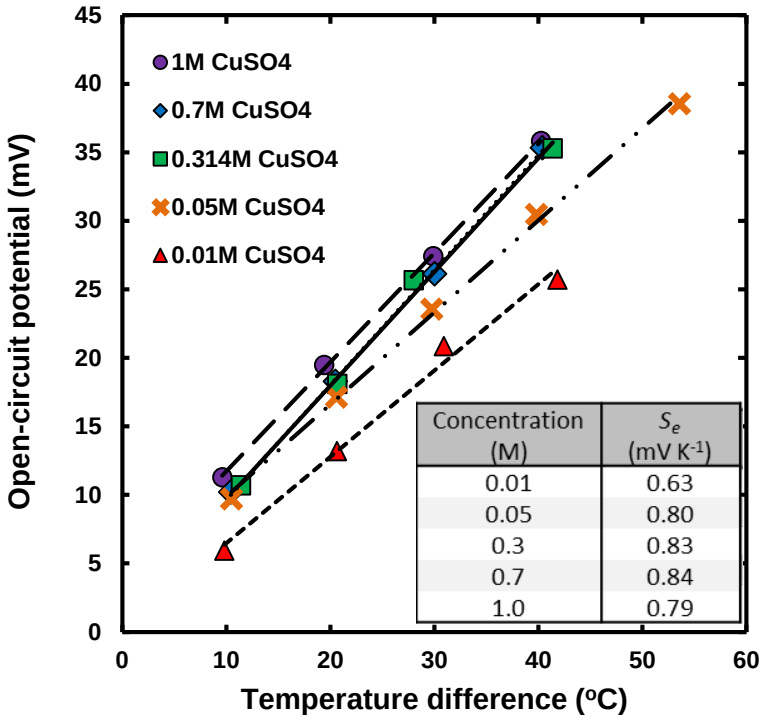

Figure 6. Plot of Seebeck Coefficients ($\alpha = E_{oc}/\Delta T$) for Various Concentrations of {x M $CuSO_4$ + 0.1 M H_2SO_4} Aqueous Electrolyte in Thermogalvanic Cells with Cu Electrodes [4]. The Values of α are Included as an Inset.

As shown in the inset of Figure 6, these values of α are in good agreement with the calculated Seebeck coefficient of a standard Cu/Cu^{2+} cell at 25 °C, i.e. $\alpha^0 = \partial E^0/\partial T =$ 0.879 mV K^{-1} from [1]. In addition, deBethune et al. [1] and Kuz'minskii [58] suggested

that each α for each molar concentration of $CuSO_4$ can be approximated with the modified Nernst equation:

$$E = E^0 + \frac{RT}{2F} \ln \frac{\gamma_{Cu^{2+}} C_{Cu^{2+}}}{\gamma_{Cu} C_{Cu}} \tag{5}$$

where E is the half-cell (reduction) potential, E^0 the standard half-cell (reduction) potential, R the universal gas constant, T the absolute temperature, γ the activity coefficients for the relevant species, C the molar concentrations, and the remaining terms have their usual meanings. Differentiating Eq. (5) with temperature ($\partial/\partial T$) will give (Note: $\gamma_{Cu} C_{Cu}$ is equal to 1)

$$\alpha = \frac{\partial E}{\partial T} = \frac{\partial E^0}{\partial T} + \frac{R}{2F} \ln(\gamma_{Cu^{2+}} C_{Cu^{2+}}) \tag{6}$$

where the activity coefficient $\gamma_{Cu^{2+}}$ varies with the molar concentrations of $CuSO_4$ aqueous electrolyte $C_{Cu^{2+}}$.

2.2 Maximum Power Output

When determining and evaluating the power-generating abilities of thermogalvanic cells, it is best to make direct measurement of the current output. Therefore, experimentally the current was obtained by simply placing a variable external load resistance (R_{ext}) in series with the cell and measuring the cell potential (E). Power output (P) was calculated from Ohm's law:

$$I = \frac{E}{R_{ext}} \tag{7}$$

$$P = E \cdot I = \frac{E^2}{R_{ext}} \tag{8}$$

The same nondimensional figure of merit $ZT = \alpha^2\sigma T/k$ [2], which is used to describe the performance of solid thermoelectric devices, is quite commonly used to express the performance of thermogalvanic cells, where σ and k are the electrical (ionic) and thermal conductivity of the electrolyte, respectively. However, one should note that in the case of thermogalvanic cell systems, σ is not necessarily constant nor necessarily ohmic in nature. Therefore, it is suggested to avoid calculating ZT when determining the power conversion efficiency of a thermogalvanic cell [56].

In cases where the *E*-*I* curve shows an approximately linear relationship (e.g., Figure 7 on the next page), the maximum power (P_{max}) is simply given by the rectangle of the greatest area under the *E*-*I* curve. Current density (j) was used as the x-axis, instead of the corresponding current (I). The greatest area occurred at $E = \frac{1}{2}E_{oc}$, where the internal resistance (R_{int}) of the cell was equal to the external resistance, $R_{int} = R_{ext}$. Consequently, P_{max} can be calculated as [2]

$$P_{max} = \left(\frac{E_{oc}}{2}\right)\left(\frac{I_{sc}}{2}\right) = \frac{{E_{oc}}^2}{4R_{int}} \tag{9}$$

where I_{sc} is the short-circuit (limiting) current delivered by the cell. In addition, because P_{max} occurs where $R_{int} = R_{ext}$, R_{int} can be calculated using E_{oc} and E measured with that specific R_{ext} [59]:

$$R_{int} = \frac{E_{oc}}{E} R_{ext} - R_{ext} \tag{10}$$

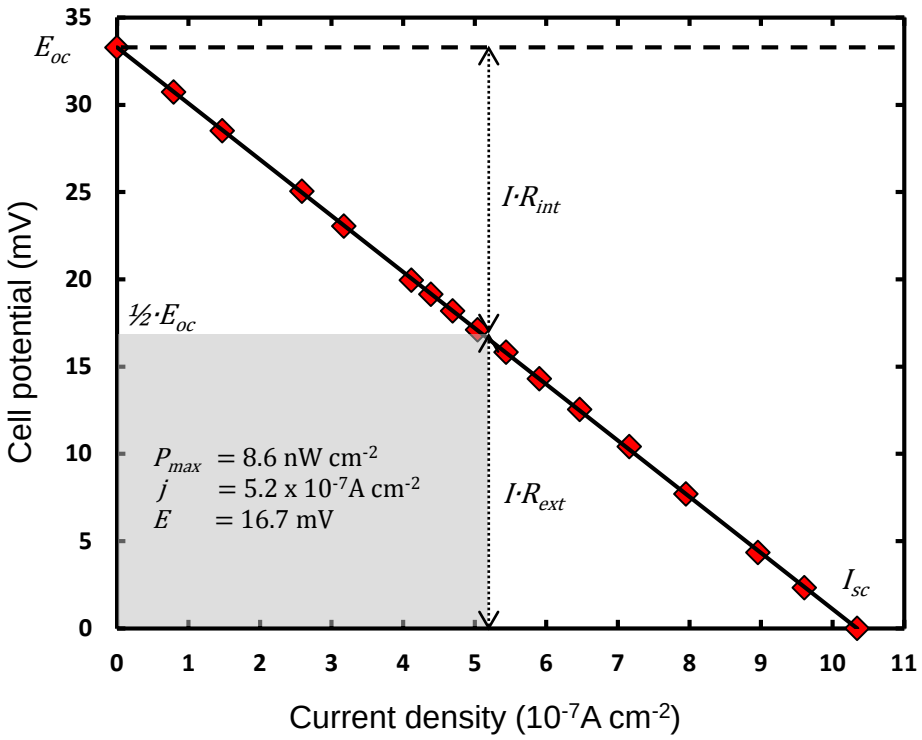

Figure 7. Characteristic *E-j* Curve of a Thermogalvanic Cell Using Cu Electrodes and {1.0 M $CuSO_4$ + 0.1 M H_2SO_4} Aqueous Electrolyte with ΔT = 40 ^oC [4]. Data Points and Error Bars Represent the Average and 95% Confidence Levels of Three Experiments, Respectively. Error Bars are not Visible because They are Smaller than the Corresponding Markers.

In the case where the *E-I* characteristic curves are nonlinear, P_{max} can still be conveniently determined from the maximum peak of the power output (P) plot, calculated using Eq. (8) as can be seen in Figure 8.

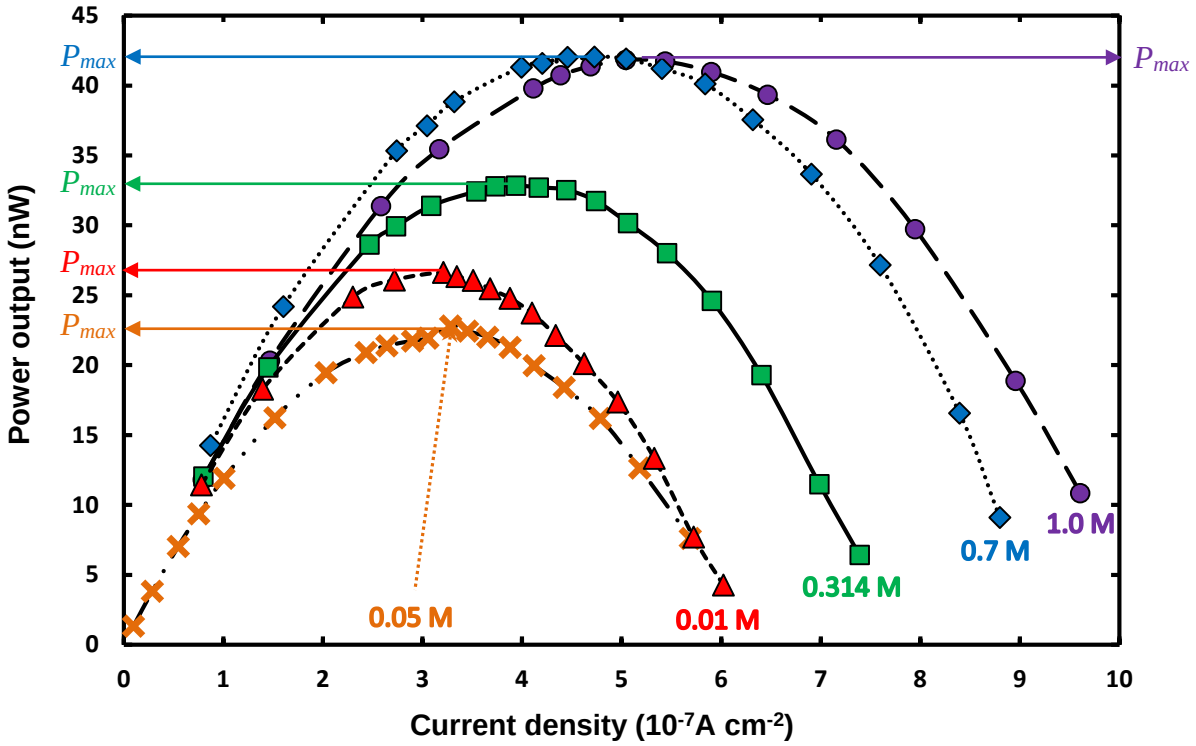

Figure 8. Experimental Results of Power Output (P) vs. Current Density (j) for Various Concentrations of $CuSO_4$ Solutions (0.01, 0.05, 0.3, 0.7, 1.0 M), Showing the Concentration Dependence of Thermogalvanic Power Generation [4].

2.3 Internal Resistance and Power Conversion Efficiency

Although it is not typically used to compare thermogalvanic cells, it is very important to understand the relationship between internal resistance and the discharge behavior of the cell to improve the thermogalvanic cell performance.

Generally, there are three primary internal resistances (see Figure 9 on the next page), i.e. activation (R_a), ohmic (R_Ω), and mass transport (R_m) resistances, which can be expressed as [39]:

$$R_{int} = R_a + R_\Omega + R_m \tag{11}$$

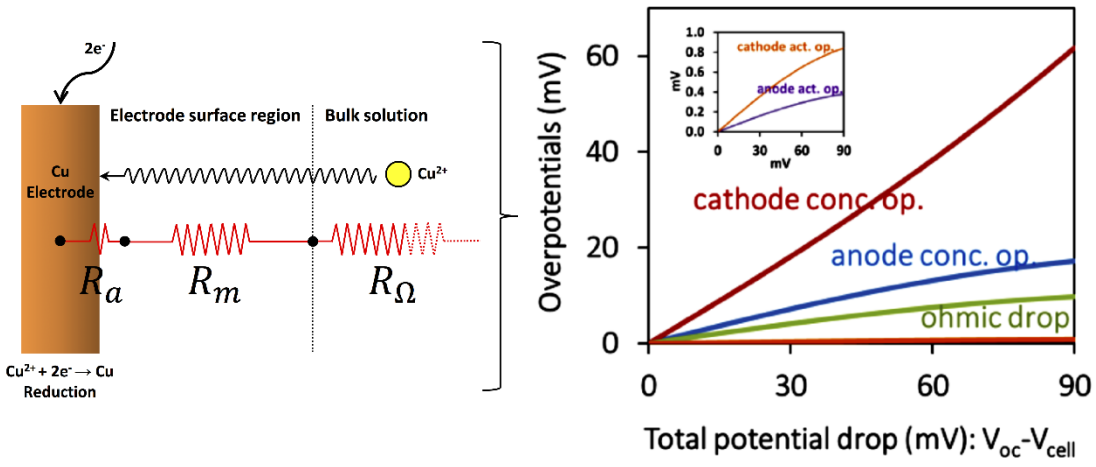

Figure 9. Three Components of the Internal Resistances in, for example, Cu-$CuSO_4$ Thermogalvanic Cell (left), i.e. Activation (R_a), Mass Transfer (R_m), and Ohmic (R_Ω) Resistances. The Relative Magnitude of the Overpotentials Associated with These Primary Internal Resistances in the Ferro/Ferricyanide Thermogalvanic Cell with Pt Electrodes is Taken from a Parametric Study (right) [40, 42].

Activation overpotential represents voltage that is sacrificed to overcome the activation barrier associated with the electron transfer reactions at the electrode/electrolyte interface. This value can be estimated from the low-field approximation to the Butler-Volmer equation [39], which gives the activation resistance (R_a) as [39]:

$$R_a \equiv \left(\frac{\partial E}{\partial I}\right)_a = \frac{RT}{AnFj_o} \tag{12}$$

where E is electrode potential, I electrode current, R the universal gas constant, T absolute temperature, A electrode surface area, n the number of electrons involved in the electrode reaction, F the Faraday constant, and j_o exchange current density. In addition to exchange current density, the charge transfer coefficients are another example of important kinetic parameters that are related to the activation overpotential. Therefore, increasing the electrode surface area (reaction sites), using higher reactant concentration,

increasing ΔT and operating temperature, and using catalytic electrodes have been applied [5, 8] to decrease the contribution to cell resistance associated with the activation barrier.

Ohmic overpotential is developed from several parts connected in series: the resistance of the electrolyte, the resistance of the electrode materials (usually negligible), and the resistance of wires and junctions. It represents the amount of voltage lost in order to force electrical current (electrons in electrodes, wires, and junction; ions in electrolyte) to flow in the cell. For thermogalvanic cells with aqueous electrolyte, however, the ohmic overpotential is mainly dominated by the electrolyte (or ionic) resistance [8, 39],

$$R_{\Omega} = \frac{L}{A\sigma} \tag{13}$$

where L is the inter-electrode spacing and σ is the ionic conductivity of the electrolyte, which can be measured experimentally using a conductivity meter or estimated from literature data.

The mass transport overpotential (or concentration polarization [8]) is highly affected by the mass (ionic) transport process in the electrolyte. In order to maintain continuous operation (current flow) of a thermogalvanic cell, reaction product formed at one electrode has to be essentially transported to the other electrode. Both activation and ohmic overpotential are influenced by mass transport overpotential. However, no direct expression derived from mass-transport theory has been published for the mass transport resistance R_m. Nevertheless, by summing R_a and R_{Ω} (from Eqs. (12 and (13) and subtracting this from measured R_{int} (Eq. (11)), R_m can be obtained [39].

Although it is not one of the goals of this thesis to investigate the power conversion efficiency of a thermogalvanic cell, η, and power conversion efficiency relative to that of a Carnot engine operating between the same temperatures, $\eta_r = \eta/(1 - T_{cold}/T_{hot})$, these two metrics will be presented for future reference. They are rarely mentioned in the recent published works, which are mostly fundamental, but for practical applications, they are as critical as R_{int} but are captured in neither α nor P_{max}. Furthermore, η_r can be used to compare such systems against other power generation technologies.

Most values of η and η_r that were published prior to [4] were still calculated by assuming no convection occurs. This may not always be valid. Therefore, a more general way to express η is

$$\eta = \frac{P_{max}}{\dot{Q}} = \frac{P_{max}R_{th}}{\Delta T} \tag{14}$$

where now the rate of heat flux through the cell, $\dot{Q}$, is more generally described as $\dot{Q} = \Delta T/R_{th}$, which recognizes that thermal transport in thermogalvanic cells is not limited to thermal conduction, as [2] suggests. Rather, thermal transport in such cells will be determined by a combination of thermal conduction, thermal convection, and even thermal radiation for high-temperature applications.

Combining Eqs. (9), (14), and $E_{oc} = \alpha \cdot \Delta T$ yields a succinct expression for the power conversion efficiency:

$$\eta = \frac{\alpha^2 R_{th}\Delta T}{4R_{int}} \tag{15}$$

Clearly, thermogalvanic cells benefit by maximizing the ratio R_{th}/R_{int}, that is, maximizing ionic transport while minimizing thermal transport. The challenge, again, is to do both simultaneously.

3. POWER OUTPUT ENHANCEMENT BY NATURAL CONVECTION

Due to the fact that advanced electrolyte and electrode materials represent a clear path to high performance, geometry and operational characteristics of the cell have been largely overlooked as an improvement route. In particular, we argue here that design configurations which utilize natural convection are a viable way to increase energy transfer within the cell.

Forced convection using rotating electrodes [60], pumps or flow cells [61], and the application of external current onto the electrodes (to generate concentration difference) [60, 62-66] to enhance convection have also been investigated by various researchers. However, these external power consumptions can be parasitic and may lead to an unfair comparison in terms of power conversion efficiency between thermogalvanic devices when energy audits are to be carried out [2, 38]. Additionally, such systems have limited practical appeal since they require moving parts to convert heat into electricity.

The aim of this study is to demonstrate that, in general, thermogalvanic power generation can be enhanced by designing an optimum cell geometry that controls and utilizes natural convection, without external forces of any kind, to increase energy and mass transfer within the cell. This study will also try to present a simple theoretical treatment aimed to provide future researchers and engineers with a useful preliminary design metric for constructing the optimum cell architecture. Before looking at our results to see if they support this hypothesis, we will first review the literature for evidence of P_{max} enhancements within cells with natural convection.

3.1 Review of Limited Existing Literature

There is relatively little evidence in the literature that discusses and validates the potential performance enhancement achievable by designing thermogalvanic cells which take advantage of natural convection. There are two numerical [40, 67] and three experimental [8, 38, 39] papers, and a PhD thesis [37]. Table 1 summarizes the literature results.

3.1.1 Numerical Literature

In his theoretical study, Sokirko [67] derived a simple analytical model to calculate the relative efficiency η_r, from general properties of thermogalvanic cells, to find the optimum parameters of the cells. This first half of the study confirmed a previous empirical conclusion by Ikeshoji et al. [62-64] that the increase in power generation due to convection was greater than that of heat flux, which was drawn from an observation that mass diffusivity (D_{AB}) was smaller compared with the thermal diffusivity (a). This conclusion could be translated to high Lewis number (Le), where Le = a /D_{AB} [68], whose significance in increasing power generation will be apparent in the simple expressions that we derive as the discussion proceeds. In addition, the author presented a more detailed analytical model to calculate concentration distribution and the current density vs. cell potential (I–E) curve to further obtain a more accurate evaluation of η_r.

Table 1. Review of Thermogalvanic Cell Experiments with Natural Convection within the Cell.

Year	Authors	Electrodes	ΔT (°C)	Electrolytes	Electrode spacing, L (mm)	Orientation	Results
Numerical							
1994	Sokirko [67]	Pt	30[a]	1.0 M $Fe(CN)_6^{4-}$ + 1.0 M $Fe(CN)_6^{3-}$ + H_2O	$L \leq 1$ ($H/L > 1$)	hot-above-cold, cold-above-hot, horizontal	No specific P_{max} or η_r enhancement reported
2014	Salazar et al. [40]	Pt /MWCNT[b]	60 (T_{cold} = 27°C)	0.4 M $Fe(CN)_6^{4-}$ + 0.4 M $Fe(CN)_6^{3-}$ + H_2O	1 (square cell)	hot-above-cold, horizontal	Enhancement of P_{max} ~723%, and η_r 444%
					$0.01 \leq L \leq 10$ (H/L kept at 1)	horizontal	Deterioration of P_{max} (from 10^3 to 10^2 μW cm^{-2}), limited enhancement of η_r
					$0.83 \leq L \leq 2.5$ ($H/L \geq 2$)	horizontal (2 - 6-series-stacked cell)	Deterioration of P_{max} (from 10^2 to 10^1 μW cm^{-2}), limited enhancement of η_r
		Pt	72 (T_{cold} = 5.4°C)	0.01 M $Fe(CN)_6^{4-}$ + 0.01 M $Fe(CN)_6^{3-}$ + H_2O	1 (H/L = 9)	hot-above-cold, cold-above-hot	Enhancement of P_{max} 200%[c]
		Pt	40 (T_{cold} = 20°C)	0.26 M $Fe(CN)_6^{4-}$ + 0.26 M $Fe(CN)_6^{3-}$ + 0.8 KCl + H_2O	$1 \leq L \leq 20$ ($11.2 \geq H/L \geq 0.56$)	cold-above-hot	Deterioration of j ~91% (from 3820 to 360 μA cm^{-2})[d]
Experimental							
1995	Quickenden and Mua [38]	Pt	20 (T_{cold} = 20°C)	0.26 M $Fe(CN)_6^{4-}$ + 0.26 M $Fe(CN)_6^{3-}$ + 0.8 KCl + H_2O	100 (H/L = ~0.1)	hot-above-cold, cold-above-hot, horizontal	Enhancement of j ~150% (from 200 to 500 μA cm^{-2})
1996	Mua and Quickenden [39]	Pt	20 (T_{cold} = 20°C)	0.26 M $Fe(CN)_6^{4-}$ + 0.26 M $Fe(CN)_6^{3-}$ + 0.8 KCl + H_2O	1, 3, 25, 50, 100, 200, 500, 1000, 1500 ($11.2 \geq H/L \geq 0.0075$)	cold-above-hot	Deterioration of P_{max} ~99%
2012	Kang et al. [8]	SWCNT[e]	20 (T_{cold} = 26.4°C)	0.10 M $Fe(CN)_6^{4-}$ + 0.10 M $Fe(CN)_6^{3-}$ + H_2O	40 (H/L = ~0.1)	hot-above-cold, cold-above-hot, horizontal	Enhancement of P_{max} 140%
					10, 20, 30, 40 ($H/L < 0.6$)	horizontal	Deterioration of P_{max} ~28%

Year	Authors	Electrodes	ΔT (°C)	Electrolytes	Electrode spacing, L (mm)	Orientation	Results
1994	Holeschovsky [37]	Cu	60 (T_{cold} = 20°C)	0.63 M $CuSO_4$ + H_2O	20 (H/L = ~2.2)	hot-above-cold, horizontal	No change, P_{max} stays constant at 1.67 μW cm^{-2}
	Current study [41]	Cu	60 (T_{cold} = 5°C)	0.70 M $CuSO_4$ + 0.1 M H_2SO_4 + H_2O	46, 80, 100 ($H/L \leq 0.82$)	hot-above-cold, cold-above-hot, horizontal	Enhancement of P_{max} up to 100% (Refer to Table 2 for more details)

a temperature of the electrodes could not be found in the paper
b multi-walled carbon nanotubes
c simulated using experimental values from [62] for model validation
d simulated using experimental values from [39] for model validation
e single-walled carbon nanotubes

The calculation [67] was based on a two-dimensional rectangular aqueous thermogalvanic cell using the $Fe(CN)_6^{4-}/Fe(CN)_6^{3-}$ redox couple with Pt electrodes ($Pt|Fe(CN)_6^{4-/3-}, H_2O|Pt$) and ΔT = 30 °C, and which was performed for three cases: hot-above-cold (Figure 10a), cold-above-hot (Figure 10b), and horizontal (Figure 10c) orientations. The height of the electrodes (H) was kept constant at 1 mm, while the electrode spacing (L) was much less than H and varied so that the aspect ratio of the cell was more than 1 ($H/L > 1$). The author concluded that the geometrical aspects of the cell, in particular, the electrode spacing L, had only a small influence on η_r. Unfortunately, the author provided only limited results and discussion regarding the effect of convection on η_r and the current generation of the cell. There was also not enough comparison between the prediction and experimental data from other literature provided in the paper; thus, formulating the general algorithm to find the optimum parameters of thermogalvanic cells has remained a challenge.

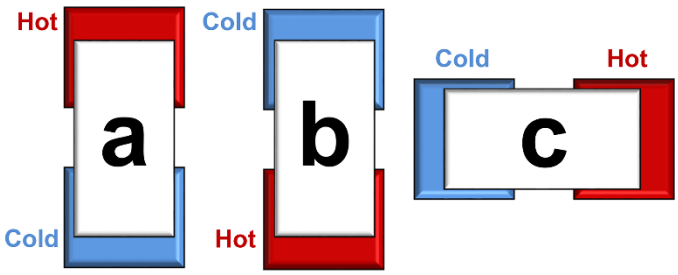

Figure 10. Three Different Cell Orientations Used in the Present Experiments: (a) Hot-above-Cold, (b) Cold-above-Hot, and (c) Horizontal.

A comprehensive answer to the above challenge has been recently brought by Salazar et al. [40]. In their parametric study, the authors developed a multiphysics model to simulate power generation and conversion efficiency of a stagnant, a series-stacked,

and a flow Pt|$Fe(CN)_6^{4-/3-}$, H_2O|Pt cell using COMSOL®. While many researchers have used nanoparticles to enhance electrical and thermal properties [69], the authors assumed multiwall carbon nanotube (MWCNT) electrodes in their simulation because of their high kinetic reactivity and use in previous experimental works [5, 9]. Their results showed that, in general, natural convection compressed concentration boundary layers, thus reducing mass-transfer (or concentration) overpotential at the electrodes that was growing and suppressing the power generation over time. The authors reported that natural convection in a 1 mm x 1mm square, stagnant, horizontal cell with ΔT of 60 °C increased P_{max} up to 8 times higher, from 56 to 461 μW cm^{-2}, while it only increased the heat flux 1.5 times higher, compared to the cell without natural convection. The η_r of the cell also increased from 0.009% to 0.049%. This once again could be explained by the high Le in their calculation, which other than the definition of Le = a / D_{AB} that has been mentioned above, high Le could also be translated into a thicker thermal boundary layer ($\delta_{thermal}$) relative to the concentration boundary layer ($\delta_{concentration}$) in the vicinity of the electrodes, where Le = $(\delta_{thermal}/\delta_{concentration})^3$ [68]. Because the actual heat transfer rate from the hot to the cold electrode is essentially impeded by the thermal boundary layers in the vicinity of both electrodes, as emphasized by Bejan [70] for natural convection within enclosures heated from below, the resulting increase in heat flux is indeed lower than the increase in P_{max} caused by the thinner $\delta_{concentration}$. Therefore, an electrolyte with high Le would be preferable, because the $\delta_{concentration}$ that impedes the diffusion rate of ionic species towards the electrodes would be compressed, thus reducing the mass-transfer overpotential and consequently increasing P_{max}. At the same time, the $\delta_{thermal}$ that impedes the heat flux would be made as large as possible, in order to maximize η_r. The model was validated

using experimental data from [62] and [39] for the cold-above-hot cells. The authors noted a slight overprediction (~22%) when they were comparing the predicted P_{max} = 9 μW cm^{-2} with the experimental P_{max} = 7.4 μW cm^{-2} from [62]. They also noted a similar overprediction (17–21%) when they were comparing the predicted current density with the experimental current density from [39]. They attributed the latter discrepancy to additional boundary layers at the side walls of the cylindrical cell, which was used by [39] for their experiments, but were not considered in their model. We assume the same is true in the former case. Overall, based on these comparisons, the authors concluded that natural convection significantly increases P_{max} of the cell, however, increasing electrode spacing L will decrease P_{max}. This happens because as L increases the ohmic overpotentials start to grow and reduce P_{max}. The authors thus noted that there is a ‘‘fundamental limit’’, where any form of convection would not improve the performance of the cell past this point, such as an optimum L of 1 mm that they calculated and that gave an optimum η_r of 6% in their study. In addition, the authors simulated series-stacking up to six stagnant 5 mm x 5 mm square thermogalvanic cells, which showed the potential to increase η_r by 100%, from ~3% to ~6%, when the cell was split in equal-sized cells and stacked in four- or five-series configuration. The authors noted, however, that consecutive cell splitting decreased the input heat flux, the power density, and eventually the efficiency, because the reduced L in the intermediate cells decreased the natural convection in them. Additionally, a cell design with forced convection using a flow cell was simulated and evaluated. We do not tabulate the results from this specific cell, because of the nature of the convection.

3.1.2 Experimental Literature

Quickenden and Mua [38] were among the first to study the potential benefits of natural convection on thermogalvanic power generation. They conducted experiments using a cylindrical Pt|$Fe(CN)_6^{4-/3-}$, H_2O|Pt cell, with aqueous solution of KCl as a background electrolyte. The ΔT between the hot and cold electrodes (L = 100 mm) were maintained at 20 °C. The geometric reactive area of each Pt electrode was 1 cm^2. The authors tested the three orientations: hot-above-cold, cold-above-hot, and horizontal. By heating up the upper electrode, in which limited or no convection takes place, they observed that current density went down to ~40% of the initial value in 55 min, from ~500 to ~200 μA cm^{-2}. In contrast, they observed a constant current density in the cells with convection, that is, when the lower electrode was heated, and when both electrodes were facing each other horizontally. The authors also calculated and observed that the η_r of the hot-above-cold cell went down over time, compared to the cold-above-hot and horizontal cells. However, since the η_r values were calculated by assuming that no convection occurs, which may not always be valid as we noted in [4], we do not discuss much of the details here. The authors concluded that ohmic resistance $R_\Omega = L/A\sigma$ (i.e. Eq. (13)), where A is the electrode area, and σ the solution conductivity (including any ohmic contributions from the anions and/or the background electrolyte) represents the largest fraction, i.e. 83–84%, of the internal resistance (R_{int}) in the cells with convection, because the mass-transfer overpotential which increases over time is suppressed by the convection. The authors suggested that using a background electrolyte with higher σ would help reduce R_Ω. The authors also suggested that operating the cell at higher ΔT would further enhance the convection and electrolyte mixing, which would considerably

suppress $\delta_{concentration}$ at the electrodes and consequently reduce the mass-transfer overpotential even more and thus improve the power generation and η_r of the cell. This conclusion again matches with our discussion so far that higher Le will ultimately lead to higher power generation.

In a separate study, Mua and Quickenden [39] observed the effect of the electrode spacing L on the performance of the cold-above-hot cell. The P_{max} decreased ~99% with L to a value of 0.14–0.36 μW cm^{-2} at L = 1500 mm from 20 μW cm^{-2} at L = 3 mm. They anticipated these results because, as they had predicted in their previous study [38] above, as the inter-electrode spacing increases, the current and power density decrease due to an increase of the R_{int} of the cell, mainly the R_Ω where $R_\Omega = L/A\sigma$. Likewise, the authors observed that η_r increased substantially with L, then started to level off after about L = 100 mm. This observation agreed very well with the Salazar et al.'s [40] conclusion described in Section 3.1.1 that as L increases, there exists an equilibrium point which they called as a ''fundamental limit'', where the positive effect of natural convection in suppressing the mass-transfer overpotential balances the negative effect of the increased electrode spacing in building up the R_Ω. Thus, further enhancing the convection by increasing L beyond this point would not improve η_r, instead, it would decrease it. However, since the η_r values were again calculated by assuming that no convection occurs, we do not discuss the details here. Nonetheless, the authors concluded that high P_{max} does not necessarily yield high η_r.

A more recent study by Kang et al. [8] observed similar dependences of cell orientation and L on power density and η_r for the same $Fe(CN)_6^{4-}/Fe(CN)_6^{3-}$ cell. However, instead of using expensive Pt electrodes, they used in-house prepared carbon-

based nanostructured electrodes. For testing the cell orientation effect, they employed a cylindrical cell with the L kept constant at 40 mm, ΔT = 20 °C, and single-walled carbon nanotube (SWCNT) electrodes with an area of 0.25 cm^2 each. They observed the same value of P_{max} = 7.2 μW cm^{-2} for both cold-above-hot and horizontal cells, which were 140% higher than the P_{max} = 3 μW cm^{-2} for a hot-above-cold cell. Moreover, since they noticed a slight fluctuation of R_{int} in the cold-above-hot cell due to vigorous convective mixing of the electrolyte, they conducted the following experiments to test the electrode spacing effect on cell performance using the horizontal orientation. The P_{max} went down ~28% from ~13.88 to ~10 μW cm^{-2}, as L increased from 10 to 40 mm. They did not specifically discuss the effect of cell orientation on η_r. Although, as reported by the other authors above, they showed that η_r increased substantially with L. They did not, however, observe that the η_r leveled off or decreased with L, because it seems that their maximum L = 40 mm was still below the equilibrium point. However, since the η_r values were also calculated by assuming that no convection occurs, we again do not discuss the details here.

All the articles above [8, 38, 39, 40, 67], so far, reached the same conclusion that natural convection is beneficial for $Fe(CN)_6^{4-}/Fe(CN)_6^{3-}$ cells because it helps electrolyte mixing and reduces the mass-transfer potential at the electrodes, thus increasing P_{max} and η_r. However, these articles also noted that increasing L would reduce P_{max} of the $Fe(CN)_6^{4-}/Fe(CN)_6^{3-}$ cells. In contrast, Holeschovsky [37] concluded that convection, either forced or natural, did not increase P_{max} of Cu/Cu^{2+} cells. The experimental data were obtained using a cylindrical cell filled with pure $CuSO_4$ aqueous electrolyte, without background electrolyte, operating at ΔT = 60 °C. The author tested the cells in

the hot-above-cold and the horizontal orientations, however, the author did not vary the inter-electrode spacing L, but kept both Cu electrodes at L = 20 mm. The surface area of the electrodes was noted to be 15 cm^2. The author reported the same values of P_{max} = 1.67 $\mu W\ cm^{-2}$ for both orientations, which he attributed to the high activation overpotentials at the electrolyte-electrode surfaces. While this observation is different compared to those previously reported for the $Fe(CN)_6^{4-}/Fe(CN)_6^{3-}$ cells, we also observe the same phenomenon in the present study with our Cu/Cu^{2+} cell. However, we vary the L of our cell to further understand its cause. And as L increases, we find out that P_{max} also increases. More detailed discussions about the dependence of L on the power generation of Cu/Cu^{2+} cells are described later in Section 3.4.2.

Indeed, it has been noted by Quickenden and Mua [2] that ‘‘various facets of thermogalvanic cell operation are still poorly understood’’ (p. 3985), which although written in 1995 would still seem true today. Therefore, we present an experimental study, by varying both the operating orientation and electrode spacing, to look more in depth at how natural convection affects the transport mechanisms in the cell, which eventually affects the power output of a thermogalvanic generator. We choose a Cu/Cu^{2+} cell in the present experiment because we already have considerable experience with the Cu/Cu^{2+} system [4, 41, 44]. Moreover, Holeschovsky [37] mentioned that ‘‘with the exception of copper formate cells, data for power densities in Cu/Cu^{2+} cells are only available from patents’’ (p. 128). Furthermore, while in $Fe(CN)_6^{4-}/Fe(CN)_6^{3-}$ cells the $Fe(CN)_6^{4-}$ and $Fe(CN)_6^{3-}$ anions need to be circulated two ways in order to continuously produce electricity [5], it should be noted that in Cu/Cu^{2+} thermogalvanic cells, continuous current and power delivery require the Cu^{2+} cations to be transferred one way

from the cold anode to the hot cathode (refer back to Figure 1). In view of the absence of the literature and the difference in ionic transfer mechanism, studying the underdeveloped Cu/Cu^{2+} system with one-way ionic transport is important to further improve and complete our understanding on the overall thermogalvanic cell operation. Continuous steady-state power generation, however, will eventually oxidize the cold Cu anode. While this is a considerable inconvenience in a practical device, this can be hindered by periodically reversing the hot and the cold electrodes, for example, as suggested by Quickenden and Vernon [56].

3.2 Experimental Testing

A cell (Figure 11) was designed specifically based on our previous experience [4] and inspiration from others [38, 39], to test various operational configurations to control the relative importance of natural convection occurring within a thermogalvanic cell.

3.2.1 Experimental Setup

Our cylindrical cell design, with inner diameter (ID) of 27 mm and outer diameter (OD) of 34 mm, has three compartments made of Pyrex glass tubes with flanges (Chemglass Life Sciences, Vineland, NJ). Six small ID 5 mm glass tubes (two on each compartment) were made as inlets/outlets for fluid and wiring.

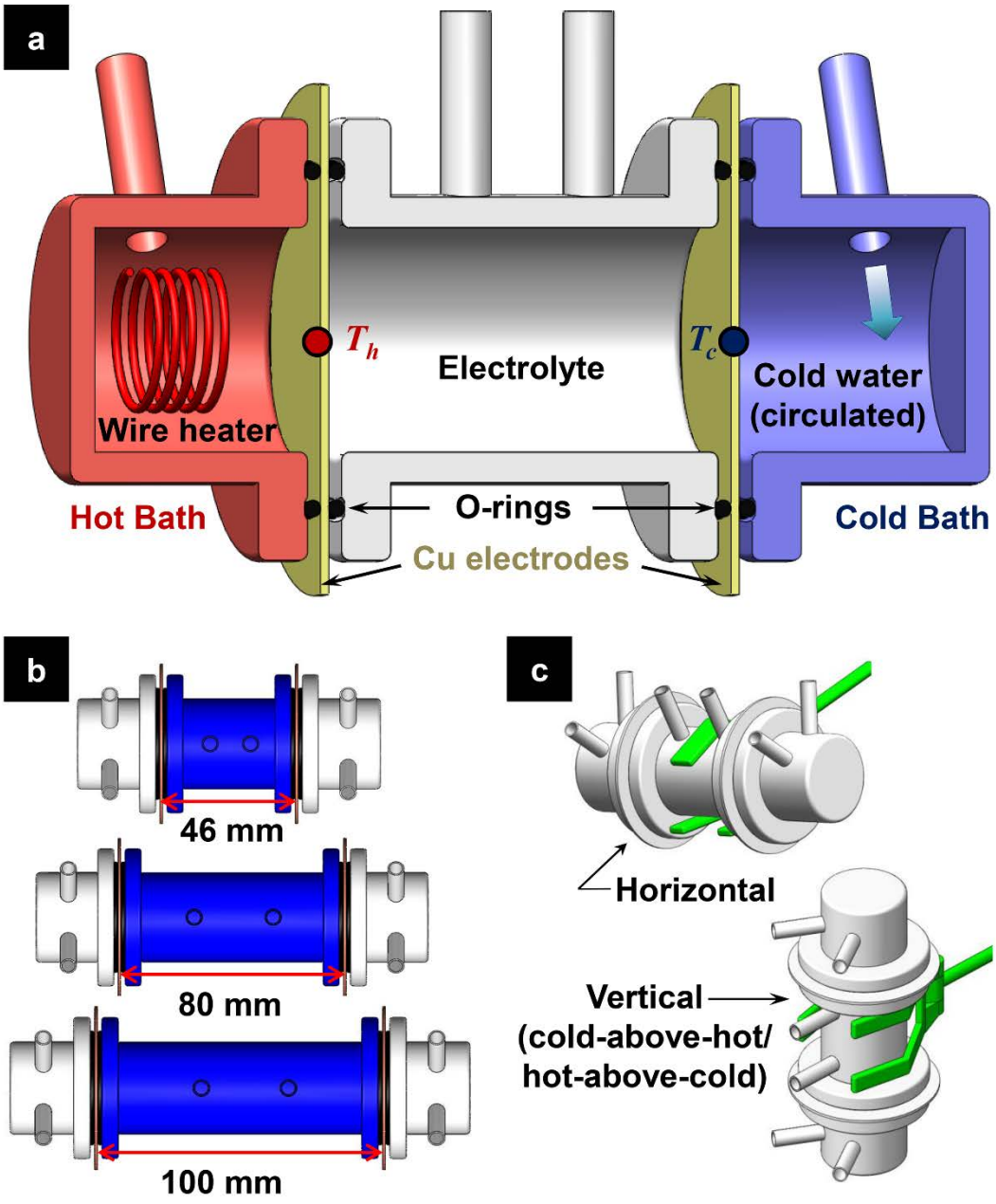

Figure 11. 3D CAD Drawings of the Cell. (a) Cross-Sectional Diagram of the Three Compartments of the Cell; (b) Three Interchangeable Middle Compartments are Made to Accommodate Variable Electrode Spacing; (c) The Assembled Cell is Held by a Clamp Arm in either Horizontal or Vertical Orientation, to Accommodate the Three Cell Orientations Described in Figure 10.

Circular metal electrodes were located between flanges, and O-rings (Chemglass Life Sciences, Vineland, NJ) were placed between the electrodes and the flanges. Two large

polytetrafluoroethylene (PTFE) clamps (Chemglass Life Sciences, Vineland, NJ) fixed the three compartments together tightly to prevent any leakage.

The schematic diagram of the cell's internal structure and the positions of each component mentioned above are shown in Figure 11a. Cold water was pumped in through polyethylene (PE) tubing to the cold bath on the right; a nichrome wire heater (Lakeshore, Westerville, OH) was immersed into warm propylene glycol (Amresco, Solon, OH, 99.5% purity) as the hot bath on the left. A Protek P6000 programmable direct current (d.c.) power supply was used to drive the wire heater in order to minimize alternating current (a.c.) noise. Three middle compartments of 46, 80, and 100 mm in length were made to vary the electrode spacing (Figure 11b). The electrodes were connected to a Fluke 8846A Digital Multimeter to measure the cell potentials. Two OMEGA type-T thermocouples were directly attached onto the outer surfaces of the electrodes to measure the temperature of the electrodes. A Campbell Scientific CR23X Micrologger was used to monitor and record the temperature differences. In all experiments, the temperature difference (ΔT) between the hot (T_h) and the cold (T_c) electrode was maintained around 60 ^{o}C. The 60 ^{o}C temperature difference was used because it was stable and easily maintained with the current setup. It should be noted that the cell was not insulated. When ΔT was increased further (usually by increasing T_h) it also increased T_c, even though the temperature of the cold bath's reservoir was well-maintained. The cell was held externally by a clamp arm in either horizontal or vertical orientation to vary the cell orientation (Figure 11c).

3.2.2 Electrolyte and Electrode Preparation

The $CuSO_4$ aqueous electrolyte was prepared by dissolving 99% pure $CuSO_4.5H_2O$ salt (PTI Process Chemicals, Ringwood, IL) into deionized water, and 0.1 M of H_2SO_4 (Amresco, Solon, OH, >95% purity) was added as a background electrolyte. The circular metal electrodes were copper (Cu), which were cut and prepared from ~0.5 mm thick ultra-conductive copper soft sheet (99.99%, McMaster-Carr, Santa Fe Springs, CA). Before each measurement, the electrodes were polished with 600 grit sandpaper (McMaster-Carr, Santa Fe Springs, CA) to remove any rust and reaction product, then rinsed with methanol and deionized water to wash away polish residue, and finally dried with compressed air. The geometric reactive area of each copper electrode was ~11.25 cm^2.

3.2.3 Experimental Procedure

After the electrolyte was added into the middle compartment, the cell was left idle (usually for 30 min) to allow the cell's open-circuit potential E_{oc} to reach steady state. Once the E_{oc} reading reached steady state, the hot electrode was heated up and the temperature difference (ΔT) between the hot and the cold electrode was maintained around 60 ^oC. After the E_{oc} reading became steady (usually requiring another 20–60 min), an Elenco RS-500 variable resistor box was then connected in parallel with the two electrodes and the digital multimeter to measure the power. The digital multimeter showed and recorded the corresponding cell potentials (E) for different resistance loads (R_{ext}) for later calculation of power output, $P = E^2/R_{ext}$ (Eq. (8)). The corresponding steady-state potentials were recorded every second and averaged over about 60–80 s,

before switching to the next resistance load. Thus, each tabulated power output, P, represents an average of 60–80 data points.

3.3 Analytical Model

A simple analytical expression that can be used to show directly the benefit of natural convection on power generation of a thermogalvanic cell, for any given geometry, will be very useful in the initial design stage of the cell. Here, we modify the power conversion efficiency expression by Salazar et al. [40], which was derived by including the effect of natural convection within the cell, to come up with a simpler ratio between the maximum power output of a thermogalvanic generator with and without convection ($P_{max,conv}/P_{max,cond}$) as a function of Sherwood number (Sh), Nusselt (Nu), and Lewis (Le) numbers.

3.3.1 Analogy between Nusselt Number and Sherwood Number

For a given geometry, the average Nu in natural convection depends on the solutal Grashof number ($\mathrm{Gr_C}$) and Prandtl number (Pr), whereas the average Sh depends on the $\mathrm{Gr_C}$ and Schmidt number (Sc). That is [68],

$$\mathrm{Nu} = f(\mathrm{Gr_C}, \mathrm{Pr})$$

$$\mathrm{Sh} = f(\mathrm{Gr_C}, \mathrm{Sc})$$

where the functional form f is an empirical correlation for that geometry, provided that the thermal and concentration boundary conditions are of the same type. Therefore, Sh can be obtained from the Nu correlation by simply replacing Pr by Sc. For natural convection inside enclosures, $\mathrm{Gr_C}$, Pr, and Sc are defined by [68]

$$\mathrm{Gr_C} = \frac{g(\Delta\rho/\rho)L^3}{\nu^2} = \frac{g\left(\rho_{a,o} - \rho_{c,o}\right)L^3}{\rho_\infty \nu^2} \tag{16}$$

$$\mathrm{Pr} = \frac{\nu}{a} \tag{17}$$

$$\mathrm{Sc} = \frac{\nu}{D_{AB}} \tag{18}$$

where g is gravitational acceleration, $\rho_{a,o}$ and $\rho_{c,o}$ are the density of the electrolyte at the anode and cathode's surface, respectively, ρ_∞ the density of the bulk electrolyte (including the anions and/or the background electrolyte), L the distance between the hot and cold electrodes (the electrode spacing), ν the kinematic viscosity, a the thermal diffusivity, and D_{AB} the diffusion coefficient (or mass diffusivity) of species A (Cu^{2+}) in mixture B (bulk electrolyte). Equation (16) is applicable to both temperature and/or concentration-driven natural convection flow, commonly known as *non-homogenous* fluids [68]. Since density differences in the bulk electrolyte of a thermogalvanic cell are due to the combined effects of temperature and concentration differences, the $\Delta\rho/\rho$ term cannot be replaced by $\beta\Delta T$, such as in the *homogenous* fluids case where $\mathrm{Gr_C}$ can be simplified and defined as *thermal* Grashof number, $\mathrm{Gr_T} = g\beta(T_h - T_c)L^3/\nu^2$; β is the coefficient of volume expansion [68].

We need no empirical correlations for the case of the hotter electrode being at the top, because no convection occurs in this case [68]; thus, Nu = Sh = 1. However, for the horizontal orientation, Bejan and Tien [71] recommend the following Nu correlation:

$$\mathrm{Nu}\,\frac{L}{H} = 1 + \left\{\left[\frac{\left((\mathrm{Gr_C Pr})\,H/L\right)^2}{362880}\right]^{-0.386} + \left(0.623\,(\mathrm{Gr_C Pr})^{1/5}\,\frac{L}{H}\right)^{-0.386}\right\}^{1/-0.386}, \qquad \mathrm{Gr_C Pr} \lesssim 10^9 \tag{19a}$$

Applying the analogy between Nu and Sh yields

$$\mathrm{Sh}\,\frac{L}{H} = 1 + \left\{\left[\frac{\left((\mathrm{Gr_C Sc})\,H/L\right)^2}{362880}\right]^{-0.386} + \left(0.623\,(\mathrm{Gr_C Sc})^{1/5}\,\frac{L}{H}\right)^{-0.386}\right\}^{1/-0.386}, \qquad \mathrm{Gr_C Sc} \lesssim 10^9 \tag{19b}$$

where H is the diameter of the geometric reactive area of each copper electrode (~37.85 mm), which gives our cells an aspect ratio of less than 1 ($H/L < 1$). While natural convection may be a classic subject, we could not find an empirical correlation for the cold-above-hot orientation that was derived specifically from an experiment using an enclosure with $H/L < 1$. Therefore, as pointed out by Bejan [70], we use the most fitting correlation for this unique case of natural convection, which is taken from a 1978 review article on the hierarchy of flow regimes and various transitions in Bénard convection by Busse [72]:

$$\mathrm{Nu} = 0.147\,(\mathrm{Gr_C Pr})^{0.247}, \qquad 2 \times 10^4 < \mathrm{Gr_C Pr} < 5 \times 10^5 \tag{20a}$$

and similarly:

$$\mathrm{Sh} = 0.147\,(\mathrm{Gr_C Sc})^{0.247}, \qquad 2 \times 10^4 < \mathrm{Gr_C Sc} < 5 \times 10^5 \tag{20b}$$

3.3.2 Ratio between the Maximum Power Output of a Thermogalvanic Generator With and Without Convection

It makes intuitive sense to maximize the efficiency of a generator, however, it is sometimes desirable instead to maximize its power output [73]. Solid-state thermoelectric generators, for example, which have similar energy conversion principles as thermogalvanic generators, can be operated at maximum power *or* maximum efficiency [74]. Where the heat source is essentially free, the minimum overall $ per W cost is achieved by operating at maximum power (not at the maximum efficiency) [75]. Since we envision that the first applications of thermogalvanic generators will be for harvesting waste heat, where the heat source is indeed free, the present treatment is limited to the maximum power operation case and the power conversion efficiency of a thermogalvanic cell (η) is defined as η operated at maximum power output (η_{mp}):

$$\eta_{mp} = \frac{\text{max. electrical power output}}{\text{thermal power input}} = \frac{P_{max}}{\dot{q}_H} \tag{21}$$

According to Salazar et al [40], the thermal power input $\dot{q}_H$ is the sum of convective heat transfer due the presence of ΔT ($\dot{q}_{conv}$), heat flux due to the Dufour effect, reversible heat due to electrochemical reactions, irreversible heat due to activation overpotential, and Joule heating. However, since the heat produced by the other thermal input components is ~3 orders of magnitude smaller compared to $\dot{q}_{conv}$, the η_{mp} for the cell with natural convection ($\eta_{mp,conv}$) can be simply represented in the following form [40]:

$$\eta_{mp,conv} \cong \frac{P_{max,conv}}{\dot{q}_{conv}} = \frac{E\, j_{max,conv}}{\dot{q}_{conv}} \tag{22}$$

where $\dot{q}_{conv} = \text{Nu}\, \dot{q}_{cond}$, $\dot{q}_{cond}$ is conductive heat transfer, and $j_{max,conv}$ the experimental maximum local current density of the cell with convection that corresponds to $P_{max,conv}$.

It should be noted that $j_{max,conv}$ does not necessarily have to be equal to the limiting current density $j_{l,conv}$. The latter can be simply calculated by $j_{l,conv}$ = Sh $n\,F\,D_{AB}\,C_\infty/L_c$ [76], where n is the number of electrons involved in the reduction/oxidation reaction, F Faraday constant, C_∞ bulk electrolyte concentration, and L_c the characteristic length. The characteristic length for the case of natural convection inside enclosures is the electrode spacing L [68], which should not be confused with the electrode diameter H as written in [76] for free convection conditions. When no convection occurs within the cell, Sh = 1; thus, the relation between the limiting current density between the cell with and without convection can be written as [64, 40]

$$j_{l,conv} = j_{l,cond}\ \text{Sh} \tag{23}$$

We observe that our experimental $j_{max,conv}$ (for the horizontal and cold-above-hot cells) is three orders of magnitude lower than the calculated $j_{l,conv}$ ($\leq 0.5\%$ of $j_{l,conv}$), while $j_{max,cond}$ is only one order of magnitude lower than the calculated $j_{l,cond}$ ($> 33\%$ of $j_{l,cond}$), which agrees with Prentice [76] that the convective flow will cause $j_{l,conv}$ to increase substantially compared with $j_{l,cond}$. While in the latter case we can safely assume that $j_{max,cond} \approx j_{l,cond}$, the relation between $j_{max,conv}$ and $j_{l,conv}$ can be expressed as $j_{max,conv} = j_{l,conv}\,(C_\infty - C_o)/C_\infty$ [76], where C_o is the concentration of the electrolyte at the electrode's surface, i.e. the hot cathode in the case of the Cu/Cu^{2+} thermogalvanic cell discussed here. Since density and concentration of a mixture are related to each other by $\rho = C\,M$, where M is the molar mass of the mixture [68], the relation between $j_{max,conv}$ and $j_{l,conv}$ can also be written as

$$j_{max,conv} = j_{l,conv}\,\frac{(\rho_\infty - \rho_{c,o})}{\rho_\infty} = j_{l,conv}\,\gamma \tag{24}$$

where constant $\gamma = (\rho_\infty - \rho_{c,o})/\rho_\infty$.

Substituting Eqs. (23) and (24) into Eq. (22) by assuming $j_{max,cond} \approx j_{l,cond}$ yields

$$\eta_{mp,conv} = \frac{E\, j_{l,cond}\, \mathrm{Sh}\, \gamma}{\dot{q}_{cond}\, \mathrm{Nu}} = \eta_{mp,cond} \frac{\mathrm{Sh}}{\mathrm{Nu}} \gamma \tag{25}$$

Subsequently, redefining $\eta_{mp,conv}$ and $\eta_{mp,cond}$ in Eq. (25) using Eq. (22) gives

$$\frac{P_{max,conv}}{\dot{q}_{conv}} = \frac{P_{max,cond}}{\dot{q}_{cond}} \frac{\mathrm{Sh}}{\mathrm{Nu}} \gamma \tag{26}$$

Consequently, rearranging the terms and using the definition of $\dot{q}_{conv}/\dot{q}_{cond} = \mathrm{Nu}$ reduces Eq. (26) to

$$\frac{P_{max,conv}}{P_{max,cond}} = \mathrm{Nu} \frac{\mathrm{Sh}}{\mathrm{Nu}}\, \gamma = \mathrm{Nu} \left(\frac{\mathrm{Sc}}{\mathrm{Pr}}\right)^x \gamma = \mathrm{Nu} \left(\frac{a}{D_{AB}}\right)^x \gamma = \mathrm{Nu}\, \mathrm{Le}^x\, \gamma \tag{27}$$

which is recommended if the empirical correlation for Nu and Sh are only a simple power law function, such as Eq. (20a) and (20b); where Le = Sc/Pr = a/D_{AB} [68], and the power x is the power quantity of the empirical correlation being used. For example, x is equal to 0.247 if Nu in Eq. (27) is calculated using Eqs. (20a). Or, since the Nu correlation in peculiar situations such as ours (with H/L <1) is sometimes more complicated, e.g., Eq. (19a), the derivation of x becomes not so trivial; thus, we recommend using a simpler form of Eq. (27):

$$\frac{P_{max,conv}}{P_{max,cond}} = \mathrm{Sh}\, \gamma \tag{28}$$

It should be noted that operating a thermogalvanic cell close to its limiting current density ($\rho_{c,o} \rightarrow 0$) will give $\gamma = (\rho_\infty - \rho_{c,o})/\rho_\infty \rightarrow 1$ that ultimately yields $P_{max,conv}/P_{max,cond} = \mathrm{Nu}\, \mathrm{Le}^x = \mathrm{Sh}$, which represents the upper limit for P_{max} enhancement within our model.

3.4 Results and Discussion

In order to validate the analytical expression developed above, which is derived under the maximum power operation case, we first run experiments to find the optimum concentration of the $CuSO_4$ aqueous electrolyte.

3.4.1 Dependence of $CuSO_4$ Concentration on Maximum Power Output

Using the same 0.1 M concentration of H_2SO_4 as background electrolyte, the shortest middle cell (L = 46 mm), constant ΔT = ~60 ^oC (T_c is maintained at around room temperature and T_h at ~85 ^oC); we observe the concentration dependence of the power generation and find that 0.7 M $CuSO_4$ produces the highest maximum power density of 3.12 μW cm^{-2} (Figure 12). For each power measurement, three rounds of load-voltage testing with different resistor sequences are performed. Between each round, the resistor box is unplugged to allow the system to return to equilibrium. The results show that the deviation between each round is less than 5%. The trend of these initial results agrees surprisingly well with the trend from our study [4] using a different cell setup, which was two beakers connected via a salt bridge of the same $CuSO_4$ mixture. The maximum power output (P_{max}) value increases with increasing $CuSO_4$ concentration until reaching 0.7 M, then it levels off and declines as the concentration is increased further to 1.0 M. For these experiments, however, only the cells with natural convection—that is, cold-above-hot (Figure 10b) and horizontal orientations (Figure 10c)—are tested. These cells are expected to generate higher P and P_{max} than the hot-above-cold cell with limited natural convection (Figure 10a).

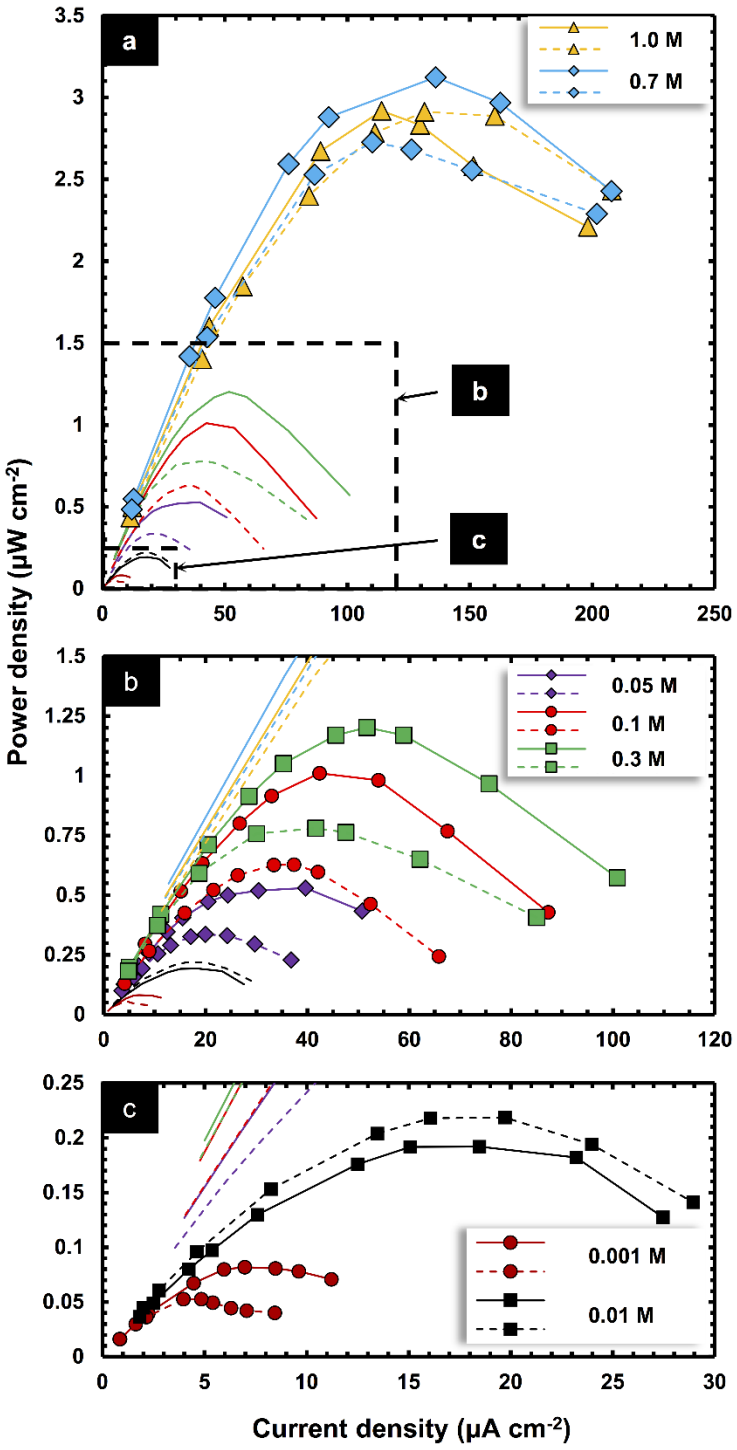

Figure 12. Concentration Dependence of Power Generation of Cu/Cu^{2+} Thermogalvanic Cells. (a) Power Density vs. Current Density for Various Concentrations of $CuSO_4$ Solutions (0.001, 0.01, 0.05, 0.1, 0.3, 0.7, 1.0 M); (b) and (c) are the Zoomed-In Views of the Dashed Rectangles in (a). Dashed and Solid Lines Indicate Cold-above-Hot and Horizontal Orientations, Respectively.

3.4.2 Dependence of Cell Orientation and Electrode Spacing on Maximum Power Output

The main experiments are carried out using the optimum 0.7 M $CuSO_4$, with the same 0.1 M H_2SO_4 as background electrolyte. The three orientations are varied for each electrode spacing, L = 46, 80, and 100 mm, to observe the natural convection effect on the power generation. At this point, however, T_c and T_h are held at lower temperatures of ~5 ^oC and ~65 ^oC, respectively, thus maintaining the 60 ^oC temperature difference. The experimental results are shown in Figure 13.

Figure 13 shows that the lower average cell temperature $T_{avg} = (T_c + T_h)/2$ of 35 ^oC compared to 55 ^oC gives a respectively lower P_{max} of ~1.09 μW cm^{-2} compared to ~3.12 μW cm^{-2} from the earlier experiments (Figure 12a) with the same molar concentration, electrode spacing, and orientation, which is consistent with Kang et al.'s [8] observation for the $Fe(CN)_6^{4-}/Fe(CN)_6^{3-}$ thermogalvanic cell. Moreover, the trend of power density vs. current density (j) curves in Figure 13a agrees very well with the trend of the same curves for the same molar concentration of 0.7 M $CuSO_4$ in Figure 12a, i.e. the horizontal cell has higher P and P_{max} compared to the cold-above-hot cell. As mentioned earlier, data for power densities in Cu/Cu^{2+} cells are only available from patents [37]. Therefore, these patent data, together with data in Holeschovsky's thesis [37], Tester et al. [59], and data from our previous study [4] are summarized in Table 2 for comparison. Our P_{max} results agree very well with Peck, Tester et al. [59], and Holeschovsky's [37]. The higher P_{max} reported by Clampitt came from the use of higher concentrations of saturated $CuSO_4$ and 2.0 M of H_2SO_4, as well as higher ΔT of 80 ^oC, as pointed out by Holeschovsky [37].

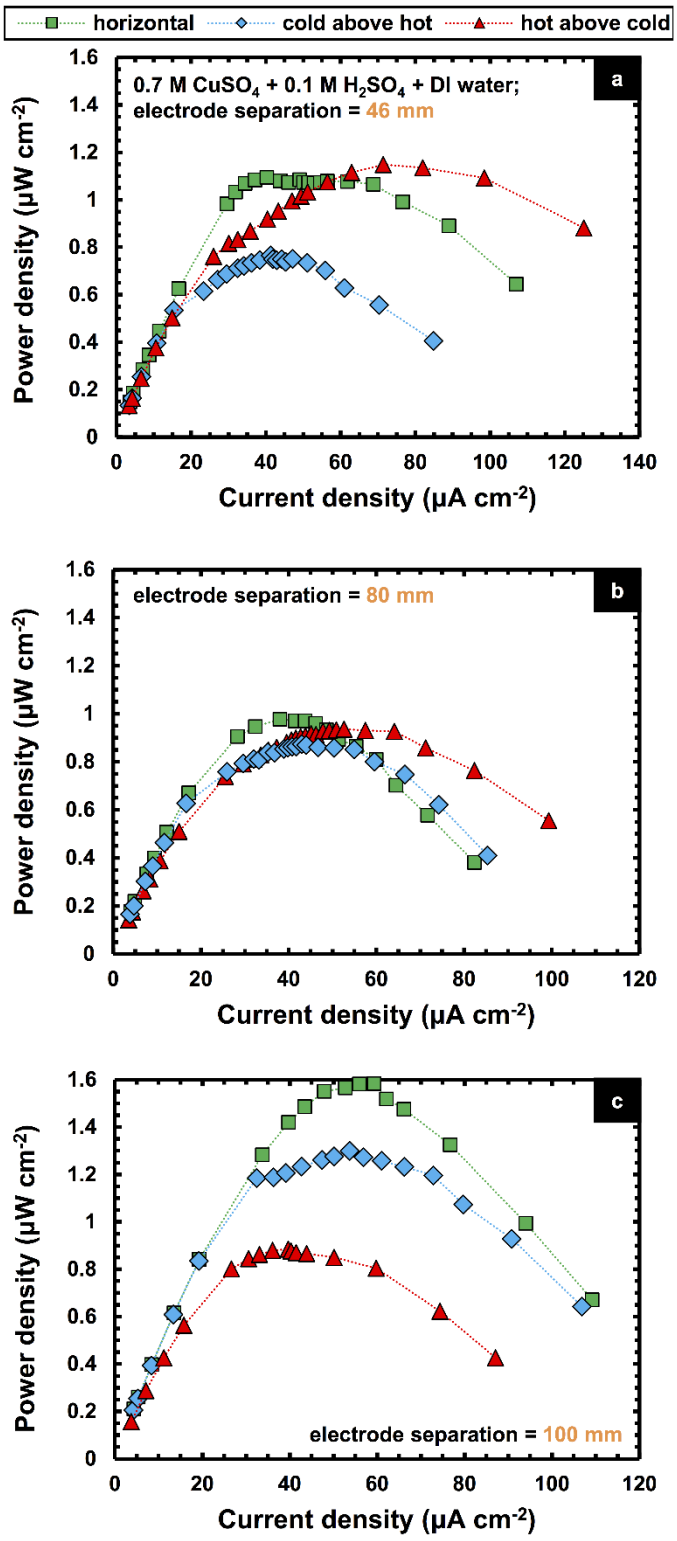

Figure 13. Power Density vs. Current Density Curves for 0.7 M $CuSO_4$ + 0.1 M H_2SO_4 Aqueous Solution with Cu Electrode in Three Different Cell Orientations, and at Three Different Electrode Spacing: (a) L = 46 mm, (b) L = 80 mm, and (c) L = 100 mm.

Table 2. Seebeck Coefficients (S_e) and Maximum Power Output (P_{max}) for Cu/Cu^{2+} Thermogalvanic Cell Systems.

Year	Authors	Electrolytes	$\lvert S_e \rvert$ (mV K^{-1})	P_{max} (μW cm^{-2})
1966	Clampitt et al.[a] (U.S. Patent)	$CuSO_4$ saturated in H_2O	0.89	30.5
		$CuSO_4$ saturated in 20 wt% H_2SO_4 + H_2O	0.89	251
1980	Peck[a] (U.S. Patent)	1.0 M $CuSO_4$ + 0.33 M Tartaric acid + H_2O	0.67	1.6
		1.0 M $CuSO_4$ + 0.33 M ethylenediaminetetracetic acid + H_2O	0.71	1.3
1992	Tester et al. [59]	0.63 M $CuSO_4$ + H_2O	0.70	1.7[b]
1994	Holeschovsky [37]	0.63 M $CuSO_4$ + H_2O	0.70	2.0
2013	Gunawan et al. [4]	0.01 M $CuSO_4$ + 0.1 M H_2SO_4 + H_2O	0.63	0.0055
		0.05 M $CuSO_4$ + 0.1 M H_2SO_4 + H_2O	0.80	0.0047
		0.3 M $CuSO_4$ + 0.1 M H_2SO_4 + H_2O	0.83	0.0068
		0.7 M $CuSO_4$ + 0.1 M H_2SO_4 + H_2O	0.84	0.0087
		1.0 M $CuSO_4$ + 0.1 M H_2SO_4 + H_2O	0.79	0.0086
	Current study (T_{avg} = 55 °C) [refer to Figure 12]	0.001 M $CuSO_4$ + 0.1 M H_2SO_4 + H_2O	0.33	0.053[c] | 0.082[d]
		0.01 M $CuSO_4$ + 0.1 M H_2SO_4 + H_2O	0.41	0.22[c] | 0.19[d]
		0.05 M $CuSO_4$ + 0.1 M H_2SO_4 + H_2O	0.56	0.34[c] | 0.53[d]
		0.1 M $CuSO_4$ + 0.1 M H_2SO_4 + H_2O	0.59	0.63[c] | 1.01[d]
		0.3 M $CuSO_4$ + 0.1 M H_2SO_4 + H_2O	0.58	0.78[c] | 1.20[d]
		0.7 M $CuSO_4$ + 0.1 M H_2SO_4 + H_2O	0.72	2.73[c] | 3.12[d]
		1.0 M $CuSO_4$ + 0.1 M H_2SO_4 + H_2O	0.70	2.91[c] | 2.91[d]
	Current study (T_{avg} = 35 °C) [refer to Figure 13]	0.7 M $CuSO_4$ + 0.1 M H_2SO_4 + H_2O (L = 46 mm)	0.72	0.77[c] | 1.09[d] | 1.15[e]
		0.7 M $CuSO_4$ + 0.1 M H_2SO_4 + H_2O (L = 80 mm)	0.72	0.87[c] | 0.98[d] | 0.94[e]

Year	Authors	Electrolytes	$\lvert S_e \rvert$ (mV K^{-1})	P_{max} (μW cm^{-2})
		0.7 M $CuSO_4$ + 0.1 M H_2SO_4 + H_2O (L = 100 mm)	0.72	1.30[c] | 1.58[d] | 0.88[e]

a cited in [37]
b values are calculated using the P_{max} and electrode area data taken from [59]
c cold-above-hot orientation
d horizontal orientation
e hot-above-cold orientation

Furthermore, the P_{max} values from our previous study [4] were quite low because of the very high internal resistance (on the order of 10 kΩ), which was imposed by the salt bridge arrangement.

Table 3. Parameters of Water and $CuSO_4$ Aqueous Electrolyte.

Parameter	Symbol	Value
For water at 35°C [68]		
Prandtl number	Pr	4.83
Density of bulk electrolyte	ρ_∞	994 kg m^{-3}
Dynamic viscosity	μ	7.2 x 10^{-4} kg m^{-1} s^{-1}
Kinematic viscosity[a]	ν	7.243 x 10^{-7} m^2 s^{-1}
Schmidt number--by Eq. (18)	Sc	985.5
Thermal conductivity	k	0.623 W m^{-1} K^{-1}
Specific heat	c_p	4178 J kg^{-1} K^{-1}
Thermal diffusivity[b]	a	1.5 x 10^{-7} m^2 s^{-1}
For water at 5°C [68]		
Density of electrolyte at the anode	$\rho_{a,o}$	999.9 kg m^{-3}
For water at 65°C [68]		
Density of electrolyte at the cathode	$\rho_{c,o}$	980.4 kg m^{-3}
Other		
Mass diffusivity of species A (Cu^{2+}) in mixture B (bulk electrolyte) [77]	D_{AB}	7.35 x 10^{-6} cm^2 s^{-1}

a Kinematic viscosity, $\nu = \mu/\rho_\infty$
b Thermal diffusivity. $a = k/\rho_\infty c_p$

No theoretical treatments of Cu/Cu^{2+} thermogalvanic power generation are available in the literature. Consequently, we compare the simple treatment of Eq. (27) and (28) with the experimental results. Ideally, the electrolyte properties at the average cell temperature of 35 ℃, where T_c = 5 ℃ and T_h = 65 ℃, are to be used in the analysis. However, because the values for properties of the 0.7 M $CuSO_4$ in 0.1 M H_2SO_4 aqueous solution are not readily available, nor easily measured, we use values of water. These values and other parameters are listed in Table 3. Considering that the water content of

the electrolytes is at least 87.5 wt. % (0.7 M $CuSO_4$ equals ~11.13 wt. %, and 0.1 M H_2SO_4 equals only ~0.98 wt. %), the resulting errors are expected to be relatively small.

The values of $Gr_C Pr$ and $Gr_C Sc$, which are calculated using Eqs. (16)–(18), are on the order of $10^8 – 10^9$ and $10^{10} – 10^{11}$, respectively. These values are beyond the range of $Gr_C Pr$ in Eq. (20a) and $Gr_C Sc$ in Eqs. (19b) and (20b). However, it was noted by Bejan and Tien [71] that for laminar natural convection in a horizontal shallow ($H/L < 1$) enclosure, the internal flow is expected to become turbulent above $Gr_C Pr \approx 10^9$. In addition, Prentice [76] noted that when the product of Gr_C and Sc is between 10^4 and 10^{12}, the flow is still considered to be laminar. Since we did not observe any sign of turbulence in our cell, we believe that Eqs. (19b), (20a) and (20b) hold very well to estimate Nu and Sh in our study.

Figure 14 on the next page demonstrates that, for the given cell's conditions and geometries, the predicted P_{max} ratio matches reasonably well with the experimental data. As we discussed earlier, the P_{max} ratio between the cold-above-hot and the hot-above cold cells is calculated by using Eq. (27) with Nu and Le^x, because of the simplicity of the power law function of Eq. (20a). However, for the horizontal and the hot-above cold cells, the P_{max} ratio is calculated by applying Eq. (28) with the Sh correlation of Eq. (19b). To test the consistency between Eqs. (27) and (28), we cross-calculate both ratios and find that the deviation is < 0.008%.

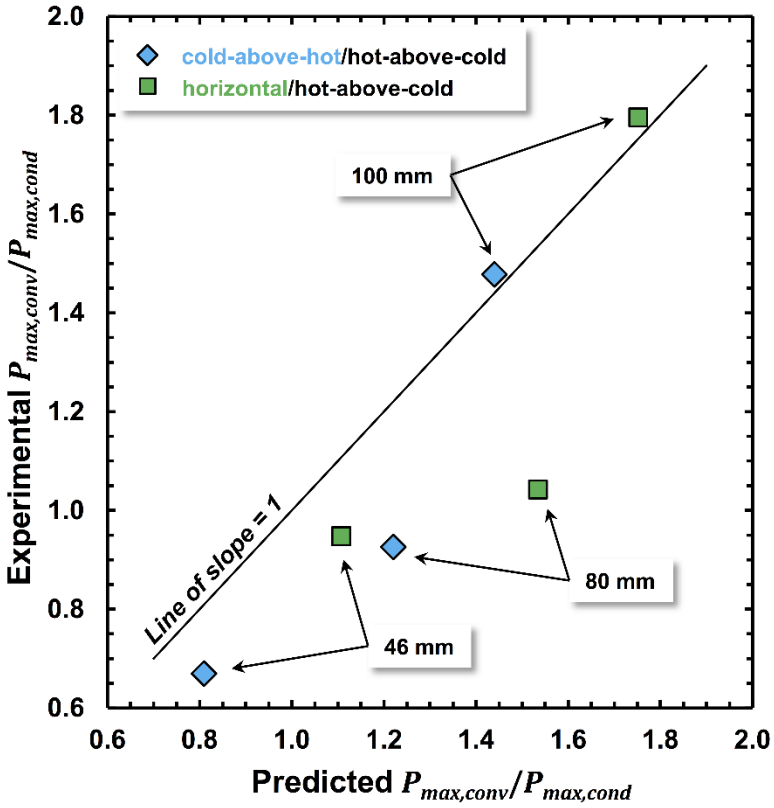

Figure 14. Comparison of Experimental Data with Prediction from the Nondimensional Analytical Expression. The *y*-axis Represents the $P_{max,conv}/P_{max,cond}$ Ratio Calculated from Experimental Data in Table 2; the *x*-axis Represents the $P_{max,conv}/P_{max,cond}$ Ratio Calculated Using Eqs. (27) and (20a) for the Cold-above-Hot/Hot-above-Cold Cells, and Eqs. (28) and (19b) for the Horizontal/Hot-above-Cold Cells.

While the power outputs of the $Fe(CN)_6^{4-}/Fe(CN)_6^{3-}$ cell in both the old-above-hot and the horizontal orientations were reported to be the same [8], it is expected that the power output of a Cu/Cu^{2+} cell in the cold-above-hot orientation should be lower than in the horizontal orientation. It happens because, in the former orientation, even though convection helps to eliminate the mass-transfer overpotential, the direction of the natural convection current from the hot cathode to the cold anode presumably opposes the Cu^{2+} cations transport (Figure 15a). In the latter orientation (Figure 15b), natural convection not only helps to mix the electrolyte, but it also helps deliver the Cu^{2+} cations from the

cold anode to the hot cathode. Nonetheless, even though these two systems have completely different charge-species transfer mechanisms, i.e. *one-way* vs. *two-ways*, we observed the same magnitude (~2-fold) of the positive amplifying effect of natural convection on the power generation of Cu/Cu^{2+} cell as has been seen for the $Fe(CN)_6^{4-}/Fe(CN)_6^{3-}$ cells [8].

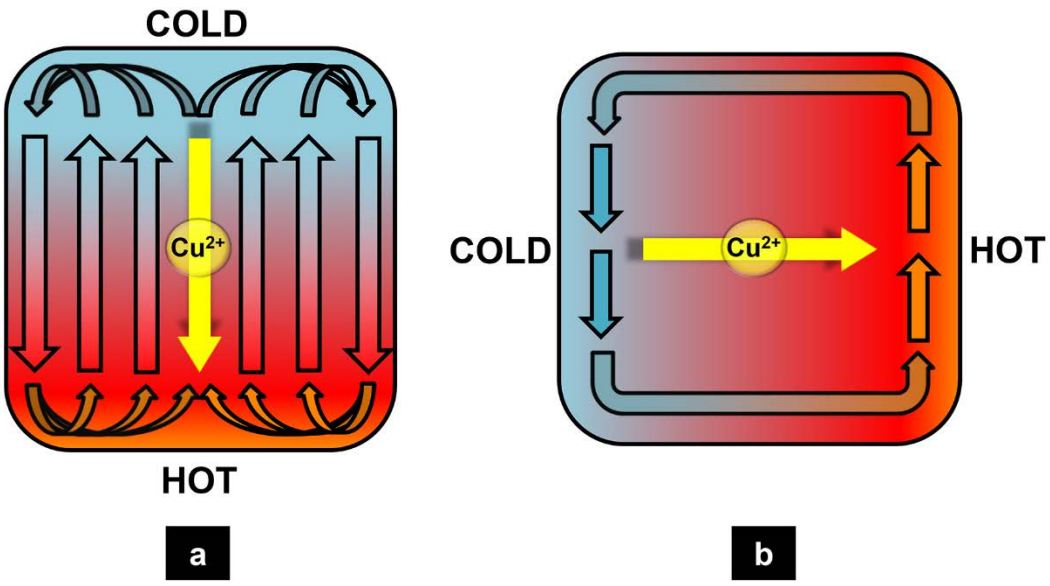

Figure 15. Illustration of Natural Convection within the (a) Cold-above-Hot and (b) Horizontal Cell Orientations.

Referring back to Figure 13a, we show that the values of P_{max} for the hot-above-cold and the horizontal orientations are almost the same, which agrees with Holeschovsky's observation [37] earlier that convection did not increase the P_{max} of Cu/Cu^{2+} cells. However, when L increases (Figure 13b and c), the P_{max} for the cells with convection, i.e. horizontal and cold-above-hot cells, also increases. These results reveal a completely different dependence of the electrode spacing L on the power generation of the Cu/Cu^{2+} cells, compared to the $Fe(CN)_6^{4-}/Fe(CN)_6^{3-}$ cells, which we believe are also caused by the difference in the ionic transfer mechanism. We depict the results in Figure

16 and compare with those of the $Fe(CN)_6^{4-}/Fe(CN)_6^{3-}$ cells [8, 39, 40] that we reviewed earlier to clearly show that as L increases, the P_{max} (or current density) of the Cu/Cu^{2+} cells increases, while those of the $Fe(CN)_6^{4-}/Fe(CN)_6^{3-}$ cells decreases.

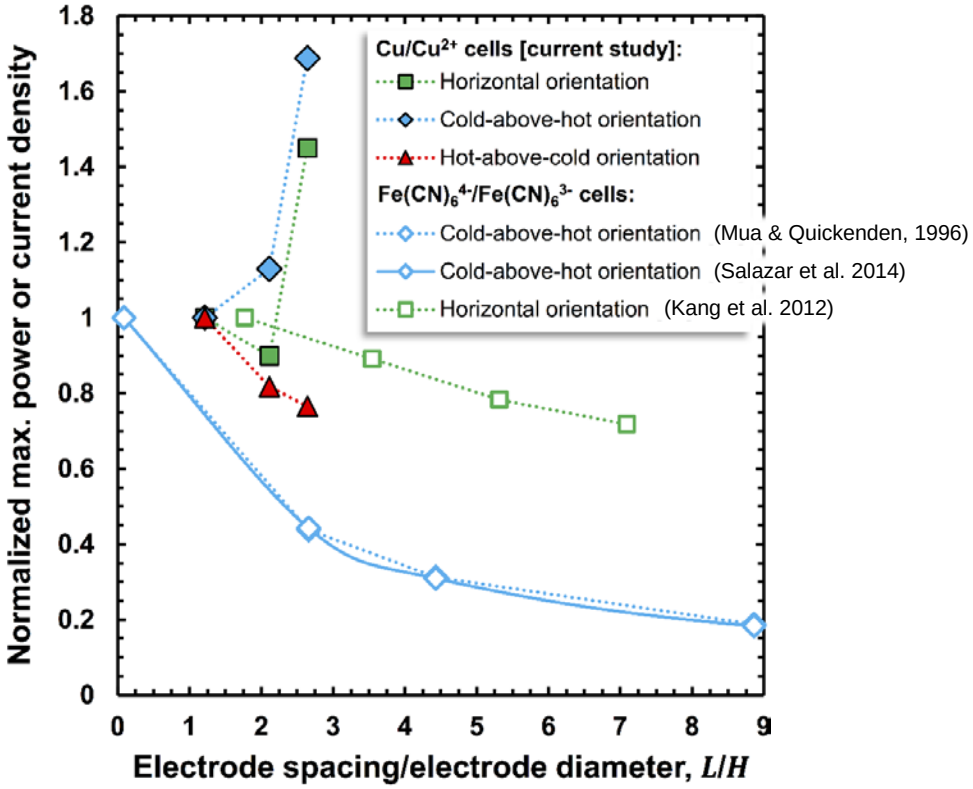

Figure 16. Comparison between the Dependence of Electrode Spacing on Power (or Current) Generation of Cu/Cu^{2+} and $Fe(CN)_6^{4-}/Fe(CN)_6^{3-}$ Cells. The Values of Maximum Current Density are Used whenever the Values of Maximum Power Density are not Included in the Literature. The *y*-axis Represents Maximum Power (or Current) Density Values that are Normalized by the Value Measured for the Same Cell with the Smallest Electrode Spacing; the *x*-axis Represents the Values of Electrode Spacing (L) that are Normalized by the Electrode Diameter (H) of the Same Cell.

The deviation of lower P and P_{max} that is observed for the 80-mm horizontal cell in Figure 13b (also shown in Figure 16) is most likely caused by imprecise temperature control of T_h and T_c (and thus, T_{avg}) during the experiment, which has been described earlier to greatly affect the power generation of the cell. This also explains the relatively

large overprediction of P_{max} ratios for the 80-mm cells in Figure 14. While Salazar et al. [40] suggested that this overprediction can be reduced with more geometrically-accurate numerical modeling, such as including the additional boundary layers at the side walls of the cylindrical cell, this discrepancy seems to be plausible concerning the simplicity of our expressions. Conversely, in the cell without convection (hot-above-cold orientation), Nu and Sh are equal to 1, which indicates that no bulk fluid motion is occurring; thus, no mixing happens. Furthermore, the cell discussed here is already ohmic-limited in nature, which is represented by the linear *I–E* curves (see Figure 17).

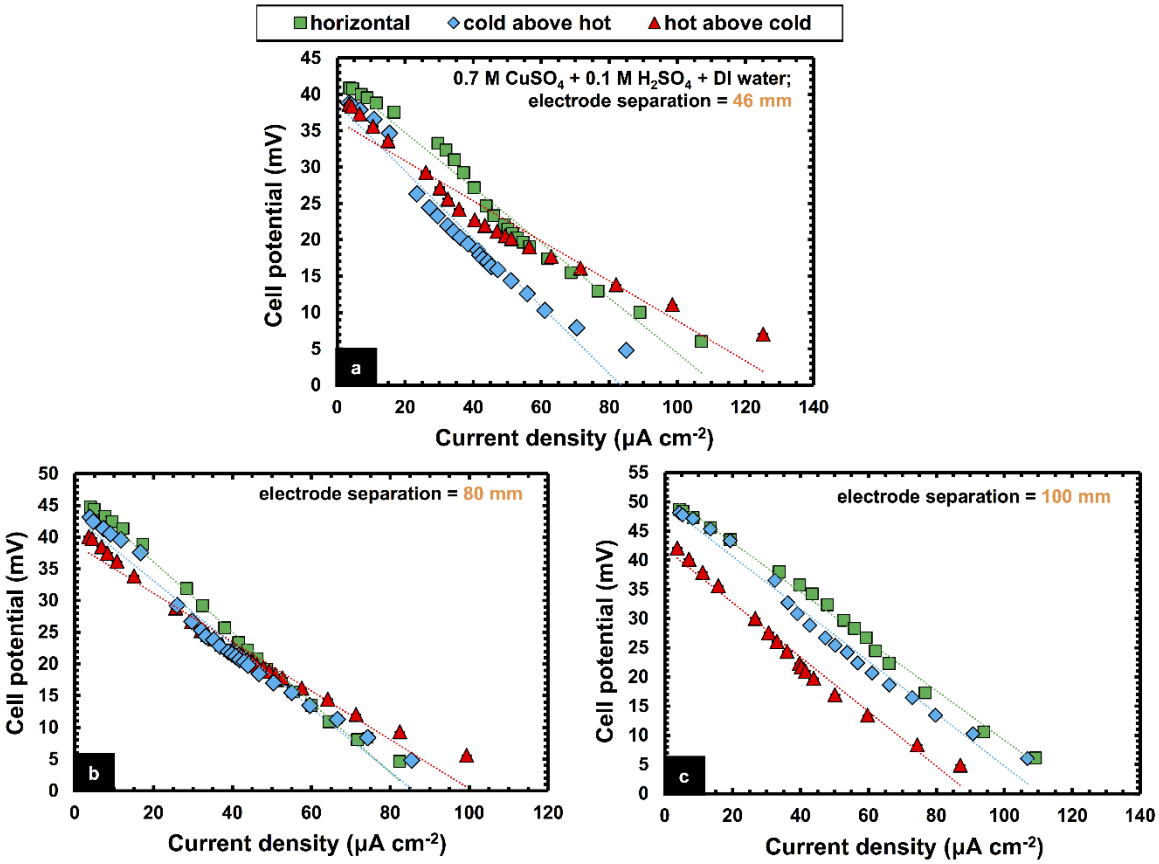

Figure 17. Cell Potential vs. Current Density (or similarly *I-E*) Curves for 0.7 M $CuSO_4$ + 0.1 M H_2SO_4 Aqueous Solution with Cu Electrodes in Three Different Cell Orientations, and at Three Different Electrode Spacing: (a) L = 46 mm, (b) L = 80 mm, and (c) L = 100 mm.

It is therefore quite obvious that when L increases, P_{max} decreases further, following the trend of $Fe(CN)_6^{4-}/Fe(CN)_6^{3-}$ cells, because of the increasing ohmic overpotential of the bulk electrolyte and the mass-transfer overpotential.

3.5 Summary

As an alternative to electrolyte and electrode materials development, I have shown that natural convection can be controlled and has a significant effect on increasing the power generation of Cu/Cu^{2+} thermogalvanic cells. With the controllable experimental configuration shown in Figure 11, which was built to allow for testing a wide variety of operational conditions, natural convection within the cell amplifies P_{max} up to 100%, from ~0.8 to ~1.6 μW cm^{-2}. In addition, P_{max} of the Cu/Cu^{2+} cell increases with the electrode spacing because of the *one-way* ionic transfer mechanism that fully utilizes the natural convection flow within the cell. This dependence of electrode spacing on thermogalvanic power generation suggests that the power generation of Cu/Cu^{2+} cells may not be limited by the cell geometry, which does restrict that of the more conventional $Fe(CN)_6^{4-}/Fe(CN)_6^{3-}$ cell. Throughout our experiments, I also found that the optimum $CuSO_4$ concentration, for the Cu/Cu^{2+} thermogalvanic cells, is 0.7 M, with 0.1 M H_2SO_4 as the background electrolyte. The average cell temperature also has a significant effect on P_{max}. Higher T_{avg} of 55 ℃ resulted in higher P_{max} of 3.12 μW cm^{-2}, while lower T_{avg} of 35 ℃ resulted in lower P_{max} of 1.09 μW cm^{-2}, which is consistent with Kang et al.'s [8] observation for $Fe(CN)_6^{4-}/Fe(CN)_6^{3-}$ cells. Moreover, the simple analytical expressions that we derived as a function of Sh, or Nu and Le numbers suggests that, an electrolyte with high Le and a generator with as high Sh and Nu as

possible, are necessary in order to maximize the power generation of thermogalvanic generators. I have not extended the analytical model beyond the case of the $CuSO_4$ aqueous electrolyte system, however, I hope that the present study will improve our understanding of the energy transfer mechanisms underlying thermogalvanic energy conversion and provide alternative approaches for future researchers and engineers to further optimize this technology.

4. WASTE HEAT RECOVERY APPLICATION IN AUTOMOBILES

Waste heat energy conversion remains an inviting subject for research, given the renewed emphasis on energy efficiency and carbon emissions reduction. The U.S. Department of Energy (DOE) has recently identified capturing waste heat in automobiles to be one of the few examples of breakthroughs—a potential game-changing solution to significantly improving today's engine and vehicle technologies [78, 79]. Solid-state thermoelectric devices have been widely investigated [80], but their practical application remains challenging due to high cost and the inability to fabricate them in geometries that are easily compatible with heat sources. An alternative to thermoelectric devices are thermogalvanic cells [4].

Thermogalvanic cells have recently received significant attention because of their immense potential in converting low-grade thermal energy to electricity (refer back to Figure 5). Hu et al. [5] and Im et al. [43] have demonstrated the feasibility of incorporating such systems to recover thermal energy from exhaust pipes using water-jacketed apparatuses. The previous chapter 3 just showed that incorporating natural convection within a Cu/Cu^{2+} cell, which compressed the concentration boundary layers in the vicinity of the electrodes and thus reduced the mass-transfer (or concentration) overpotential, improved the maximum power output of the cell up to 100% [41].

Motivated by this result, here we investigate the feasibility of incorporating a thermogalvanic system into automobiles. The experimental setup is designed to provide an equivalent real-world condition. We simulate three temperature differences based on quad-monthly average ambient temperatures in Phoenix, AZ. The lower average ambient temperature in November-February, compared to May-August, is expected to impose a

higher temperature difference, which is expected to produce higher power output. However, the experimental results suggest that average cell temperature, which has in general been ignored, may play a bigger role when designing a practical system to ensure optimum power generation.

4.1 Experimental Testing

4.1.1 Annular Thermogalvanic Cell

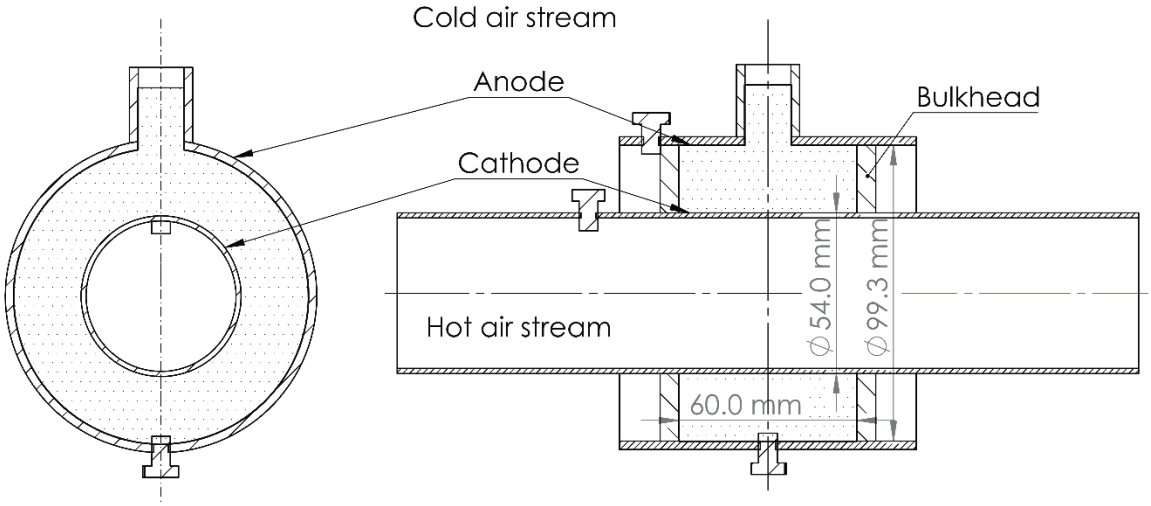

Figure 18. Cross-Sectional Diagram of the Annular Cu/Cu^{2+} Thermogalvanic Cell. The Cold Outer Cu Pipe Acts as the Anode, and the Hot Inner Cu Pipe the Cathode. The Dotted Fill Denotes the Electrolyte.

The annular cell (Figure 18) consisted of two concentric Cu pipes (>99.9%, Thomas Pipe & Supply LLC, Phoenix, AZ) bounded by 2.5-cm-thick high-temperature chlorinated polyvinyl chloride (CPVC) bulkheads (McMaster-Carr, Santa Fe Springs, CA), all sealed with household GE Silicone II Almond sealant. The inner diameter (ID) of the outer Cu pipe, i.e. the cold electrode, was 99 mm and the pipe wall was 3 mm thick. The outer diameter (OD) of the inner Cu pipe, the hot electrode, was 54 mm and

the wall was 2 mm thick. The two CPVC bulkheads were approximately 60 mm apart. Two 22 gauge OMEGA type-K thermocouples and two OMEGA hermetically sealed type-K thermocouples were epoxied onto the air sides and electrolyte sides of the electrodes, respectively, to measure the temperatures of the hot (T_h) and the cold (T_c) electrodes. These and other thermocouples, which will be discussed in the next subsection, were read and recorded every second and averaged over 60 s intervals by a Campbell Scientific CR23X Micrologger with built-in compensation. However, it should be noted that one of the hermetically sealed thermocouples, which was initially epoxied onto the electrolyte side of the cold electrode, was found detached and could not be put back together without dismantling the cell. Cell potentials were probed every second by a Fluke 8846A Digital Multimeter, which then were downloaded and recorded on a PC using LabView. A small polyvinyl chloride (PVC) pipe (The Home Depot, Tempe, AZ) was attached on top of the cell as a filling tube, and a nylon screw was used to plug the drain hole on the bottom.

4.1.2 Climate-Controlled Wind Tunnel

A closed-loop, climate-controlled wind tunnel (Figure 19) was built to provide equivalent conditions to the ambient air stream under the car. The air was driven by a 2700 CFM Dri-Eaz Sahara Pro X3 115V blower. The average air velocity was observed to be 6 m s^{-1}, which is equivalent to 13 mph, at a window in the test section via a UEI DAFM3 anemometer. Ambient air temperature (T_a) inside the wind tunnel was controlled using a combination of 12,000 Btu hr^{-1} LG LW1214ER window air conditioner for cooling and a Master Appliance HG-201A heat gun for heating. These temperatures were measured 70 cm upwind of the test section by two 30 gauge OMEGA

type-K thermocouples sheathed in stainless steel tubing. Another heat gun was used to provide the equivalent of a low-temperature exhaust gas stream of 110 ^{o}C, and was monitored using the same type of thermocouples located at 5 and 10 cm upwind and downwind of the cell inside the inner Cu pipe. This heat gun was connected to a PVC pipe, which was routed through 60 cm of straight section into the cell, to make sure that the flow is fully developed when entering the inner pipe of the cell.

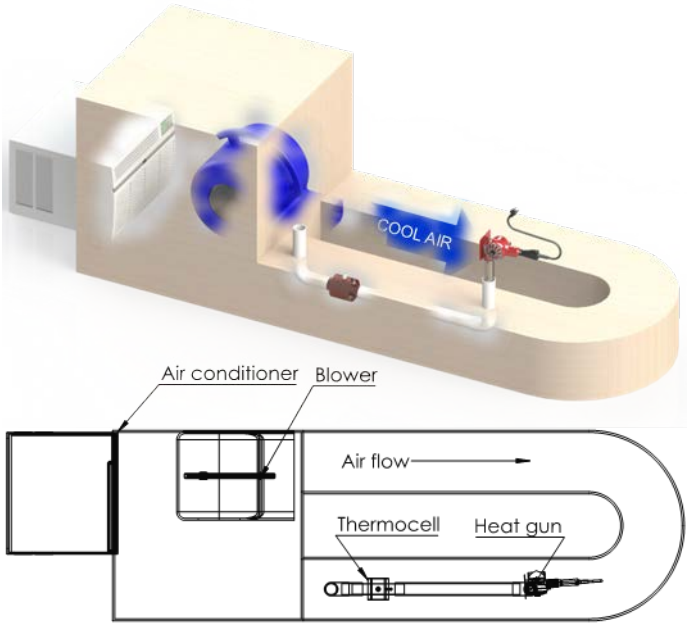

Figure 19. Isometric View and Top View of the Climate-Controlled Wind Tunnel

4.1.3 Electrolyte and Electrode Preparations

The copper sulfate ($CuSO_4$) aqueous electrolyte was prepared identically as described in section 3.2.2. After each measurement, the cell was flushed with technical-grade methanol and deionized water to wash away the reaction product.

4.1.4 Experimental Procedure

After the electrolyte was added into the cell, the cell was left idle, usually for 30 minutes, to make sure there is no leak and to allow the cell's open-circuit potential (E_{oc}) to reach steady state. Once the E_{oc} reading reached steady state, the blower, the window air conditioner and the heat gun were turned on. It took another 30-60 minutes for T_a and T_h to reach the expected set temperatures. Consecutively, after the E_{oc} reading became steady (usually requiring another 20-60 minutes), an Elenco RS-500 variable resistor box was then connected in parallel with the two electrodes and the digital multimeter to measure the power. The digital multimeter showed and recorded the corresponding cell potentials (E) for different resistance loads (R_{ext}), as R_{ext} was manually varied down to 1.1 Ω, for later calculation of power outputs, $P = E^2/R_{ext}$ (Eq. (8). The corresponding steady-state potentials $E(R_{ext})$ were recorded every second and averaged over 80 s, before switching to the next resistance load. The power density was subsequently calculated based on the geometric reactive area of the hot Cu electrode, the cathode, of ~101.8 cm^2, where the heat is captured. At least two runs of experiments were performed; thus, each plotted power density represents an average of 160 data points. The results show that the deviation was usually smaller than 20% but was as high as 64% in some cases. Nevertheless, the cell potential vs. current density (or E-I) curves showed an approximately linear relationship, which are consistent with our previous observations [4, 41].

During the potential sampling phase of the experiment, instead of a thermal steady state, compressor cycling led to a limit cycle. The thermal limit cycle period did not match the potential sampling period; therefore during each 80-s averaging window,

temperature was unsteady, with phase changing at each sampling period. However, only one averaged temperature data point was recorded per 60 s interval. This causes a loss of information that prevents the independent calculation of electrode temperature bias and noise uncertainties associated with each *E-I* data point and is considered to be the primary source of uncertainty. The uncertainty calculation could be made possible by increasing the rate of temperature data recordings, and uncertainty could be reduced by replacing the off-the-shelf window cooler with a unit utilizing variable compression ratio or otherwise improved range and controls.

4.2 Thermal Resistance Model

A simple thermal network analysis can be used to better understand the thermal behavior of the cell and provide insight into design optimization of the experimental setup in the future. Figure 20 on the next page shows the thermal resistance network of the thermogalvanic cell with the associated parameters used in the thermal resistance model.

The heat is transferred from the hot air stream (T_{ha}) to the cold air stream (T_a) through three convection resistances, which are associated with internal forced convection between the inner Cu pipe (T_h) and the hot air stream ($R_{\text{conv},1}$), natural convection of the electrolyte in the annular space between the pipes ($R_{\text{conv,el}}$), and another internal forced convection between the outer Cu pipe (T_c) and the cold air stream ($R_{\text{conv},2}$). The conduction resistances of the Cu pipes are neglected in the model because they are calculated to be four orders of magnitude smaller compared to the three convection resistances.

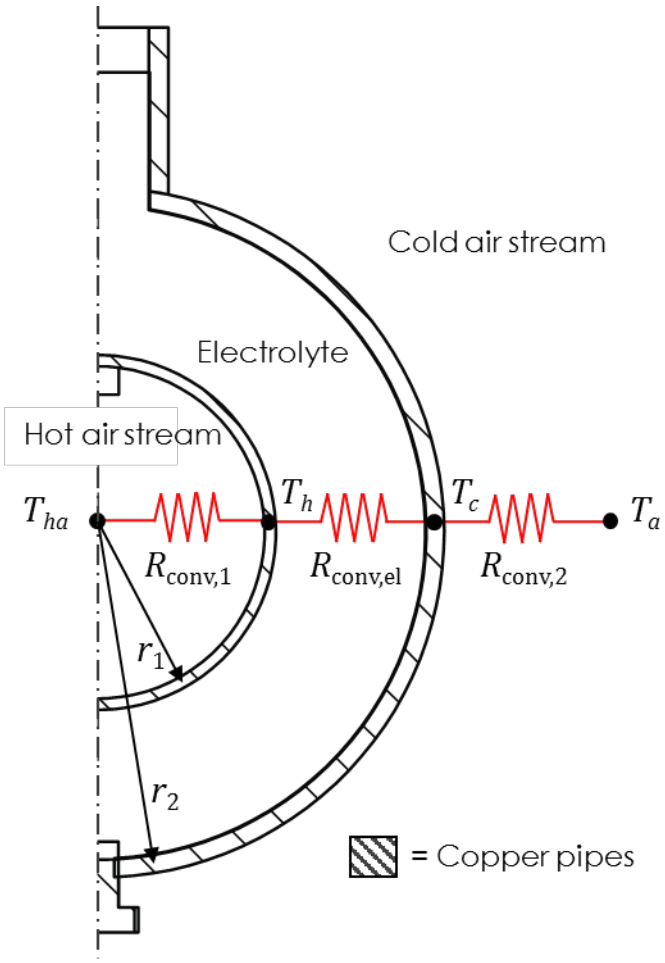

Figure 20. One-Dimensional Thermal Resistance Model of the Thermogalvanic Cell.

The first internal forced convection resistance $R_{conv,1}$ is given by

$$R_{conv,1} = \frac{1}{h_1 A_{s,1}} \tag{29}$$

where

$$h_1 = \frac{\mathrm{Nu}_{ha} k_{ha}}{D_1} \tag{30}$$

$$A_{s,1} = \pi D_1 L \tag{31}$$

h_1 is the heat transfer coefficient, $A_{s,1}$ the heat transfer surface area, Nu_{ha} the Nusselt number, k_{ha} the thermal conductivity of the hot air stream, D_1 (= $2r_1$) the mean diameter

of the inner Cu pipe, and L the length of the thermogalvanic cell, that is the distance between the CPVC bulkheads. Assuming that the hot air stream is turbulent, where Reynolds number, $\mathrm{Re}_{ha} = 4\dot{m}_{ha}/\mu_{ha}\pi D_1$, is larger than 4000; $\dot{m}_{ha}$ and μ_{ha} are respectively the mass flow rate and the dynamic viscosity of the hot air stream, Çengel and Ghajar [81] recommend the following Nu_{ha} correlation:

$$\mathrm{Nu}_{ha} = \frac{\left(\frac{f_{ha}}{8}\right)(\mathrm{Re}_{ha} - 1000)\mathrm{Pr}_{ha}}{1 + 12.7\left(\frac{f_{ha}}{8}\right)^{0.5}\left(\mathrm{Pr}_{ha}{}^{\frac{2}{3}} - 1\right)} \tag{32}$$

assuming that the surface of the Cu pipe is smooth, the friction factor (f_{ha}) is given by [81]

$$f_{ha} = (0.79 \ln \mathrm{Re}_{ha} - 1.64)^{-2} \tag{33}$$

This Nu_{ha} correlation in Eq. (32) is applicable for Reynolds and Prandtl number values between $3 \times 10^3 \leq \mathrm{Re}_{ha} \leq 5 \times 10^6$ and $0.5 \leq \mathrm{Pr}_{ha} \leq 2000$, respectively.

Next, the natural convection resistance of the electrolyte $R_{\mathrm{conv,el}}$ is given by [81]

$$R_{\mathrm{conv,el}} = \frac{\ln(D_2/D_1)}{2\pi k_{el}\mathrm{Nu}_{el}L_c} \tag{34}$$

where D_2 (= $2r_2$) is the mean diameter of the outer Cu pipe, and k_{el} the thermal conductivity of the electrolyte. The characteristic length (L_c) is the spacing between the two Cu pipes, $L_c = (D_2 - D_1)/2$. The Nu_{el} correlation is given by [81]

$$\mathrm{Nu}_{el} = 0.386\left(\frac{\mathrm{Pr}_{el}}{0.861 + \mathrm{Pr}_{el}}\right)^{1/4}\left(F_{\mathrm{cyl}}\mathrm{Ra}_{L,el}\right)^{1/4} \tag{35}$$

where F_{cyl} is the geometric factor for concentric cylinders given by

$$F_{\mathrm{cyl}} = \frac{[\ln(D_2/D_1)]^4}{{L_c}^3\left({D_1}^{-3/5} + {D_2}^{-3/5}\right)^5}, \tag{36}$$

and $\mathrm{Ra}_{L,el}$ is the Rayleigh number for an enclosure which is determined from

$$\mathrm{Ra}_{L,el} = \frac{g\beta_{el}(T_h - T_c){L_c}^3}{{\nu_{el}}^2}\mathrm{Pr}_{el} \tag{37}$$

where g is gravitational acceleration, β_{el} the coefficient of volume expansion of the electrolyte, T_h and T_c are respectively the temperature of the inner (hot) and outer (cold) Cu pipes, Pr_{el} the Prandtl number of the electrolyte, and ν_{el} the kinematic viscosity of the electrolyte. The Nu_{el} correlation in Eq. (35) is applicable for $0.7 \leq \mathrm{Pr}_{el} \leq 6000$ and $10^2 \leq F_{\mathrm{cyl}}\mathrm{Ra}_{L,el} \leq 10^7$.

Ideally, the electrolyte properties at the average cell temperature T_{avg} are to be used in the analysis. However, because the values for properties of the 0.7 M $CuSO_4$ in 0.1 M H_2SO_4 aqueous solution are not readily available, nor easily measured, we again use values of water (see Table 3). Considering that the water content of the electrolytes is at least 87.5 wt.% (0.7 M $CuSO_4$ equals ~11.13 wt.%, and 0.1 M H_2SO_4 equals only ~0.98 wt.%), the resulting errors are expected to be relatively small.

Finally, the second internal forced convection resistance $R_{\mathrm{conv},2}$ is given by

$$R_{\mathrm{conv},2} = \frac{1}{h_2 A_{s,2}} \tag{38}$$

where

$$h_2 = \frac{\mathrm{Nu}_\infty k_\infty}{D_{h,2}} \tag{39}$$

$$A_{s,2} = \pi D_2 L \tag{40}$$

Assuming that the cold air stream is also turbulent, the space between the cell and the surrounding walls of the wind tunnel can be treated as a non-circular duct with a hydraulic diameter, $D_{h,2}$, given by [81]

$$D_{h,2} = D_{h,\text{duct}} - D_2 \tag{41}$$

where the hydraulic diameter of the wind tunnel ($D_{h,\text{duct}}$) is given by

$$D_{h,\text{duct}} = \frac{2ab}{a+b} \tag{42}$$

a and *b* are respectively the height and the width of the square cross-section of the wind tunnel, where $a = b = 30$ cm. The Nu_∞ is calculated using the same Nusselt number correlation described in Eq. (32) by simply substituting the values of f_{ha}, Re_{ha}, and Pr_{ha} with f_∞, Re_∞, and Pr_∞, respectively.

Noting that all three resistances are in series, the total resistance is

$$R_{\text{total}} = R_{\text{conv},1} + R_{\text{conv,el}} + R_{\text{conv},2} \tag{43}$$

Then the steady rate of heat transfer through the cell ($\dot{Q}_{\text{cell}}$) becomes

$$\dot{Q}_{\text{cell}} = \frac{T_{ha} - T_a}{R_{\text{total}}} \tag{44}$$

By keeping T_{ha} constant at 110 ^{o}C while varying T_a, the temperatures of the hot (T_h) and the cold (T_c) electrodes are solved in an iterative method with updating the thermophysical parameters at each iteration step *via* Engineering Equation Solver (EES) v.9.699.

4.3 Results and Discussion

The experiments are carried out using the optimum concentrations of 0.7 M $CuSO_4$, with 0.1 M H_2SO_4 as background electrolyte, which was found and described in the previous study (see section 3.4.1). T_c is varied based on the quad-monthly average ambient air temperature T_a in Phoenix, AZ of 32, 23, and 14 ^{o}C. The experimental values of T_h and T_c are shown next to their resultant plots in Figure 21. Since the

resistance loads R_{ext} in the current Elenco RS-500 resistor box could only be varied down to 1.1 Ω, we could not admit enough current to show the maximum power output (P_{max}) peaks for T_a values of 32 and 23 °C.

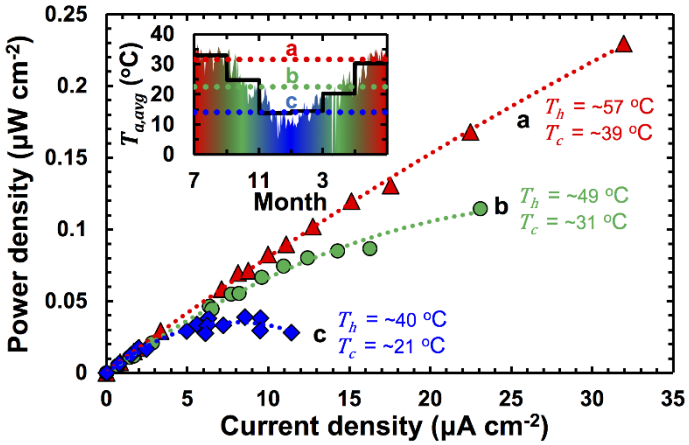

Figure 21. Power Density vs. Current Density Curves for the Annular Cu/Cu^{2+} Thermogalvanic System Tested at Three Average Ambient Temperatures T_a of (a) 32, (b) 23, and (c) 14 °C. T_h and T_c are Respectively the Temperatures of the Hot and Cold Electrodes. The Inset Shows Historical Data of Average Ambient Air Temperature in the Greater Phoenix Area, AZ from July 1, 2013 to June 30, 2014, Imported from the Arizona State University Weather Station [82]; Solid and Dotted Lines in the Inset Indicate Bi-Monthly and Quad-Monthly Average Ambient Air Temperatures, Respectively.

It was expected that the lower average ambient temperature T_a would impose higher temperature difference (ΔT), thus producing higher maximum power output P_{max}. However, these results conversely show that higher T_a yields a higher power density, because of the higher average cell temperature, $T_{avg} = (T_h + T_c)/2$. Increasing T_{avg}, i.e. increasing both T_h and T_c, increases the redox reactivity at these electrodes, as well as the ionic conductivity of the electrolyte, while simultaneously reduces the mass-transfer resistance of the cell [8, 41]. Moreover, changing the temperature has an exponential effect on the exchange current density as described by the Bulter–Volmer equation [8].

This trend agrees with our previous study [41] and another observation for a cell using conventional $Fe(CN)_6^{4-}/Fe(CN)_6^{3-}$ redox couple [8]. In addition, the magnitudes of power output P and P_{max} are consistent with ours and other previously reported studies of Cu/Cu^{2+} cells that had been reviewed in Table 2. A summary of the dependence of temperatures on maximum power output of the Cu/Cu^{2+} thermogalvanic waste heat recovery system is provided in Table 4.

Table 4. Summary of the Dependence of Temperatures on Maximum Power Output of the Cu/Cu^{2+} Thermogalvanic Waste Heat Recovery System.

T_a (°C)	T_h (°C)	T_c (°C)	ΔT (°C)	T_{avg} (°C)	P_{max} (μW cm^{-2})
14	40	21	19	30.5	~0.04
23	49	31	18	40	~0.11
32	57	39	18	48	N/A

The results of the simple thermal resistance analysis, which includes all temperatures that are tabulated in Table 4 minus the maximum power output (P_{max}), in comparison to the experimental results for the three quad-monthly average ambient air temperature T_a, are shown in Figure 22.

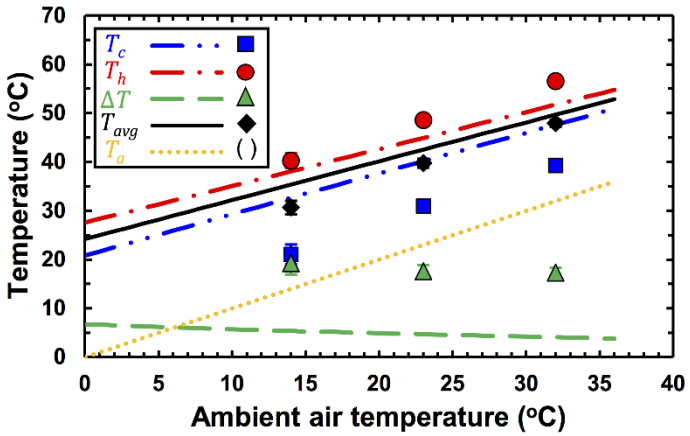

Figure 22. Comparison between Experimental Data (markers) and Calculated Results (lines) of Dependence of Ambient Air Temperature (T_a) on Temperatures of the Cold (T_c) and Hot (T_h) Electrodes, Temperature Difference (ΔT), and Average Cell Temperature (T_{avg}) of the Cell. Error Bars Represent 95% Confidence Intervals. Most of the Error Bars are not Visible because They are Smaller than the Corresponding Markers.

This simple model is shown to be in fair agreement with the experiments. The bigger discrepancy between the calculated and experimental values of the cold electrode temperature T_c is most likely caused by the inaccuracy in the measurement. As we mentioned earlier in the experimental setup section, we lost the thermocouple reading on the electrolyte side of the cold electrode. Therefore, the experimental data of T_c (rectangular markers) is lower than the calculated data (double-dotted dashed line) because it represents only the air-side temperature of the cold electrolyte, instead of the average temperature between the air-side and the electrolyte-side, which is exposed to the cooler ambient air temperature T_a. The average temperature different between the air-side and the electrolyte-side of the hot electrode throughout the experiments, for an example, is ~10 ^{o}C. This error is being carried over in the following calculations of ΔT and T_{avg}, which also causes the discrepancy between their calculated and experimental values. Nevertheless, the figure shows that both T_c and T_h increase linearly with T_a,

hence, the average cell temperature T_{avg} also increases. On the other hand, the temperature difference between the electrodes, ΔT, decreases slightly with the increasing of T_a, which also agrees very well with the trend of the experimental data.

It should also be noted that the measured ΔT for the three cases are almost the same. It is probably caused by the lost reading of the temperature of the electrolyte side of the cold electrode. Nonetheless, the errors are expected to be relatively small. Moreover, the temperatures of the hot electrode T_h are measured to be much lower than the hot air stream's temperature of 110 ^{o}C. This happens because heat is lost due to convection along the inner Cu pipe. The simple thermal resistance analysis shows that the convection resistance between the inner Cu pipe and the hot air stream ($R_{\text{conv},1}$) contribute up to 75% of the total thermal resistance, while the convection resistance between the outer Cu pipe and the cold air stream ($R_{\text{conv},2}$) and the convection resistance of the electrolyte ($R_{\text{conv,el}}$) contributes only up to 20% and 5% of the the total thermal resistance, respectively. This translates into, approximately, only 31–38% of the total thermal energy from the hot air stream that is captured and transferred through the cell.

$$\frac{\dot{Q}_{\text{cell}}}{\dot{Q}_{\text{total}}} = \frac{\text{Eq. (44)}}{\dot{m}_{ha} c_{p,ha} (T_{in} - T_{out})} \approx 38\%$$

where $\dot{Q}_{\text{cell}}$ is the steady rate of heat transfer through the cell that is calculated using Eq. (44), $\dot{m}_{ha}$ the mass flow rate of the hot air stream through the inner Cu pipe of the cell, $c_{p,ha}$ the constant pressure specific heat of hot air at the average temperature of 110 ^{o}C, T_{in} and T_{out} are the temperature of the hot air stream at the inlet and outlet of the inner Cu pipe of the cell, respectively.

More thermal energy, up to 38%, is captured and transferred through the cell at lower ambient temperature T_a because of the slightly higher ΔT. However, since it has been shown that the dependence of power generation on the average cell temperature T_{avg} is stronger than on ΔT, especially in this particular annular thermogalvanic cell, this does not translate into a higher power output, P_{max}. Further improvement of this system requires designing an optimum heat exchanger that will maximize the heat transfer from the hot air stream to the hot electrode, especially, and from the ambient air to the cold electrode. This will maximize the ΔT across the cell; thus, maximizing the electric power output.

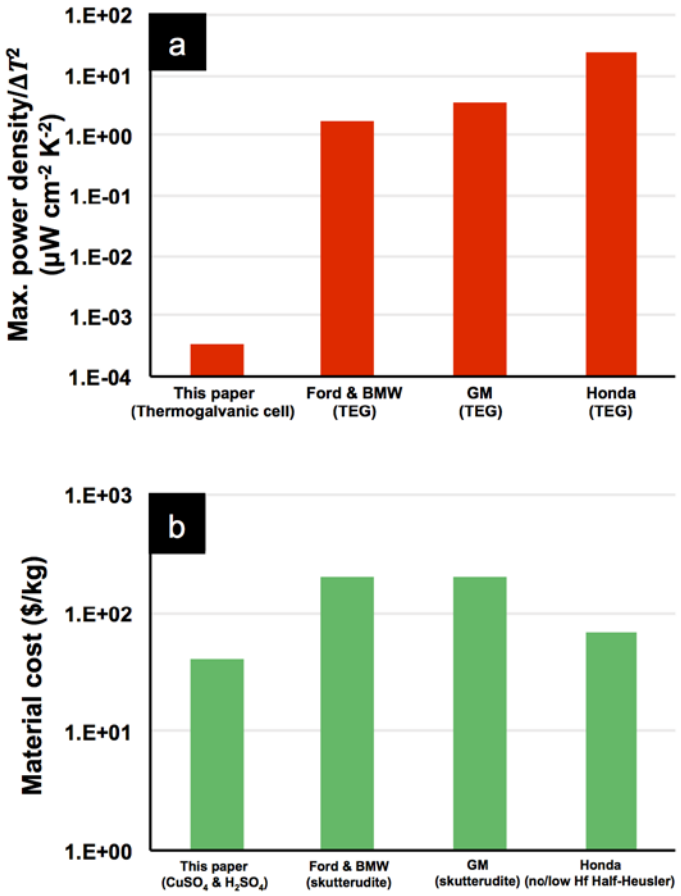

Figure 23. Comparison of Normalized Specific Power Density (a) and Pure Material Costs (b) between the Cu/Cu^{2+} Annular Thermogalvanic Waste Heat Recovery System and Solid-State Thermoelectric Generators (TEGs).

To illustrate a simple economic assessment, Figure 23a shows the comparison between normalized specific power density ($P_{max}/\Delta T^2$) of Cu/Cu^{2+} annular thermogalvanic waste heat recovery system that we assembled and tested, and data from solid-state thermoelectric generators (TEGs) that are currently being implemented and tested for a light-duty vehicle by General Motors, Honda, BMW and Ford. The TEG data are adapted from the Fiscal Year 2014 Annual Progress Report for the Advanced Combustion Engine R&D program, which was published recently by the DOE Vehicle Technologies Office [83]. The power density of the TEGs is calculated based on

geometric area of the hot side of the devices where heat is captured. Per data from the DOE report [83], unless otherwise stated specifically by the manufacturer, all TEGs are assumed to be operating with a 'cold' side temperature of 100 ^{o}C, and 'hot' side temperature of 500 ^{o}C. Figure 23a may not show the highest achievable experimental data of the TEGs because more tests are still underway. Additionally, since the dimensions of the geometric area of the hot side of Honda's TEG are unavailable in the report, the plotted data are adapted from a paper published by their university partner [84]. This comparison shows that the power density of thermogalvanic cells is 4 to 5 orders of magnitude lower compared to the TEGs. Figure 23b puts the comparison in monetary forms based on the cost of the raw materials alone. It indicates that the costs of the raw materials for both the Cu/Cu^{2+} thermogalvanic cells (the electrolyte) and the TEGs are almost the same. The prices of skutterudite and no/low Hf Half-Housler are adapted from [85].

Indeed, Joshi et al. [84] mentioned that raw material contributes only ~10% of the total produced energy cost ($ per W) of TEGs. The rest of the cost is contributed by other processes such as material processing, device assembly and system integration. Therefore, we calculated and estimated the cost to build our Cu/Cu^{2+} thermogalvanic cell to be around $36 in total (see Table 5). Expensive, cleanroom-based manufacturing processes are not required for assembling the cell. Additionally, we have demonstrated that the fluid (liquid) nature of the electrolyte enables a thermogalvanic device to be integrated seamlessly onto a car's exhaust pipe. The highest reported maximum power output, a P_{max} of 1.8 W m^{-2} corresponding to a power conversion efficiency relative to that of a Carnot engine operating between the same temperatures, $\eta_r = \eta/(1 - T_c/T_h) =$

1.4%, was achieved by [5] with carbon-multiwalled nanotubes buckypaper electrodes in a $Fe(CN)_6^{4-}/Fe(CN)_6^{3-}$ aqueous electrolyte. In that case, if we assume that this P_{max} can still be further improved, it is feasible to ultimately achieve energy production cost of about $1/Watt.

Table 5. Total Cost to Build Our Cu/Cu^{2+} Annular Thermogalvanic Waste Heat Recovery System.

Material	Needed (approx.)	Est. $
Electrodes		
Inner Cu pipe	25 cm	$ 14.27
Outer Cu pipe	8 cm	$ 15.00
Electrolyte		
$CuSO_4 \cdot 5H_2O$ salts	61.17 gram	$ 2.43
H_2SO_4 solution	3.43 gram	$ 0.05
Misc.		
CPVC bulkhead	55.64 cm^2	$ 4.07
Silicone sealant		(negligible)
TOTAL		$ 35.81

4.4 Summary

We have discussed the feasibility of incorporating Cu/Cu^{2+} thermogalvanic system into automobiles, to recover waste heat energy from exhaust gases. The power outputs are typically small, between a tenth and tens of mW m^{-2}, but as pointed out by Ball [51], aside from the initial outlay on the cell, that energy is essentially free when it comes from an exhaust pipe of a car that would otherwise just be left to warm the air. It was also found that the average cell temperature, $T_{avg} = (T_h + T_c)/2$, had a more substantial effect on the power generation than the temperature difference did.

Furthermore, the fluid (liquid) nature of the electrolyte and potential to be manufactured inexpensively will lead to widespread applications. These have also resulted in thermogalvanic cells becoming an intriguing alternative to solid-state thermoelectric devices.

5. SEEBECK COEFFICIENT ENHANCEMENTS BY NOVEL ELECTROLYTES

Ideally, an electrolyte for a thermogalvanic cell should have high intrinsic Seebeck coefficient, in addition to high intrinsic R_{th}/R_{int} ratio. However, identifying such an ideal system is not an easy task. There are lots of options available out there; some of them can be bought off-the-shelf, but others can only be manufactured in particular labs.

Based on our recent review article [4], between 1995 and 2013 four studies have reported results using molten salt and ionic liquids [6, 86-88], two have pursued and reported results for non-aqueous (organic) redox couple electrolytes [7, 15], and six have chosen to continue using aqueous redox couples [5, 8, 58, 39, 89]. These numbers have grown considerably since as shown in Figure 5 on p. 7.

The Seebeck coefficient of a thermogalvanic cell is directly proportional to the change in entropy of the redox reaction in the cell through the relation $\alpha = \partial E/\partial T = \Delta S/nF$ (Eq. (4)). In an ideal thermogalvanic cell, one therefore prefers to employ a redox couple exhibiting the largest ΔS, which leads to a correspondingly largest α. Therefore, this study focuses on ways to couple the Cu/Cu^{2+} redox process to solution phase complexation to increase the entropy change (ΔS) for the electron transfer process. The idea is to complex the Cu^{2+} species with a dissolved polymer, such as poly(acrylic acid) (PAA), that will be cross-linked by the metal dication (Figure 24).

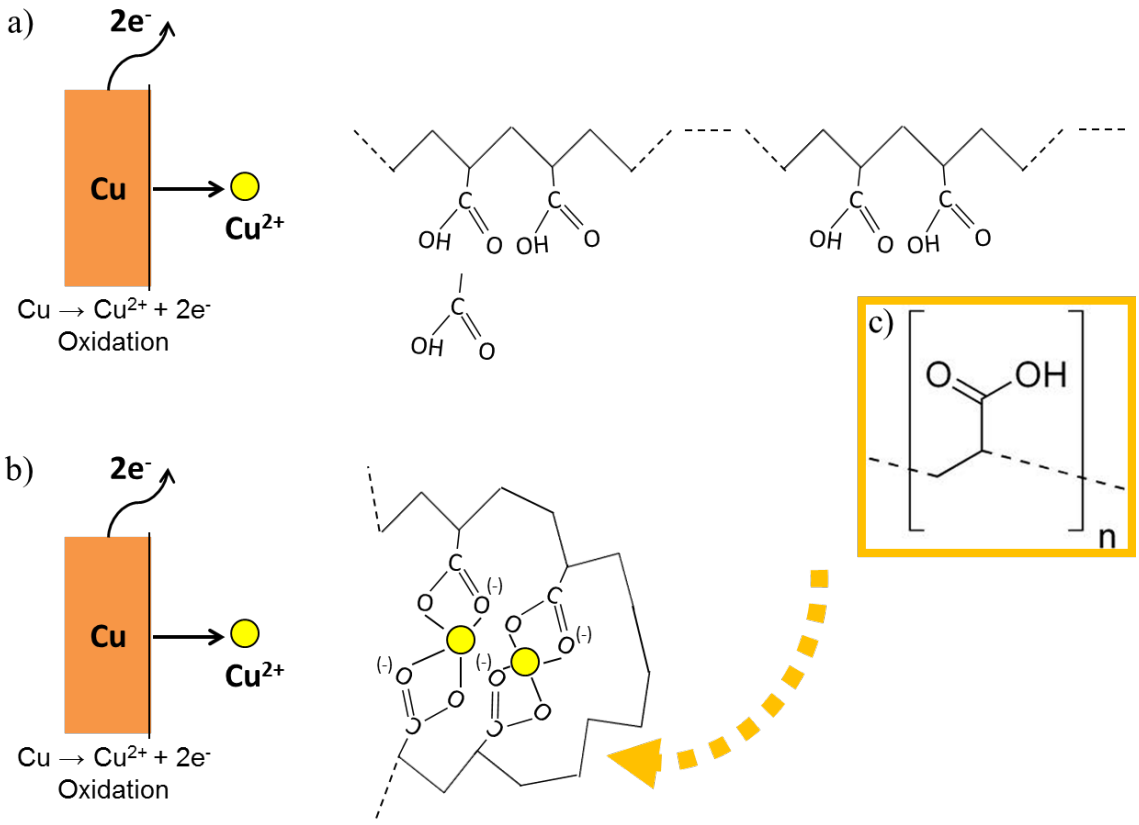

Figure 24. Illustration of the Complexation of the Cu^{2+} Species with Dissolved Polymer (e.g., PAA) that is Cross-Linked by Metal Dication. The Density of Final Configurational States S_{final} (a) is much Lower than the Density of Initial Configurational States $S_{initial}$ (b), which Leads to an "Amplified" Entropy Change ΔS, and Correspondingly Larger α. Inset (c) Shows the Chemical Structure of PAA.

The density of configurational states of the polymer, which is expressed as S (entropy), will be substantially decreased in the complexed state [90]:

$$S_{final} \ll S_{initial} \tag{45}$$

Reduction of Cu^{2+} to Cu metal will release the complexed polymer, resulting in a dramatic increase in the configurational entropy of the polymer,

$$\Delta S_{[\mathrm{PAA+Cu,\ Cu^{2+}}]} = S_{initial} - S_{final} \tag{46}$$

leading to an "amplified" entropy change for the redox process,

$$\Delta S_{[\mathrm{PAA+Cu,\ Cu^{2+}}]} \gg \Delta S_{[\mathrm{Cu,\ Cu^{2+}(without\ PAA)}]} \quad (47)$$

and a correspondingly larger Seebeck coefficient:

$$\frac{\Delta S_{[\mathrm{PAA+Cu,\ Cu^{2+}}]}}{nF} = \alpha \uparrow \quad (48)$$

Previous studies have described solution conditions under which Cu^{2+} and PAA can coexist in solution [91], which will be a starting point for this part of our study. We are not aware of any previous investigations of the use of such "amplified" entropy changes in thermogalvanic cells, so this work will represent a completely new approach to enhancing Seebeck coefficients.

5.1 Experimental Testing

We choose to focus on the Cu/Cu^{2+} cell because we already have considerable experience with the Cu/Cu^{2+} system [4, 41], which has a relatively simple electrochemical behavior and the ion can be chelated with chemical agents like Ethylenediaminetetraacetic acid (EDTA) [92] to explore the role of the entropy change in the generation of thermoelectric power.

5.1.1 Experimental Setup

The experimental setup (Figure 25) was inspired by [61] and [6]. The electrolyte was contained in two 10-ml glass beakers, with a stopper holding an electrode and a thermocouple in each beaker. A 14-cm-long tubing (Tygon R-3603, Cole-Parmer, Vernon Hills, IL) filled with the same electrolyte connected the two beakers as a salt bridge. A Keithley 6517B Electrometer/High Resistance Meter was used to measure the

cell potentials. A thermoelectric cooler (TE Technology, Inc.CP-031) was attached at the bottom of the hot beaker with Arctic Silvers thermal paste (Arctic Silver, Inc., Visalia, CA) to enhance heat conductance. The thermoelectric cooler was controlled by a programmable Newport 3040 temperature controller. The cold side was maintained at room temperature by natural cooling.

OMEGA hermetically sealed type-T thermocouples were connected to a Campbell Scientific CR23X Micrologger to monitor and record temperature differences. This temperature measurement system was calibrated, and its mean relative error was estimated to be around ± 1.0%, and with a maximum uncertainty of ± 1.3%.

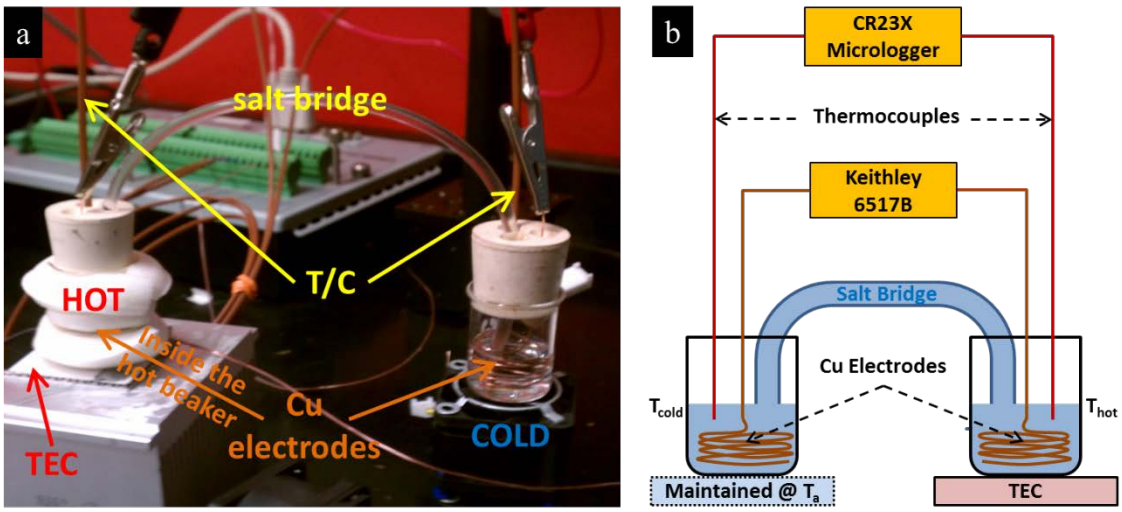

Figure 25. (a) Photograph of the Cell Configuration for the Current Experiment. (b) Schematic Diagram of the Overall System.

5.1.2 Electrolyte and Electrode Preparation

Copper sulfate ($CuSO_4$) solution was prepared by dissolving 99% purity $CuSO_4.5H_2O$ salt (PTI Process Chemicals, Ringwood, IL) into deionized water. The polymer electrolyte (polyelectrolyte) was prepared by dissolving Polyacrylic acid sodium

salt (Sigma-Aldrich, average molecular weight (M_w) ~2,100) into the $CuSO_4$ aqueous solution, and stirring the solution slowly. After the stirring process, 0.1 M K_2SO_4 was added into the solution as a background electrolyte. Ionic conductivity and pH of the polyelectrolyte were measured using a Hach CO150 Conductivity Meter and a Hach EC10 pH Meter, respectively. Thirty-centimeter-long Cu electrodes were prepared by winding 22 American Wire Gauge bare copper wires (99.9%, Arcor Electronics, Northbrook, IL). The Cu electrodes were rinsed with methanol and deionized water at the onset of each experiment, and were used immediately after air drying.

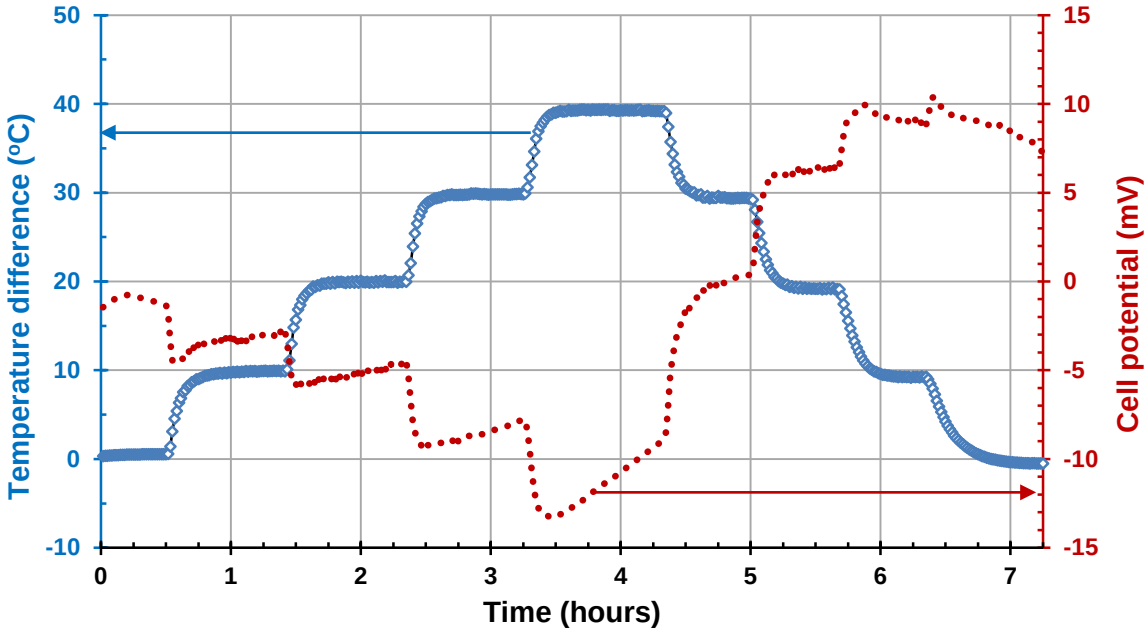

Figure 26. Plots of Temperature Difference ΔT and Corresponding Potential Difference Across the Cell ΔE vs. Time, for a Thermogalvanic Cell with Cu Electrodes in 1 mM $CuSO_4$ + 100 mM PAA Aqueous Electrolyte. The Solution Contained 0.1 M Potassium Sulfate and was at Its Natural pH of ~8.0.

5.1.3 Experimental Procedure

Figure 26 shows an example of one complete run. After the electrolyte was added into the cell, the cell was left idle (usually for 30 min) to allow the cell's open-circuit

potential (E_{oc}) to reach steady state. Once the E_{oc} reading reached steady state, the hot electrode was heated up and the temperature difference (ΔT) between the hot and the cold electrode was maintained around 10 °C. After the ΔT and E_{oc} readings became steady, i.e. when the readings varied between ± ~0.3 °C and ± ~2.5 mV over the average values, respectively, the hot electrode was heated up to the next ΔT of 20 °C. This usually required another 55–65 min. The same procedure was repeated for the following ΔTs of 30 and 40 °C. In addition, for reversibility check, the ΔT was consecutively brought down to 30, 20, 10, and back to 0 °C by following the same procedure, but with less time (~40 min) in between ΔT's.

5.2 Results and Discussion

We use a low concentration of $CuSO_4$ (i.e. 1 mM) to avoid precipitation issues with the polymer. For a first approximation, we calculate the Seebeck coefficient (α) of 1 mM $CuSO_4$ aqueous solution using Eq. (6) [1]:

$$\begin{aligned} \alpha &= \frac{\partial E^0}{\partial T} + \frac{R}{nF}\ln(\gamma_{Cu^{2+}} C_{Cu^{2+}}) \\ &= 0.879 + \frac{R}{2F}\ln(1.674 \times 0.001) = 0.604 \text{ mV K}^{-1} \end{aligned} \tag{49}$$

where $\partial E^0/\partial T$ = 0.879 mV K^{-1}, again, is the Seebeck coefficient of a standard Cu/Cu^{2+} cell at 25 °C taken from [1], R the universal gas constant, n the number of electrons involved in the redox reaction, F the Faraday constant, $C_{Cu^{2+}}$ the molar concentration of the $CuSO_4$ aqueous solution, and $\gamma_{Cu^{2+}}$ the activity coefficient for the cupric ion. deBethune et al. [1] only listed the values of $\gamma_{Cu^{2+}}$ for $C_{Cu^{2+}}$ between 0.08 and 1.4 M. Therefore, the $\gamma_{Cu^{2+}}$value for 1 mM $CuSO_4$ above is quantified using a best-fit curve.

We consequently run an experiment in order to validate the approximate value of $\alpha = 0.604$ mV K^{-1} from Eq. (49). As noted by deBethune et al [1], the calculation agrees very well within $\pm$ 0.05 mV K^{-1} with the experimental value depicted in Figure 27 below. We therefore use this experimental value of $\alpha = 0.619$ mV K^{-1} as a benchmark for the following discussion.

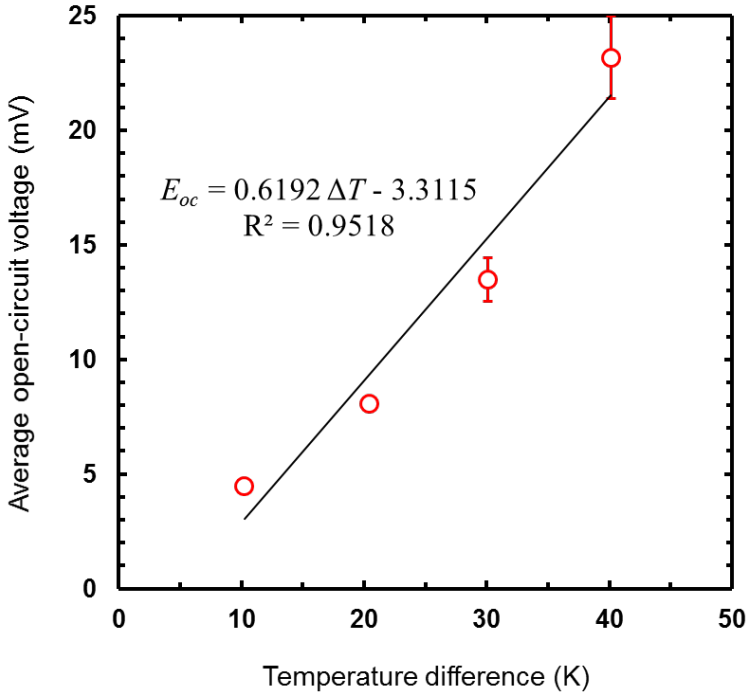

Figure 27. Seebeck Coefficient ($\alpha = E_{oc}/\Delta T$) of 1 mM $CuSO_4$ Aqueous Electrolyte in a Thermogalvanic Cell with Cu Electrodes. The Solution Contained 0.1 M Potassium Sulfate and was Adjusted to pH 5, from the Natural pH of ~5.7, Using 0.1 M Sulfuric Acid. Error Bars Represent 95% Confidence Intervals. Most of the Error Bars are not Visible because They are Smaller than the Corresponding Markers.

5.2.1 Aqueous Polyelectrolytes

Figure 26 has previously shown a typical Seebeck coefficient measurement for aqueous polyelectrolyte with Cu/Cu^{2+} redox process complexed with a polymer, i.e.

poly(acrylic acid) or PAA. The temperature dependence of the electrode potential of this particular polyelectrolyte is unfortunately irreversible, as shown below in Figure 28.

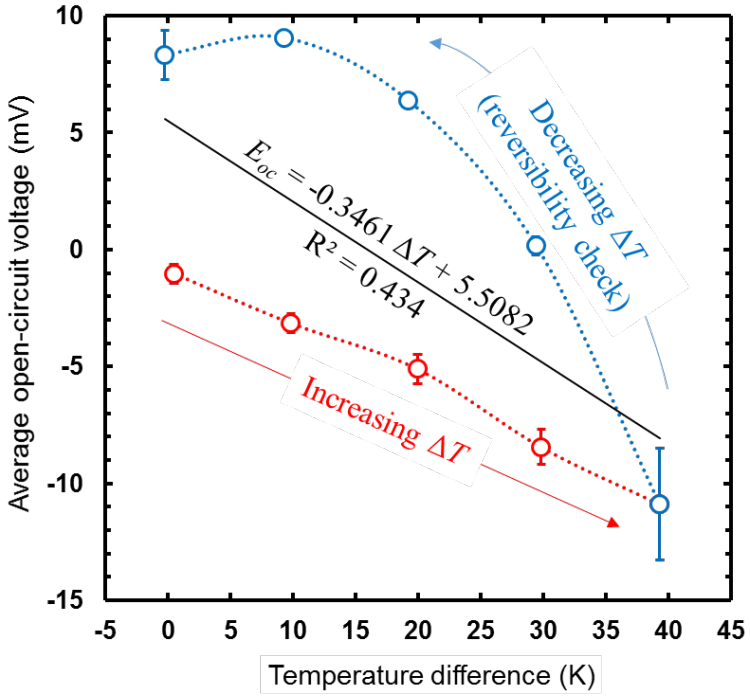

Figure 28. Seebeck Coefficient ($\alpha = E_{oc}/\Delta T$) of 1 mM $CuSO_4$ + 100 mM PAA Aqueous Electrolyte. The Plot was Depicted from ΔE and ΔT vs. Time Data for the Same Electrolyte in Figure 26. Error Bars Represent 95% Confidence Intervals. Most of the Error Bars are not Visible because They are Smaller than the Corresponding Markers. Dotted Lines were Added to Guide the Eye.

We have attempted to solve this irreversibility issue by shortening the total experiment time, in addition to varying the pH and the molar concentration ratio of PAA:$CuSO_4$. The concentration of $CuSO_4$ is kept constant at all times at 1 mM to avoid the aforementioned precipitation issue. Nevertheless, we observe the same behavior of the corresponding open-circuit voltage of the cell (see Figure 29). The cell potential, or the open-circuit voltage E_{oc}, starts to deviate when the temperature difference ΔT reaches 40 ^{o}C, as indicated by the grey rectangle in Figure 29a. This phenomenon was also

observed in Figure 26, for different molar concentration ratio of PAA:$CuSO_4$, pH, and longer total experiment time. The Seebeck coefficients of these aqueous polyelectrolytes are therefore invalid. It should be noted, however, that the Seebeck coefficients between the $CuSO_4$ (Figure 27) and the $CuSO_4$-PAA (Figure 28) are opposite in sign. This change of sign will be discussed later in the following section.

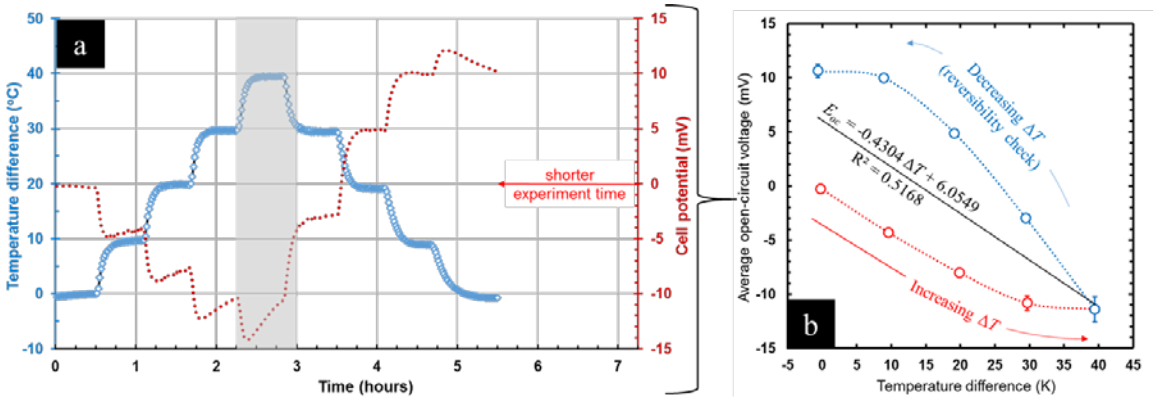

Figure 29. (a) *Shortening* the Total Experiment Time for a Thermogalvanic Cell with Cu Electrodes in 1 mM CuSO4 + *10 mM* PAA Aqueous Electrolyte. The Solution Contained 0.1 M Potassium Sulfate and was at Its Natural pH of ~*6.8*. (b) Seebeck Coefficient Plot for the Same Electrolyte Depicted from (a). Error Bars Represent 95% Confidence Intervals. Most of the Error Bars are not Visible because They are Smaller than the Corresponding Markers. Dotted Lines were Added to Guide the Eye.

5.2.2 Mixed-Ligand Complexes Aqueous Electrolytes

Since we found out that there was an irreversibility issue in the Seebeck coefficient measurement of Cu/Cu^{2+} redox process with PAA, we use a simpler chelating agent, i.e. Ethylenediaminetetraacetic acid (EDTA), instead to explore the role of the entropy change in the generation of thermoelectric power. Using the same experimental setup, electrolyte and electrode preparation, as well as experimental procedure, we

observe no irreversibility issue of the temperature dependence of the electrode potential of the Cu-EDTA aqueous electrolyte in eight independent runs (Figure 30).

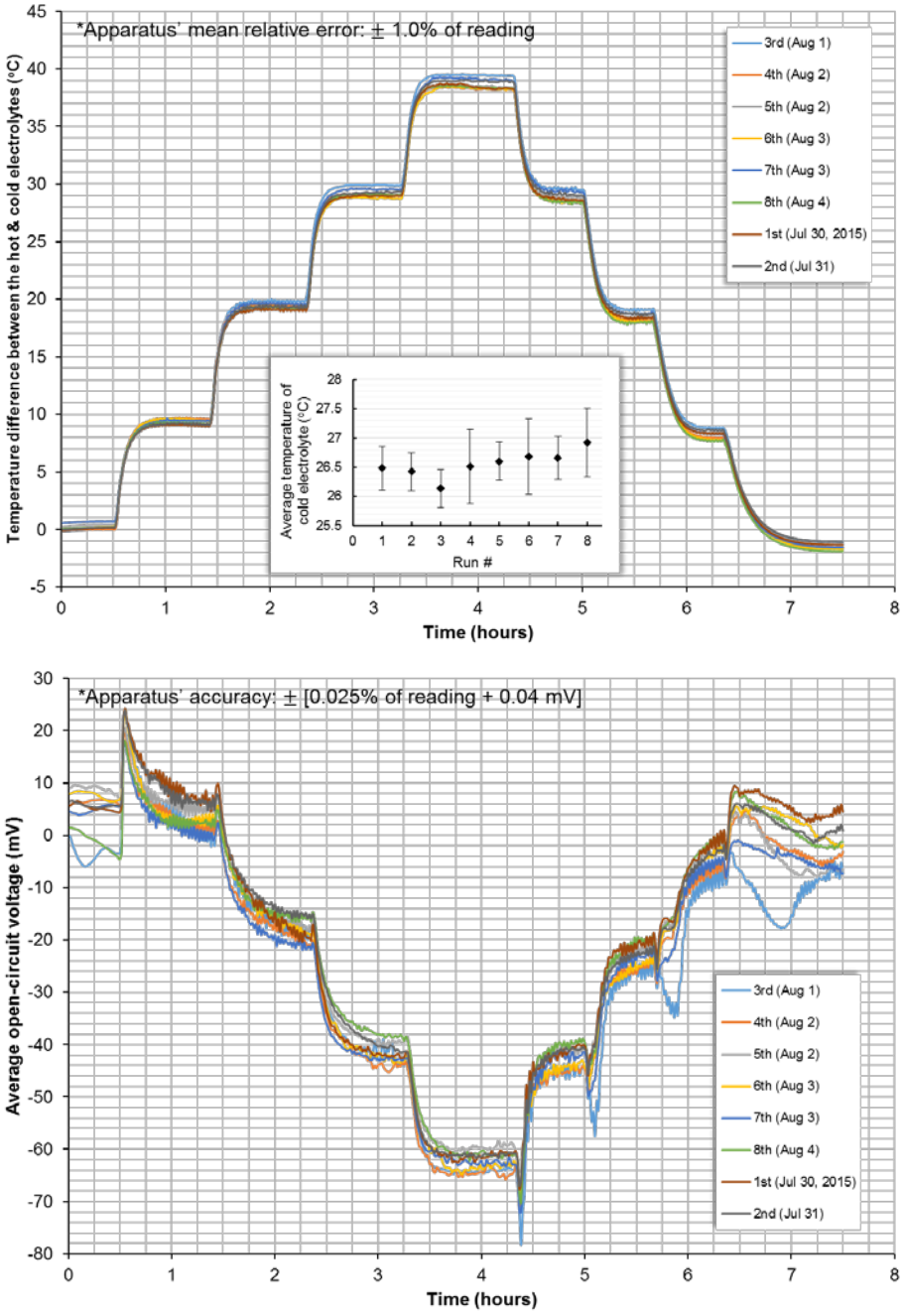

Figure 30. Temperature Difference (above) and Open-Circuit Potential (below) of Cu-EDTA Experiments, Showing Reproducibility. There is a Small, Systematic Issue with the Initial and Final Thermal Situation in the Cell, but It is Negligible.

It seems pretty clear that the new data are reproducible. There is no deviation in the open-circuit voltage versus time plot that results for the aqueous polyelectrolyte cells, when temperature difference reached 40 ºC (Figure 26 and Figure 29a). There are small systematic issues with the initial and final thermal situation in the cell, however, they are trivial as the data are consequently compiled and depicted in Figure 31, then Figure 32 below.

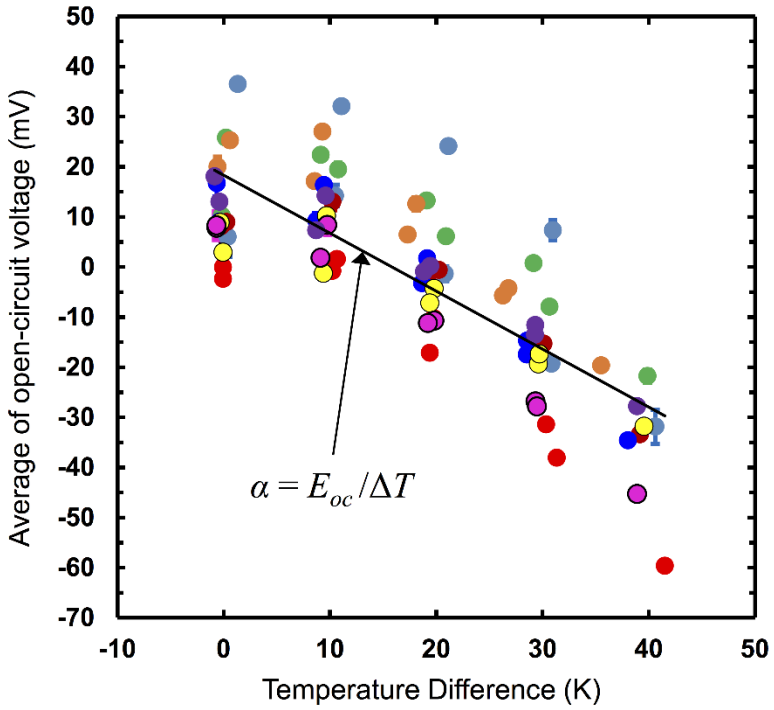

Figure 31. Plots of Average Open-Circuit Voltage E_{oc} vs. Temperature Difference ΔT of Eight Independent Runs from Figure 30, of a Thermogalvanic Cell with Cu Electrodes in 10 mM EDTA + 1 mM $CuSO_4$ Aqueous Electrolyte. These Data are Summarized in a More Concise Figure 32, with More Details Regarding the Electrolyte in the Caption.

Figure 32 provides more concrete evidence of irreversibility. We find no evidence of irreversibility, which was found in the aqueous polyelectrolyte cells (Figure 28 and Figure 29b). In addition, this set of results shows that the averaged experimental run of Cu-EDTA aqueous electrolyte gives a Seebeck coefficient ($|\alpha|$ = 1.108 mV K^{-1})

that is much larger than the traditional 1 mM $CuSO_4$ result of 0.619 mV K^{-1}, an 80% increase.

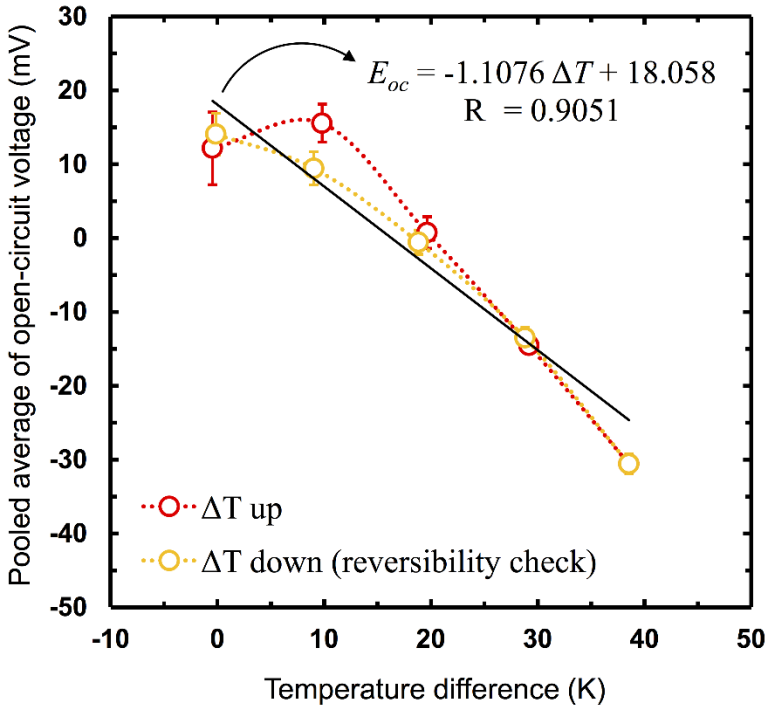

Figure 32. Seebeck Coefficient of 10 mM EDTA + 1 mM $CuSO_4$. The Solution Contained 0.1 M Potassium Sulfate and was Adjusted to pH 6, from the Natural pH of ~3.6, Using 0.1 M Sodium Hydroxide. Error Bars Represent 95% Confidence Intervals. Some Error Bars are not Visible because They are Smaller than the Corresponding Markers. Dotted Lines were Added to Guide the Eye.

Furthermore, we are motivated by unusually large entropic contributions from 2CuEDTA-$(CH_2)_2(NH_2)_2$ and 2CuEDTA-$(CH_2)_6(NH_2)_2$ dimers compared to the monomeric case [92, 93]. These papers suggested that, for example, adding half of mole fraction of 1,6-diaminohexane, i.e. $(CH_2)_6(NH_2)_2$, into the Cu-EDTA experiments will result in a dimeric species of EDTACu-$H_2N(CH_2)_6NH_2$-CuEDTA, where the two ends of diamine (i.e. NH_2) bridge between the Cu centers. Consequently, the formation of the dimeric species of 2CuEDTA-$(CH_2)_6(NH_2)_2$ results in a large negative entropy change

(ΔS) of -145.2 J mol^{-1} K^{-1}, while the ΔS for the formation of the dimeric species of 2CuEDTA-$(CH_2)_2(NH_2)_2$ is -75.1 J mol^{-1} K^{-1}; a smaller but still a negative entropy.

Therefore, we do eight independent runs for each 2CuEDTA-$(CH_2)_6(NH_2)_2$ and 2CuEDTA-$(CH_2)_2(NH_2)_2$ aqueous electrolyte to check the irreversibility of the Seebeck coefficient measurements. The results are shown in Figure 33 and Figure 34.

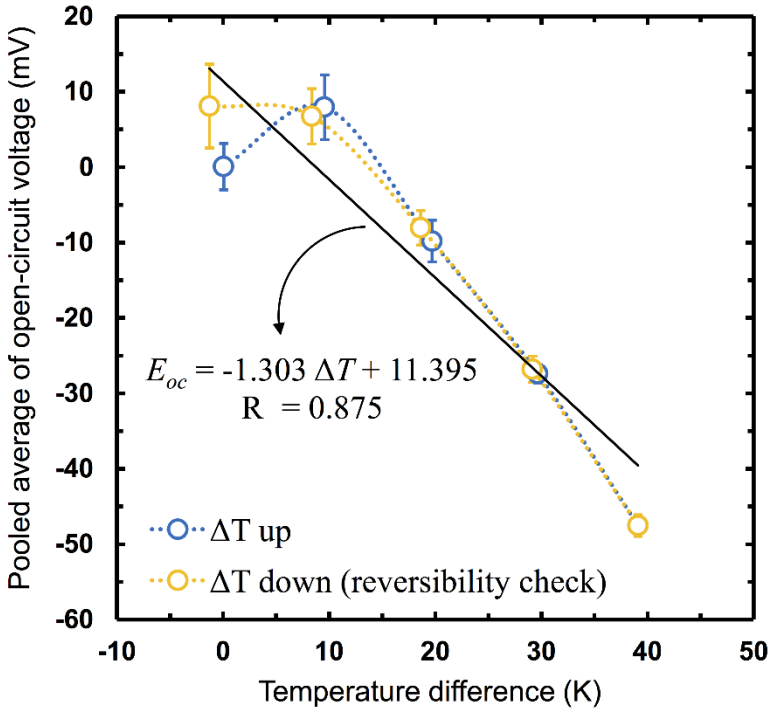

Figure 33. Seebeck Coefficient of 0.5 mM $(NH_2)_2(CH_2)_6$ + 10 mM EDTA + 1 mM $CuSO_4$. The Solution Contained 0.1 M Potassium Sulfate and was Adjusted to pH 6, from the Natural pH of ~4, Using 0.1 M Sodium Hydroxide. Error Bars Represent 95% Confidence Intervals. Some Error Bars are not Visible because They are Smaller than the Corresponding Markers. Dotted Lines were Added to Guide the Eye.

As expected, there is no sign of irreversibility found in both the Seebeck measurements of 2CuEDTA-$(CH_2)_6(NH_2)_2$ and 2CuEDTA-$(CH_2)_2(NH_2)_2$ aqueous electrolytes. Figure 33 shows that simply adding a half mole fraction of 1,6-diaminohexane into a Cu-EDTA aqueous electrolyte further increases the Seebeck

coefficient of traditional 1 mM $CuSO_4$ aqueous electrolyte up to $|\alpha|$ = 1.303 mV K^{-1}, which is more than double the traditional value of 0.619 mV K^{-1}.

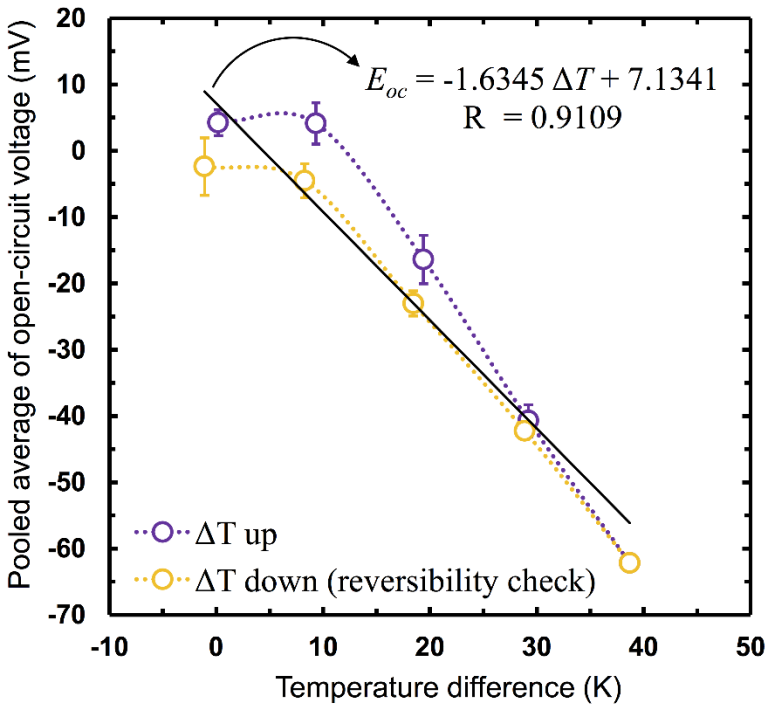

Figure 34. Seebeck Coefficient of 0.5 mM $(NH_2)_2(CH_2)_2$ + 10 mM EDTA + 1 mM $CuSO_4$. The Solution Contained 0.1 M Potassium Sulfate and was Adjusted to pH 6, from the Natural pH of ~4, Using 0.1 M Sodium Hydroxide. Error Bars Represent 95% Confidence Intervals. Some Error Bars are not Visible because They are Smaller than the Corresponding Markers. Dotted Lines were Added to Guide the Eye.

Moreover, adding the same half mole fraction of 1,2-diaminoethane, i.e. $(CH_2)_2(NH_2)_2$, into a Cu-EDTA aqueous electrolyte amplifies the Seebeck coefficient to an even higher value of $|\alpha|$ = 1.635 mV K^{-1}. This value is higher than the benchmark value of 1.4 – 1.5 mV K^{-1}, which is the Seebeck coefficient of ferro/ferricyanide ($Fe(CN)_6^{4-}/Fe(CN)_6^{3-}$) aqueous electrolyte [2, 8, 9, 94].

These Seebeck coefficient values together with their corresponding change of entropy are tabulated in Table 6 for comparison.

Table 6. Summary of Standard Change of Entropy at 25°C (ΔS^o) and Seebeck Coefficient (α) for Cu^{2+} (only), Cu-EDTA, Its Complexes, and Ferro/Ferricyanide Thermogalvanic Cell Systems.

Electrolyte	ΔS^o (J mol-1 K-1)	α (mv K-1)
$Cu + 4H_2O \leftrightarrow 4Cu(H_2O)^{2+} + 2e^-$	+130.4[a]	+0.62
$Cu + EDTA^{2-} \leftrightarrow CuEDTA^{2-} + 2e^-$	-326.2[b]	-1.16
$2CuEDTA^{2-} + (NH_2)_2(CH_2)_6 \leftrightarrow (CuEDTA)_2(NH_2)_2(CH_2)_6^{4-}$	-145.2[c]	-1.30
$2CuEDTA^{2-} + (NH_2)_2(CH_2)_2 \leftrightarrow (CuEDTA)_2(NH_2)_2(CH_2)_2^{4-}$	-75.1[c]	-1.63
$Fe(CN)6^{4-} \leftrightarrow Fe(CN)6^{3-} + e^-$	-	+1.4[d] – 1.5[e]

a $\Delta S^o = S^o(Cu) - S^o(Cu^{2+})$; S^o values are taken from [95]
b unpublished computational results
c Table 4 of Bazanova et al. [93]
d taken from Hu et al. [5]
e taken from Salazar et al. [9]

5.3 Summary

Measurement of Seebeck coefficients in simple electrochemical systems with mixed-ligand complex formations of Cu/Cu^{+2} electrolyte suggests that these electrolytes improve the thermoelectric power (or Seebeck coefficient) of the Cu/Cu^{2+} system up to 160% (Figure 35). This is an important step in understanding the much more complex behavior of polyelectrolytes, which show reproducibility issues whose origin needs further investigation. I have also found that the Seebeck coefficient between the CuSO4 and the CuSO4-EDTA, CuSO4-EDTA-1,6-diaminohexane, or CuSO4-EDTA-1,2-diaminoethane are opposite in sign. This will allow construction of thermodynamically more efficient thermogalvanic devices, such as a thermally regenerative electrochemical cycle (TREC), which utilizes two copper-based half-cells that have opposite signs of Seebeck coefficients, in which electrodes discharged at a low temperature can be recharged at a higher temperature [96-98]. The 160% enhancement of Seebeck

coefficient of Cu/Cu^{2+} electrolyte will also benefit another similar thermally regenerative ammonia-based battery (TRAB), which is also copper based [99, 100].

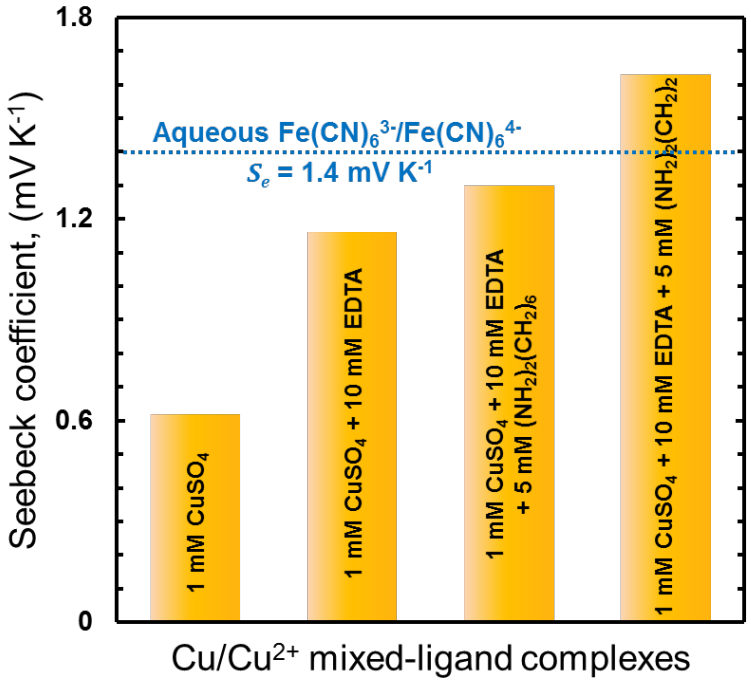

Figure 35. Seebeck Coefficient Comparison between Aqueous $CuSO_4$ Electrolyte and Its Mixed-Ligand Complexes with EDTA, EDTA+1,6-Diaminohexane, and EDTA+1,2-Diaminoethane in Thermogalvanic Cells Using Cu Electrodes and 0.1 M Potassium Sulfate as Background Electrolyte.

6. CONCLUSIONS

As an alternative to electrolyte and electrode materials development, I have shown that natural convection can be controlled and has a significant effect on increasing the power generation of Cu/Cu^{2+} thermogalvanic cells. I concluded that natural convection, which could be induced by orienting the cell either horizontally or vertically, and heating the bottom electrode at the same time, is a plausible aid to improve power generation of thermogalvanic cells. I observed the same magnitude (~2-fold) of the positive amplifying effect of natural convection on the power generation of Cu/Cu^{2+} cell as has been reported for the $Fe(CN)_6^{4-}/Fe(CN)_6^{3-}$ cells in the literature (Figure 36).

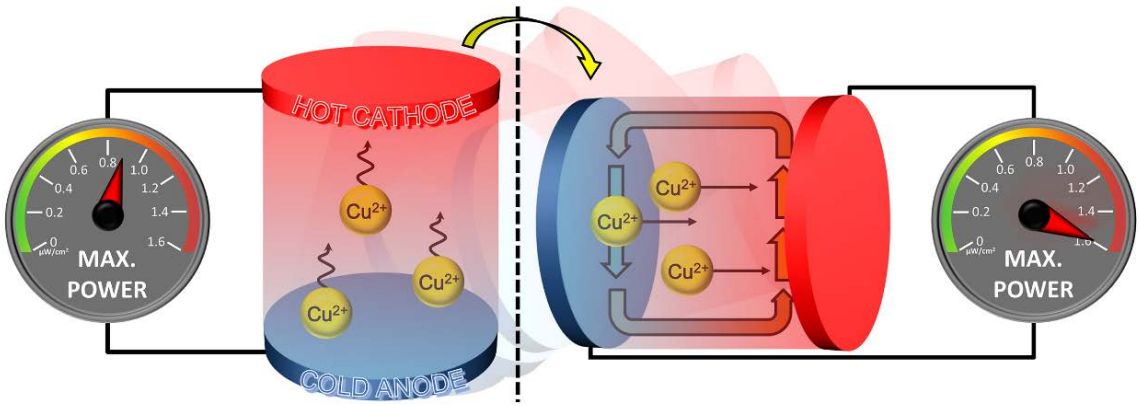

Figure 36. Graphical Summary of Chapter 3: Power Output Enhancement by Natural Convection.

Moreover, I developed a simple analytical model that predicts the ratio between the P_{max} of a thermogalvanic generator with and without convection in terms of Sherwood, Nusselt, and Lewis numbers. The predictions are in reasonable agreement with our experimental data; they show that convection is primarily responsible for the

enhancement in P_{max} of thermogalvanic generators. Comparison with the conventional $Fe(CN)_6^{4-}/Fe(CN)_6^{3-}$ cells revealed a completely different dependence of the electrode spacing on the power generation of Cu/Cu^{2+} thermogalvanic cells, namely that the maximum power output (P_{max}) of Cu/Cu^{2+} cell increases, instead of decreasing, with the electrode spacing because of the one-way ionic transfer mechanism that fully utilizes the natural convection flow within the cell. This dependence of electrode spacing on thermogalvanic power generation suggests that the power generation of Cu/Cu^{2+} cells may not be limited by the cell geometry, which restricts that of the more conventional $Fe(CN)_6^{4-}/Fe(CN)_6^{3-}$ cells. Based on literature review (section 3.1), I confirmed the expectation that the enhancement in mass (ionic) transport, caused by the natural convection, dominates the enhancement in heat transfer. This has also been proven in the analytical model, which shows that higher Lewis number (Le = a /D_{AB}) will ultimately lead to higher power generation; a is thermal diffusivity and D_{AB} mass diffusivity. Throughout my experiments, I also found that the optimum $CuSO_4$ concentration, for the Cu/Cu^{2+} thermogalvanic cells, is 0.7 M, with 0.1 M H_2SO_4 as the background electrolyte. The average cell temperature also has a significant effect on P_{max}. Higher T_{avg} of 55 ^oC resulted in higher P_{max} of 3.12 $\mu W\ cm^{-2}$, while lower T_{avg} of 35 ^oC resulted in lower P_{max} of 1.09 $\mu W\ cm^{-2}$, which is consistent with Kang et al.'s [8] observation for $Fe(CN)_6^{4-}/Fe(CN)_6^{3-}$ cells. The achieved P_{max} still has room to improve by designing a system which uses an electrolyte with higher Lewis number and a generator with Sherwood and Nusselt numbers as high as possible, a prediction from the simple analytical method that I developed. Moreover, the P_{max} in this system can potentially be improved by increasing the mean electrolyte temperature (T_{avg}), either by adopting a

pressurized container and/or alternatively adding propylene glycol to the electrolyte. Although it may increase the complexity of the system, increasing the T_{avg} will increase its thermal efficiency. These results improve our understanding of the energy transfer mechanisms underlying thermogalvanic energy conversion and provide alternative approaches for future researchers and engineers to further optimize this technology.

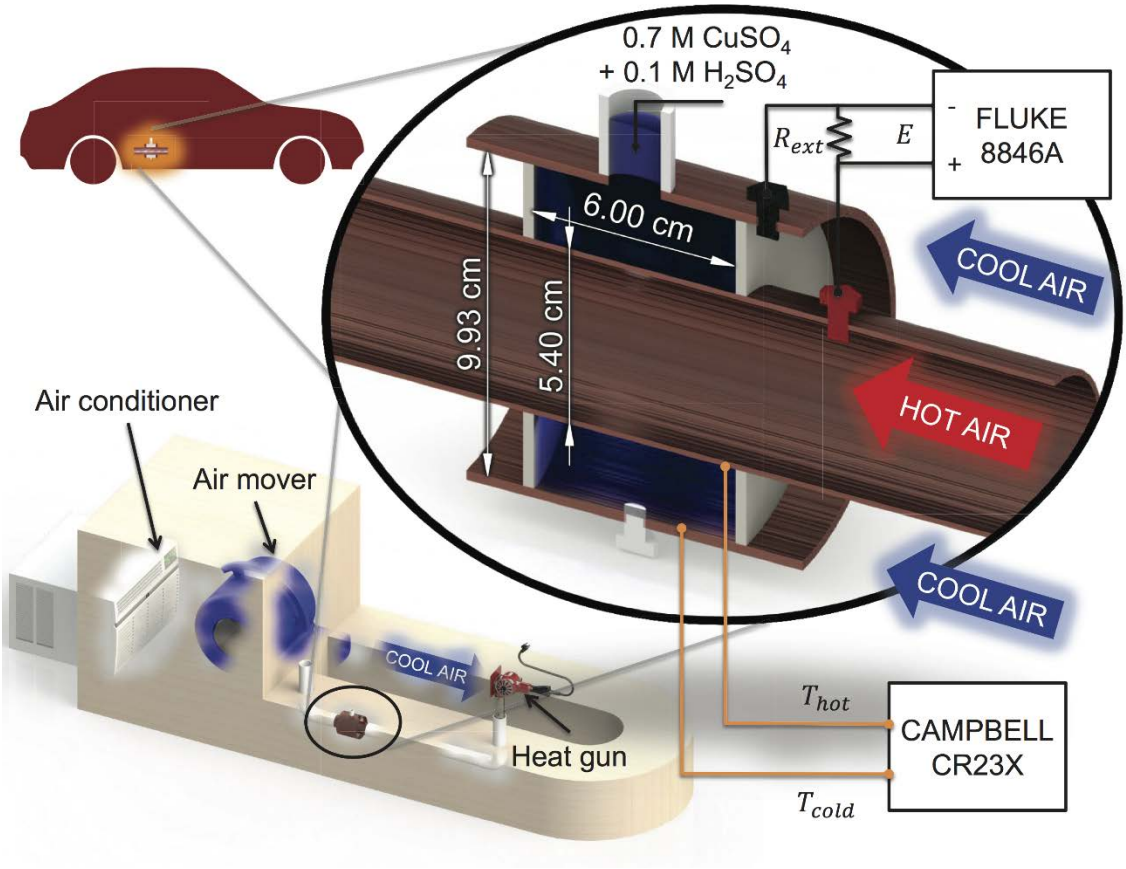

Figure 37. Graphical Summary of Chapter 4: Waste Heat Recovery Application in Automobiles.

In addition, Chapter 4 (Figure 37), which details the feasibility of incorporating a thermogalvanic system into automobiles that would convert waste thermal energy from vehicles' exhaust pipes into electricity, has demonstrated that the liquid nature of the

electrolyte enables a thermogalvanic device to conform to the shape of automotive exhaust pipes much more readily than a solid-state thermoelectric device. Expensive, cleanroom-based manufacturing processes are not required for constructing the cell, which means that their production costs are likely to be substantially lower than for high-performance solid-state thermoelectrics. The power outputs are typically small, between a tenth and tens of mW m^{-2}, but as pointed out by Ball [51], aside from the initial outlay on the cell, that energy is essentially free when it comes from an exhaust pipe of a car that would otherwise just be left to warm the air. The achieved power density indeed still has room to improve. Moreover, more waste thermal energy from the car's radiator can be harvested by designing and developing a flowing cell. Although it may increase the complexity of the system, it will also potentially increase the total thermal efficiency of the system.

Finally, this research has identified simple electrochemical systems with mixed-ligand complex formations of Cu/Cu^{+2} electrolyte, which improve the thermoelectric power (or Seebeck coefficient) of the Cu/Cu^{2+} system up to 160% (Figure 38). This finding has shined some light on the influence of the entropy on the thermoelectric power using simple chelating agents like Ethylenediaminetetraacetic acid (EDTA).

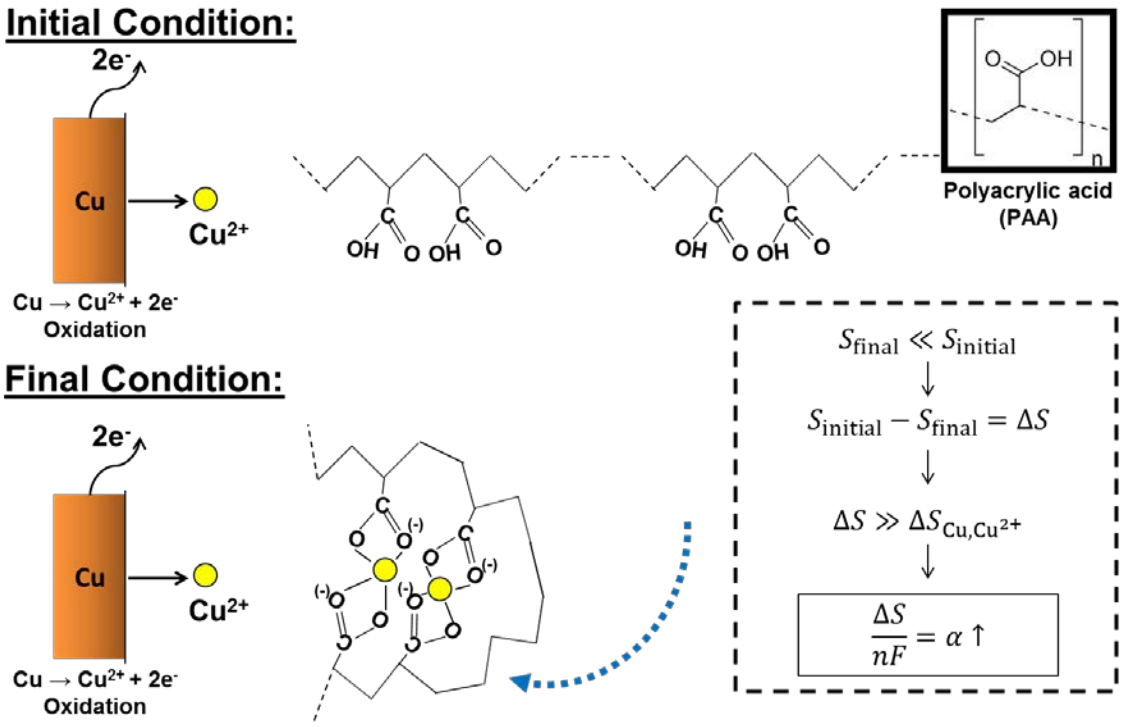

Figure 38. Graphical Summary of Chapter 5: Seebeck Coefficient Enhancements by Novel Electrolytes.

This is an important step in understanding the much more complex behavior of polyelectrolytes, which show reproducibility issues whose origin needs further investigation. It has a huge potential to open a new field of energy conversion application of polymer science. It should also be noted that it will be the sustainable and renewable energy application field, because, first, I have envisioned that the first applications of thermogalvanic generators will be for waste heat cogeneration, e.g., from vehicle exhaust pipes. It is also be renewable, because this concept could be applied to other reversible redox couple and electrode pairs, such as the ferro/ferricyanide redox couple with carbon-nanotubes electrodes. I have shown that the Seebeck coefficient between $CuSO_4$ and the $CuSO_4$-EDTA, $CuSO_4$-EDTA-1,6-diaminohexane, or $CuSO_4$-

EDTA-1,2-diaminoethane are opposite in sign. This will allow construction of thermodynamically more efficient thermogalvanic devices, such as MIT-Stanford's thermally regenerative electrochemical cycle (TREC), which utilizes two copper-based half-cells that have opposite signs of Seebeck coefficients, in which electrodes discharged at a low temperature can be recharged at a higher temperature [96-98]. The 160% enhancement of Seebeck coefficient of Cu/Cu^{2+} electrolyte will also benefit another similar thermally regenerative ammonia-based battery (TRAB), that is also copper based, which was recently proposed by Penn State University [99, 100]. On a bigger picture, this finding has paved a way for the development of 'materials by design' approach to thermogalvanic materials that would enable researchers to predict from theory the expected thermoelectric power, meaning that theory could be used to screen large numbers of compounds without ever having to walk into the lab.

7. FUTURE WORK

The experimental and analytical work presented here has shown some of the potential improvements afforded by using thermogalvanic cells for waste heat recovery systems. A variety of questions and further improvements still remain which should be addressed in future work to bring this concept to real-world applications:

1. Nanostructured Carbon Membrane: Recent reports [101-104] observed that liquid (water) transport through multistep-process-fabricated membranes, in which vertically aligned multi-walled carbon nanotubes (MWCNTs) were grown across a thin permeable polymer film, is orders of magnitude larger than in any other known materials with nanometer-scale pores. On the other hand, however, the thermal conductivity *k* of a packed bed of randomly oriented three-dimensional random networks of single and multi-walled CNTs has been reported to be smaller than that of thermally insulating amorphous polymers [105, 106]. Consequently, how can nanostructured membranes be used to limit the thermal transport while enhancing the mass (ionic) transport?
2. Nanofluids-enhanced thermogalvanic cell: Will mixing specific nanoparticles into the electrolyte (nanofluids) enhance the performance of a thermogalvanic system [16], e.g., sub-freezing thermogalvanic cell using graphene-based nanofluid [107]?
3. Thermally Regenerative Electrochemical Cycle (TREC) and Thermally Regenerative Ammonia-based Battery (TRAB): Both TREC and TRAB that were recently discussed in the literature [96-100] are utilizing copper-based aqueous electrolytes. For a TREC device operating between 283 K and 333 K

[96], the theoretical efficiency is Carnot efficiency, i.e. 15%. However this rejuvenated technology is limited by certain physical parameters, such as the heat capacity of materials, the internal resistance of the cell, and the effectiveness of thermal management [96-98]. To date, the highest demonstrated thermal efficiency (η_{th}) of TREC has been 3.7% [96]. While the highest demonstrated η_{th} of a non-optimized TRAB is lower (i.e. 0.86%) for a device operating between 298 K and 323 K [99], it produces higher maximum power density [100] and shows greater scalability potential than the TRECs.

4. Thermally Chargeable Supercapacitor (TCS) or Thermal Chargeable Capacitor (TCC): This thermal-to-electrical energy conversion system has also been recently discussed in the literature [108-110]. It works based on the temperature dependence of surface ion density in the vicinity of the electrode (i.e. capacitive effect), which relatively distinguish it from thermogalvanic cells.
5. Novel application: Since this work only showed a prototype of automotive thermogalvanic waste heat recovery system, which produced electrical power between 0.1 – 10 mW m^{-2}, other applications such as body-heat powered wearable electronics will be more suitable for this magnitude of converted electrical power.

REFERENCES

[1] A. J. deBethune, T. S. Licht and N. Swendeman, "The Temperature Coefficients of Electrode Potentials," *Journal of The Electrochemical Society,* vol. 106, no. 7, pp. 616-625, 1959.

[2] T. I. Quickenden and Y. Mua, "A Review of Power Generation in Aqueous Thermogalvanic Cells," *Journal of The Electrochemical Society,* vol. 142, no. 11, pp. 3985-3994, 1995.

[3] Y. V. Kuzminskii, V. A. Zasukha and G. Y. Kuzminskaya, "Thermoelectric Effects in Electrochemical Systems. Nonconventional Thermogalvanic Cell," *Journal of Power Sources,* vol. 52, no. 2, pp. 231-242, 1994.

[4] A. Gunawan, C.-H. Lin, D. A. Buttry, V. Mujica, R. A. Taylor, R. S. Prasher and P. E. Phelan, "Liquid Thermoelectrics: Review of Recent and Limited New Data of Thermogalvanic Cell Experiments," *Nanoscale and Microscale Thermophysical Engineering,* vol. 17, no. 4, pp. 304-323, 2013.

[5] R. Hu, B. A. Cola, N. Haram, J. N. Barisci, S. Lee, S. Stoughton, G. Wallace, C. Too, M. Thomas, A. Gestos, M. E. dela Cruz, J. P. Ferraris, A. A. Zakhidov and R. H. Baughman, "Harvesting Waste Thermal Energy Using a Carbon-Nanotube-Based Thermo-Electrochemical Cell," *Nano Letters,* vol. 10, no. 3, pp. 838-846, 2010.

[6] T. J. Abraham, D. R. MacFarlane and J. M. Pringle, "Seebeck Coefficients in Ionic Liquids–Prospects for Thermo-Electrochemical Cells.," *Chemical Communications,* vol. 47, no. 22, pp. 6260-6262, 2011.

[7] M. Bonetti, S. Nakamae, M. Roger and P. Guenon, "Huge Seebeck Coefficients in Nonaqueous Electrolytes," *Journal of Chemical Physics,* vol. 134, no. 11, p. 114513, 2011.

[8] T. J. Kang, S. Fang, M. E. Kozlov, C. S. Haines, N. Li, Y. H. Kim, Y. Chen and R. H. Baughman, "Electrical Power from Nanotube and Graphene Electrochemical Thermal Energy Harvesters," *Advanced Functional Materials,* vol. 22, no. 3, p. 477–489, 2012.

[9] P. F. Salazar, S. Kumar and B. A. Cola, "Nitrogen- and Boron-Doped Carbon Nanotube Electrodes in a Thermo-Electrochemical Cell," *Journal of The Electrochemical Society,* vol. 159, no. 5, pp. B483-B488, 2012.

[10] Y. Yamato, Y. Katayama and T. Miura, "Effects of the Interaction between Ionic Liquids and Redox Couples on their Reaction Entropies," *Journal of The Electrochemical Society,* vol. 160, no. 6, pp. H309-H314, 2013.

[11] T. J. Abraham, D. R. MacFarlane and J. M. Pringle, "High Seebeck Coefficient Redox Ionic Liquid Electrolytes for Thermal Energy Harvesting," *Energy and Environmental Science,* vol. 6, no. 9, pp. 2639–2645, 2013.

[12] M. S. Romano, S. Gambhir, J. M. Razal, A. Gestos, G. G. Wallace and J. Chen, "Novel Carbon Materials for Thermal Energy Harvesting," *Journal of Thermal Analysis and Calorimetry,* vol. 109, no. 3, pp. 1229-1235, 2012.

[13] M. S. Romano, N. Li, D. Antiohos, J. M. Razal, A. Nattestad, S. Beirne, S. Fang, Y. Chen, R. Jalili, G. G. Wallace, R. Baughman and J. Chen, "Carbon Nanotube – Reduced Graphene Oxide Composites for Thermal Energy Harvesting Applications," *Advanced Materials,* vol. 25, no. 45, pp. 6602-6606, 2013.

[14] T. J. Abraham, D. R. MacFarlane, R. H. Baughman, L. Jin, N. Li and J. M. Pringle, "Towards Ionic Liquid-Based Thermoelectrochemical Cells for The Harvesting of Thermal Energy," *Electrochimica Acta,* vol. 113, pp. 87-93, 2013.

[15] N. S. Hudak and G. G. Amatucci, "Energy Harvesting and Storage with Lithium-Ion Thermogalvanic Cells," *Journal of The Electrochemical Society,* vol. 158, no. 5, pp. A572, 2011.

[16] P. F. Salazar, S. T. Stephens, A. H. Kazim, J. M. Pringle and B. A. Cola, "Enhanced Thermo-Electrochemical Power Using Carbon Nanotube Additives in Ionic Liquid Redox Electrolytes," *Journal of Materials Chemistry A,* vol. 2, no. 48, pp. 20676-20682, 2014.

[17] X. Kang, M. T. Børset, O. S. Burheim, G. M. Haarberg, Q. Xu and S. Kjelstrup, "Seebeck Coefficients of Cells with Molten Carbonates Relevant for the Metallurgical Industry," *Electrochimica Acta,* vol. 182, pp. 342–350, 2015.

[18] M. T. Børset, X. Kang, O. S. Burheim, G. M. Haarberg, Q. Xu and S. Kjelstrup, "Seebeck Coefficients of Cells with Lithium Carbonate and Gas Electrodes," *Electrochimica Acta,* vol. 182, pp. 699–706, 2015.

[19] H. A. Alzahrani, J. J. Black, D. Goonetilleke, J. Panchompoo and L. Aldous, "Combining Thermogalvanic Corrosion and Thermogalvanic Redox Couples for Improved Electrochemical Waste Heat Harvesting," *Electrochemistry Communications,* vol. 58, pp. 76–79, 2015.

[20] B. T. Huang, M. Roger, M. Bonetti, T. J. Salez, C. Wiertel-Gasquet, E. Dubois, R. Cabreira Gomes, G. Demouchy, G. Mériguet, V. Peyre, M. Kouyaté, C. L. Filomeno, J. Depeyrot, F. A. Tourinho, R. Perzynski and S. Nakamae, "Thermoelectricity and Thermodiffusion in Charged Colloids," *The Journal of Chemical Physics,* vol. 143, pp. 054902, 2015.

[21] W. Kobayashi, A. Kinoshita and Y. Moritomo, "Seebeck Effect in a Battery-Type Thermocell," *Applied Physics Letters,* vol. 107, pp. 073906, 2015.

[22] K. Touati, M. Depriester, M. Kuriakose and A. H. Sahraoui, "New Methodology for the Thermal Characterization of Thermoelectric Liquids," *Review of Scientific Instruments,* vol. 86, pp. 094901, 2015.

[23] S. Krebs, "Performance Analysis of a Copper II Sulfate Pentahydrate Based Thermogalvanic Cell," University of Louisville, Louisville, 2015.

[24] R. Koerver, D. R. MacFarlane and J. M. Pringle, "Evaluation of Electrochemical Methods for Determination of the Seebeck Coefficient of Redox Electrolytes," *Electrochimica Acta,* vol. 184, pp. 186-192, 2015.

[25] W. Qian, M. Li, L. Chen, J. Zhang and C. Dong, "Improving Thermo-Electrochemical Cell Performances by Constructing Ag-MgO-CNTs Nanocomposite Electrodes," *RSC Advances,* 2015, doi: 10.1039/C5RA19182C.

[26] E. H. Anari, M. Romano, W. X. Teh, J. J. Black, E. Jiang, J. Chen, T. Q. To, J. Panchompoo and L. Aldous, "Substituted Ferrocenes and Iodine as Synergistic Thermoelectrochemical Heat Harvesting Redox Couples in Ionic Liquids," *Chemical Communications,* 2015, doi: 10.1039/C5CC05889A.

[27] M. Stijepovic and P. Linke, "Optimal Waste Heat Recovery and Reuse in Industrial Zones," *Energy,* vol. 36, pp. 4019 - 4031, 2011.

[28] C.-T. Hsu, D.-J. Yao, K.-J. Ye and B. Yu, "Renewable Energy of Waste Heat Recovery System for Automobiles," *Journal of Renewable and Sustainable Energy,* vol. 2, pp. 013105, 2010.

[29] I. Dincer, "On Thermal Energy Storage Systems and Applications in Buildings," *Energy and Buildings,* vol. 34, pp. 377 – 388, 2002.

[30] International Energy Agency, "World Energy Outlook 2011," International Energy Agency, 2010.

[31] United Nations, "United Nations Decade of Sustainable Energy for All 2014-2024," October 2014. [Online]. Available: http://www.se4all.org/decade/.

[32] J. N. Agar, "Thermogalvanic Cells," in *Advances in Electrochemistry and Electrochemical Engineering*, New York, Interscience, 1963, pp. 31-121.

[33] E. Bouty, "Phénomènes Thermo-électriques et Électro-thermiques au Contact d'un Métal et d'un Liquid," *Journal de Physique*, vol. 9, pp. 229-241, 1880.

[34] R. Venkatasubramanian, E. Siivola, T. Colpitts and B. O'Quinn, "Thin-Film Thermoelectric Devices with High Room-Temperature Figures of Merit," *Nature*, vol. 413, pp. 597-602, 2001.

[35] Y. Ito and T. Nohira, "Non-Conventional Electrolytes for Electrochemical Applications," *Electrochimica Acta*, vol. 45, pp. 2611-2622, 2000.

[36] R. H. Hammond and W. M. Risen, Jr., "An Electrochemical Heat Engine for Direct Solar Energy Conversion," *Solar Energy*, vol. 23, pp. 443-449, 1979.

[37] U. B. Holeschovsky, "Analysis of Flooded Flow Fuel Cells and Thermogalvanic Generators," Massachusetts Institute of Technology, Boston, 1994.

[38] T. I. Quickenden and Y. Mua, "The Power Conversion Efficiencies of a Thermogalvanic Cell Operated in Three Different Orientations," *Journal of The Electrochemical Society*, vol. 142, no. 11, pp. 3652-3659, 1995.

[39] Y. Mua and T. I. Quickenden, "Power Conversion Efficiency, Electrode Separation, and Overpotential in the Ferricyanide/Ferrocyanide Thermogalvanic Cell," *Journal of The Electrochemical Society*, vol. 143, no. 8, pp. 2558-2564, 1996.

[40] P. F. Salazar, S. Kumar and B. A. Cola, "Design and Optimization of Thermo-Electrochemical Cells," *Journal of Applied Electrochemistry*, vol. 44, no. 2, pp. 325-336, 2014.

[41] A. Gunawan, H. Li, C.-H. Lin, D. A. Buttry, V. Mujica, R. A. Taylor, R. S. Prasher and P. E. Phelan, "The amplifying effect of natural convection on power generation of thermogalvanic cells," *International Journal of Heat and Mass Transfer*, vol. 78, pp. 423-434, 2014.

[42] P. F. Salazar, "Modeling and Experiments to Develop Thermo-Electrochemical Cells," Georgia Institute of Technology, Atlanta, 2014.

[43] H. Im, H. G. Moon, J. S. Lee, I. Y. Chung, T. J. Kang and Y. H. Kim, "Flexible Thermocells for Utilization of Body Heat," *Nano Research,* vol. 7, no. 4, pp. 443-452, 2014.

[44] A. Gunawan, F. W. Nicholas and P. E. Phelan, "Thermogalvanic Waste Heat Recovery System in Automobiles," in *Proceedings of the ASME 2015 Power Conference*, POWER2015-49094, San Diego, 2015.

[45] P. Pichanusakorn and P. Bandaru, "Nanostructured thermoelectrics," *Materials Science and Engineering R,* vol. 67, pp. 19-63, 2010.

[46] S. Uhl, E. Laux, T. Journot, L. Jeandupeux, J. Charmet and H. Keppner, "Development of Flexible Micro-Thermo-Electrochemical Generators Based on Ionic Liquids," *Journal of Electronic Materials,* vol. 43, no. 10, pp. 3758-3764, 2014.

[47] H. D. Yang, L. T. Tufa, K. M. Bae and T. J. Kang, "A Tubing Shaped, Flexible Thermal Energy Harvester Based on a Carbon Nanotube Sheet Electrode," *Carbon,* vol. 86, pp. 118-123, 2015.

[48] K. M. Bae, H. D. Yang, L. T. Tufa and T. J. Kang, "Thermobattery based on CNT Coated Carbon Textile and Thermoelectric Electrolyte," *International Journal of Precision Engineering and Manufacturing,* vol. 16, no. 7, pp. 1245-1250, 2015.

[49] M. T. S. Chani, K. S. Karimov, S. B. Khan and A. M. Asiri, "Fabrication and Investigation of Flexible Photo-Thermo Electrochemical Cells based on Cu/orange dye aqueous solution/Cu," *International Journal of Electrochemical Science,* vol. 10, pp. 5694 - 5701, 2015.

[50] S. Uhl, M. Pellet, J. Tschanz, E. Laux, T. Journot, L. Jeandupeux and H. Keppner, "Fabrication of Highly-integrated Thermoelectric Generators Based on Ionic Liquids," *Materials Today: Proceedings,* vol. 2, no. 2, pp. 669-674, 2015.

[51] P. Ball, "Material Witness: Pipe dreams," *Nature Materials,* vol. 9, no. 4, p. 290, 2010.

[52] T. J. Abraham, "Ionic Liquid Electrolytes in Thermoelectrochemical Cells," Monash University, Melbourne, 2013.

[53] T. J. Abraham, N. Tachikawa, D. R. MacFarlane and J. M. Pringle, "Investigation of The Kinetic and Mass Transport Limitations in Thermoelectrochemical Cells with Different Electrode Materials," *Physical Chemistry Chemical Physics,* vol. 16, pp. 2527-2532, 2014.

[54] N. Jiao, T. J. Abraham, D. R. MacFarlane and J. M. Pringle, "Ionic Liquid Electrolytes for Thermal Energy Harvesting Using a Cobalt Redox Couple," *Journal of The Electrochemical Society,* vol. 161, no. 7, pp. D3061-D3065, 2014.

[55] M. A. Lazar, D. Al-Masri, D. R. MacFarlane and J. M. Pringle, "Enhanced Thermal Energy Harvesting Performance of a Cobalt Redox Couple in Ionic Liquid–Solvent Mixtures," *Physical Chemistry Chemical Physics,* 2015, doi:10.1039/c5cp04305k.

[56] T. I. Quickenden and C. F. Vernon, "Thermogalvanic Conversion of Heat to Electricity," *Solar Energy,* vol. 36, no. 1, pp. 63-72, 1986.

[57] H. J. V. Tyrell, Diffusion and Heat Flow in Liquids, London: Butterworth & Co. Ltd., 1961.

[58] E. V. Kuz'minskii, "Coefficients of Initial Thermoelectromotive Force for the Thermogalvanic Cell Cu|CuSO4,H2O|Cu," *Russian Journal of Electrochemistry,* vol. 31, no. 6, pp. 600-602, 1995.

[59] J. W. Tester, U. B. Holeschovsky, K. C. Link and J. Corbett, "Evaluation of Thermogalvanic Cells for the Conversion of Heat to Electricity," MIT Energy Lab, Boston, 1992.

[60] B. Burrows, "Discharge Behavior of Redox Thermogalvanic Cells," *Journal of The Electrochemical Society,* vol. 123, no. 2, pp. 154-159, 1976.

[61] J. M. Hornut and A. Storck, "Experimental and Theoretical Analysis of A Thermogalvanic Undivided Flow Cell with Two Aqueous Electrolytes at Different Temperatures," *Journal of Applied Electrochemistry,* vol. 21, no. 12, pp. 1103-1113, 1991.

[62] T. Ikeshoji, "Thermoelectric Conversion by Thin-Layer Thermogalvanic Cells with Soluble Redox Couples," *Bulletin of the Chemical Society of Japan,* vol. 60, pp. 1505-1514, 1987.

[63] T. Ikeshoji, S. Kimura, F. N. B. de Nahui and M. Yoneya, "Computer Analysis of Natural Convection in Thin-Layer Thermocells with A Soluble Redox Couple. Part 1. Method and The Unsteady Problem," *Journal of Electroanalytical Chemistry,* vol. 307, pp. 29-45, 1991.

[64] T. Ikeshoji, F. N. B. de Nahui, S. Kimura and M. Yoneya, "Computer analysis on natural convection in thin-layer thermocells with a soluble redox couple. Part 2. E-I relation, electric power, heat flux and electrochemical heat pump," *Journal of Electroanalytical Chemistry,* vol. 312, pp. 43-56, 1991.

[65] R. S. Gonçalves and T. Ikeshoji, "Comparative Studies of a Thermoelectric Converter by a Thermogalvanic Cell with a Mixture of Concentrated Potassium Ferrocyanide and Potassium Ferricyanide Aqueous Solutions at Great Temperatures Differences," *Journal of The Brazilian Chemical Society,* vol. 3, no. 3, pp. 98-101, 1992.

[66] T. Ikeshoji and R. S. Goncalves, "Thermogalvanic Cells with Aqueous Redox Couples and Temperature Differences Larger than 100 K," *Journal of Applied Electrochemistry,* vol. 23, pp. 516-519, 1993.

[67] A. V. Sokirko, "Theoretical Study of Thermogalvanic Cells in Steady State," *Electrochimica Acta,* vol. 39, no. 4, pp. 597-609, 1994.

[68] Y. A. Çengel, Heat and mass transfer: A practical approach, New York: McGraw-Hill Companies, Inc., 2007.

[69] R. Taylor, S. Coulombe, T. Otanicar, P. Phelan, A. Gunawan, W. Lv, G. Rosengarten, R. Prasher and H. Tyagi, "Small Particles, Big Impacts: A Review of the Diverse Applications of Nanofluids," *Journal of Applied Physics,* vol. 113, pp. 011301, 2013.

[70] A. Bejan, Convection Heat Transfer, Hoboken, New Jersey: John Willey & Sons, 2004.

[71] A. Bejan and C. L. Tien, "Laminar Natural Convection Heat Transfer in a Horizontal Cavity with Different End Temperatures," *Journal of Heat Transfer,* vol. 100, pp. 641-647, 1978.

[72] F. H. Busse, "Non-Linear Properties of Thermal Convection," *Report on Progress in Physics,* vol. 41, pp. 1929-1967, 1978.

[73] S. W. Angrist, Direct Energy Conversion, 4th ed., F. Kreith, Ed., Boston, MA: Allyn and Bacon, Inc., 1982.

[74] R. A. Taylor and G. L. Solbrekken, "Comprehensive System-Level Optimization of Thermoelectric Devices for Electronic Cooling Applications," *IEEE Transaction on Components and Packaging Technologies,* vol. 31, no. 1, pp. 23-31, 2008.

[75] S. K. Yee, S. LeBlanc, K. E. Goodson and C. Dames, "$ per W metrics for thermoelectric power generation: beyond ZT," *Energy & Environmental Science,* vol. 6, pp. 2561-2571, 2013.

[76] G. Prentice, Electrochemical Engineering Principles, Englewood Cliffs, New Jersey: Prentice Hall, 1991.

[77] T. I. Quickenden and Q. Xu, "Toward a Reliable Value for the Diffusion Coefficient of Cupric Ion in Aqueous Solution," *Journal of The Electrochemical Society,* vol. 143, no. 4, pp. 1248-1253, 1996.

[78] S. Chu and A. Majumdar, "Opportunities and Challenges for a Sustainable Energy Future," *Nature,* vol. 488, pp. 294-303, 2012.

[79] U.S. Department of Energy, "Report on the First Quadrennial Technology Review," 2011. [Online]. Available: http://energy.gov/sites/prod/files/QTR_report.pdf. [Accessed October 2014].

[80] J. R. Armstead and S. A. Miers, "Review of Waste Heat Recovery Mechanisms for Internal Combustion Engines," *ASME Journal of Thermal Science and Engineering Applications,* vol. 6, no. 1, pp. 014001, 2014.

[81] Y. A. Çengel and A. J. Ghajar, Heat and Mass Transfer: Fundamentals & Applications, 5th ed., New York: McGraw-Hill Education, 2015.

[82] Arizona State University, "ASU Weather Station," Ameresco, 2014. [Online]. Available: http://cm.asu.edu/weather/. [Accessed 1 June 2014].

[83] U.S. Department of Energy, "FY 2014 Progress Report for Advanced Combustion Engine Research and Development," December 2014. [Online]. Available: http://energy.gov/sites/prod/files/2015/03/f20/FY2014%20Advanced%20Combustion%20Engine%20R%26D%20Annual%20Report_0.pdf. [Accessed March 2015].

[84] G. Joshi, R. He, M. Engber, G. Samsonidze, T. Pantha, E. Dahal, K. Dahal, J. Yang, Y. Lan, B. Kozinsky and Z. Ren, "NbFeSb-based p-type Half-Heuslers for Power Generation Applications," *Energy and Environmental Science,* vol. 7, no. 12, pp. 4070-4076, 2014.

[85] S. LeBlanc, "Thermoelectric Generators: Linking Material Properties and Systems Engineering for Waste Heat Recovery Applications," *Sustainable Materials and Technologies,* vol. 1, pp. 26-35, 2014.

[86] K. Amezawa, N. Yamamoto, Y. Tomii and Y. Ito, "Single-Electrode Peltier Heats of Li-Si Alloy Electrodes in LiCl-KCl Eutectic Melt," *Journal of The Electrochemical Society,* vol. 145, no. 6, pp. 1986-1993, 1998.

[87] K. Amezawa, N. Yamamoto, Y. Tomii and Y. Ito, "Thermodynamic Properties and Single-Electrode Peltier Heats of a Li-Al Alloy in a LiCl-KCl Eutectic Melt," *Journal of The Electrochemical Society,* vol. 146, no. 3, pp. 1069-1074, 1999.

[88] T. Murakami, T. Nishikiori, T. Nohira and Y. Ito, "Thermoelectric Power of M-H Systems in Molten Salts and Application to M-H Thermogalvanic Cell," *Journal of The Electrochemical Society,* vol. 150, no. 7, pp. A928-A932, 2003.

[89] K. Shindo, M. Arakawa and T. Hirai, "Effect of Non-graphitized Carbon Electrodes on The Electrochemical Characteristics of A Thermocell with A Br2/Br- Redox Couple," *Journal of Power Sources,* vol. 70, no. 2, pp. 228-234, 1998.

[90] J. Kim, B. Min, J. Won and Y. Kang, "Analysis of the Glass Transition Behavior of Polymer-Salt Complexes: An Extended Configurational Entropy Model," *Journal of Physical Chemistry B,* vol. 107, pp. 5901-5905, 2003.

[91] Z. Iatridi, G. Bokias and J. Kallitsis, "Physicochemical Study of the Complexation of Poly(acrylic acid) with Cu2+ Ions in Water," *Journal of Applied Polymer Science,* vol. 108, pp. 769-776, 2008.

[92] D. F. Pyreu and E. V. Kozlovskii, "Thermodynamics of Mixed-Ligand Complex Formation of Copper (II) Ethylenediaminetetraacetate with Hexamethylenediamine in an Aqueous Solution," *Journal of Thermal Analysis and Calorimetry,* vol. 100, no. 1, pp. 355-360, 2010.

[93] M. A. Bazanova, D. F. Pyreu and E. V. Kozlovskii, "Thermodynamics of Mixed-Ligand Complex Formation of Copper (II) Ethylenediaminetetraacetate with Amino Acids in Solution," *Journal of Thermal Analysis and Calorimetry,* vol. 112, no. 3, pp. 1545-1551, 2013.

[94] R. Hu, "Thermogalvanic Cells Using Carbon Nanotubes as Electrode Materials," The University of Texas at Dallas, Dallas, 2007.

[95] A. J. Bard and L. R. Faulkner, Electrochemical Methods: Fundamentals and Applications, New York: John Wiley & Sons, Inc, 2001.

[96] S. W. Lee, Y. Yang, H.-W. Lee, H. Ghasemi, D. Kraemer, G. Chen and Y. Cui, "An Electrochemical System for Efficiently Harvesting Low-grade Heat Energy," *Nature Communications,* vol. 5, pp. 3942, 2014.

[97] Y. Yang, J. Loomis, H. Ghasemi, S. W. Lee, Y. J. Wang, Y. Cui and G. Chen, "Membrane-Free Battery for Harvesting Low-Grade Thermal Energy," *Nano Letters,* vol. 14, no. 11, pp. 6578-6583, 2014.

[98] Y. Yang, S. W. Lee, H. Ghasemi, J. Loomis, X. Li, D. Kraemer, G. Zheng, Y. Cui and G. Chen, "Charging-Free Electrochemical System for Harvesting Low-Grade Thermal Energy," *Proceedings of the National Academy of Sciences,* vol. 111, no. 48, p. 17011–17016, 2014.

[99] F. Zhang, J. Liu, W. Yang and B. E. Logan, "A Thermally Regenerative Ammonia-based Battery for Efficient Harvesting of Low-Grade Thermal Energy as Electrical Power," *Energy & Enviromental Science,* vol. 8, no. 1, pp. 343-349, 2015.

[100] F. Zhang, N. LaBarge, W. Yang, J. Liu and B. E. Logan, "Enhancing Low-Grade Thermal Energy Recovery in aThermally Regenerative Ammonia Battery Using Elevated Temperatures," *ChemSusChem,* vol. 8, no. 6, pp. 1043-1048, 2015.

[101] B. J. Hinds, N. Chopra, T. Rantell, R. Andrews, V. Gavalas and L. G. Bachas, "Aligned Multiwalled Carbon Nanotube Membranes," *Science,* vol. 303, pp. 62-65, 2004.

[102] M. Majumder, N. Chopra, R. Andrews and B. J. Hinds, "Enchanced flow in carbon nanotubes," *Nature,* vol. 438, p. 44, 2005.

[103] J. K. Holt, H. G. Park, Y. Wang, M. Stadermann, A. B. Artyukhin, C. P. Grigoropoulos, A. Noy and O. Bakajin, "Fast Mass Transport Through Sub-2-Nanometer Carbon Nanotubes," *Science,* vol. 312, pp. 1034-1037, 2006.

[104] D. S. Sholl and J. K. Johnson, "Making High-Flux Membranes with Carbon Nanotubes," *Science,* vol. 312, pp. 1003-1004, 2006.

[105] R. Prasher, X. Hu, Y. Chalopin, N. Mingo, K. Lofgreen, S. Volz, F. Cleri and P. Keblinski, "Tuning Carbon Nanotubes from Exceptional Heat Conductors into Insulators," *Physical Review Letters,* vol. 102, pp. 1-4, 2009.

[106] J. Chen, X. Gui, Z. Wang, Z. Li, R. Xiang, K. Wang, D. Wu, X. Xia, Y. Zhou, Q. Wang, Z. Tang and L. Chen, "Superlow Thermal Conductivity 3D Carbon Nanotube Network for Thermoelectric Applications," *ACS Applied Materials & Interfaces,* vol. 4, no. 1, pp. 81-86, 2012.

[107] R. Zheng, J. Gao, J. Wang and G. Chen, "Reversible temperature regulation of electrical and thermal conductivity using liquid–solid phase transitions," *Nature Communications,* vol. 2, pp. 289, 2011.

[108] Y. Qiao, V. K. Punyamurtual, A. Han and H. Lim, "Thermal-to-electric Energy Conversion of A Nanoporous Carbon," *Journal of Power Sources,* vol. 183, no. 1, pp. 403-405, 2008.

[109] H. Lim, "Recycling of Wasted Energy: Thermal to Electrical Energy Conversion," University of California, San Diego, San Diego, 2011.

[110] M. Bonetti, S. Nakamae, B. T. Huang, T. J. Salez, C. Wiertel-Gasquet and M. Roger, "Thermoelectric Energy Recovery at Ionic-Liquid/Electrode Interface," *The Journal of Chemical Physics,* vol. 142, pp. 244708, 2015.